To My Parents

THE PENETRATION OF MAGNETIC FIELD INTO SUPERIMPOSED FILMS OF NORMAL AND SUPERCONDUCTING METALS

Thesis submitted

by

Abdulmohamed Adatia

for the

Degree of Doctor of Philosophy

of the University of London

Physics Department,
Imperial College of Science and Technology
London

1976

ABSTRACT

The variation of the a.c. susceptibility of plane superimposed films of normal and superconducting metals as a function of an applied d.c. field has been used to investigate the electromagnetic screening that the normal metal displays as a result of induced superconductivity.The measurements were made by the Schawlow-Devlin technique using an 800 kHz back-diode oscillator.All the specimens studied had pure Pb as the superconductor with Ag and its dilute magnetic and non-magnetic alloys, Zn, Cd and CdMg variously constituting the normal film. Comparison of the results with theoretical calculations of Deutscher shows that the qualitative agreement between the two improves as the dirty limit, the domain of validity of the model, is approached, yielding an estimate of ~ -0.07 for the BCS interaction parameter NV in Ag. The reliability of this method for estimating NV and possible refinements to theoretical calculations are discussed. Measurements on dilute AgMn are shown to demonstrate clearly the pair-breaking effect of the magnetic atoms.

The so-called "saturation" effects in the normal part of NS layers that have been observed by the Orsay Group in the course of experiments similar to ours were looked for throughout our investigation. No such effects were observed in any of the normal metals studied. This has led to a close examination of the existing theory of "saturation" effects and the theory is shown to be open to criticism in several respects. On the experimental side, possible explanations to account for the reported observations of these effects are put forward and supported by experimental evidence. Finally, areas of further investigation in this field are set out.

ACKNOWLEDGEMENTS

I wish to express my sincere thanks to my supervisor, Dr. J.G. Park, who proposed the subject for my research and has, throughout the course of this work, been a constant source of help, ideas and encouragement. My thanks are also due to Professor B.R. Coles for his valuable guidance and numerous helpful suggestions; to Dr. D. Griffiths and Dr. H.E.N. Stone for assistance at various stages of this project; to Dr. S.M. Freake and Dr. A.P. Murani whose help and advice have been invaluable; and to all the members of the Metal Physics group who provided a congenial and stimulating atmosphere to work in.

I am deeply grateful to Professor Coles and Dr. Park for their kindness and understanding during the grave events of 1972 in Uganda, which was a period of considerable personal stress for me.

Finally, I would like to thank Molly Chock for her patience in typing the manuscript.

CONTENTS

		Page
ABSTRACT		II
ACKNOWLEDGEMENTS		III
CONTENTS		IV
CHAPTER I	INTRODUCTION	
1.1	The Proximity Effect	1.1
1.2	Discovery and Early Experiments	1.2
1.3	BCS Theory-Interaction Parameter	1.3
1.4	Interaction Parameter of a Normal Metal	1.5
1.5	Post-BCS Proximity Experiments	1.7
	EXPERIMENTS IN ZERO FIELDS	
1.6	Transition Temperature of NS Layers	1.8
1.7	T_{CNS} for Magnetic 'Normal' Films	1.11
1.8	Specific Heat Measurements	1.14
1.9	Critical Current of SNS Sandwiches	1.16
1.10	Resistance of SNS Junctions	1.17
1.11	Tunnelling Experiments on NS Layers	1.20
	PROXIMITY EFFECT IN THE PRESENCE OF A MAGNETIC FIELD	
1.12	Parallel Upper Critical Field of NS Layers	1.22
1.13	Thermal Conductivity Measurements	1.24
1.14	Critical Field of N: Breakdown Field H_b	1.25
1.15	'Meissner' Screening in N	1.30
1.16	The Present Work	1.32

		Page
CHAPTER II	THEORY	
2.1	Introduction	2.1
2.2	Gor'kov's Formulation of Microscopic Theory	2.1
2.3	Variation of $\Delta(\underline{r})$ in Normal Metal for $T \lesssim T_{CNS}$	2.3
2.4	Boundary Conditions on $\Delta(x)$	2.9
2.5	Werthamer Approximation for Evaluating T_{CNS}	2.10
2.6	Electrodynamics of Superconductors	2.12
2.7	Generalised Ginzburg-Landau Equations	2.14
2.8	Description of Δ at Lower Temperatures	2.18
2.9	Magnetic Effects on N Side	2.23
2.10	G-L Parameter in N	2.25
2.11	Screening Distance δ in Thick N Layer	2.26
2.12	Breakdown Effect, Normal Layer Thin	2.28
2.13	(a) Improved Calculation of $\lambda(\Delta)$	2.33
	(b) Deutscher's Numerical Calculation	2.34
	(c) Discussion of the Model	2.35
2.14	'Saturation' Effects	2.37
CHAPTER III	SPECIMEN PREPARATION	
3.1	Choice of Materials	3.1
3.2	The Evaporator	3.2
3.3	Substrate Cleaning Procedure	3.3
3.4	Film Geometry and Film Trimming	3.5
3.5	Preparation of Alloys	3.6

		Page
3.6	Necessity for Use of Pellets	3.7
3.7	Evaporation Procedure	3.9
3.8	Film Thickness Measurement	3.10
3.9	Order of Evaporation	3.14
3.10	Storage of Specimens	3.16
CHAPTER IV	APPARATUS	
4.1	Introduction	4.1
4.2	The Cryostat	4.2
4.3	Temperature Control and Measurement	4.2
4.4	Cryostat Insert	4.3
4.5	Reasons for Use of He Gas Chamber	4.7
4.6	Field Coils and Magnet Power Supply	4.8
4.7	Back-Diode Oscillator	4.9
4.8	Estimation of r.f. Field	4.16
4.9	Frequency Measurement	4.17
4.10	Oscillator Stability	4.18
4.11	Effect on Frequency of Circuit Losses	4.18
4.12	Specimen Heater and Thermal Contacts	4.23
CHAPTER V	EXPERIMENTAL PROCEDURE AND DATA ANALYSIS	
5.1	Coil Winding and Specimen Mounting	5.1
5.2	Data Recording and Measurement of δ	5.2
5.3	Magnetic Transitions of Pb of NS Layers	5.4
5.4	Frozen Flux	5.11
5.5	Field Alignment	5.13
5.6	The Empty Coil Effect	5.15
5.7	Measurement of Residual Resistivity	5.17

		Page
5.8	Effect of Earth's Field	5.18
CHAPTER VI	RESULTS AND DISCUSSION	
6.1	δ for Ag Alloys	6.1
6.2	Resistance of Ag Alloys	6.9
6.3	Zn and Cd	6.14
6.4	'Saturation' Effects	6.18
6.5	Effect of Order of Evaporation and Time Lag	6.26
6.6	Assessment of Technique and Suggestions for Future Work	6.31
REFERENCES		R.1

CHAPTER I

INTRODUCTION

This thesis is based on an experimental investigation of the proximity effect between superimposed normal and superconducting films. This is done by studying the electromagnetic screening properties of such a system in response to an applied magnetic field. The normal film in such systems, under suitable conditions, exhibits a diamagnetic response to the applied field and thus behaves like a superconductor. Conversely, the superconducting film displays weakened superconductivity near the interface which, in our kind of experiment, would be shown by a lowering of its critical field at the interface. The above, however, is but one of many observable effects produced in the properties of the two films by their proximity. In this chapter we briefly examine why the superconducting proximity effect has come to be regarded as an important tool in physical investigations and review just some of the wide variety of experiments based on this phenomenon that have been done. This will put the present series of experiments in its proper perspective.

1.1 The Proximity Effect

A large number of experiments over the recent years have firmly established the existence of the superconducting proximity effect, whereby the properties of normal (N) and superconducting (S) metals in good electrical contact are modified in the vicinity of the boundary between the two (1a).

The ideal proximity effect in this context is understood as resulting from the movement of electrons across a clean, well-defined boundary where effects due to atomic inter-diffusion, alloying or compound formation are absent. The range of the proximity effect, that is, the distance into N that the 'superelectrons' or Cooper pairs from S penetrate is of the order of a few coherence lengths or a few thousand angstroms. This necessitates its study by the use of specimens such as superimposed films or laminated structures where at least one dimension is of a comparable magnitude.

A closely analogous situation is believed to exist between ferromagnetic and non-magnetic metals in contact. However, the distances to which spin-polarised electrons can be detected in the non-magnetic material is much shorter. For example, Hauser (69) has reported a range of only ~ 20 Å for the magnetic proximity effect between Fe and Pd.

1.2 Discovery and Early Experiments

Around 1930, Burton, Wilhelm and Misener (2) carried out an investigation into the resistive transition temperatures of superconducting films. In the course of these experiments, they found that Pb and Sn films electroplated onto constantan subtrates showed a large drop in the transition temperature with a decrease in thickness below about 5000 Å. This was in marked contrast to the behavior of similar films on glass subtrates. No satisfactory explanation could be found to account for these observations and they were attributed to alloying and atomic diffusion at the boundary. Apparently,

no more experiments were conducted on these lines until after the advent of the microscopic theory of Bardeen, Cooper and Shrieffer, commonly referred to as the BCS theory, in 1957 (3).

1.3 BCS Theory-Interaction Parameter

The BCS theory was preceded by numerous phenomenological theories and models constructed to account for the observed properties of superconductors. The current universal acceptance of the theory as the basis of a microscopic description of the superconducting state derives from its remarkable success in being able to explain and correlate all the observed properties of superconductors and in leading to the rather diverse phenomenological models in the appropriate limits. The essential feature of the theory is to show, in general, that in the presence of an attractive interaction, no matter how weak, between pairs of electrons in a metal the free electron gas in its ground state is unstable against the formation of a lower energy state consisting of electrons bound in pairs (4). In particular they showed that such an attractive interaction could arise out of electron-phonon coupling as first suggested by Frölich, and proposed the following simplified form for the nett interaction $V_{kk'}$, between electrons of momenta $\underline{k}$ and $\underline{k}'$:

$$V_{kk'} = V \quad \text{for } |\varepsilon_k|, |\varepsilon_{k'}| \leq \hbar\omega_q$$

$$= 0 \qquad \text{otherwise} \qquad \text{(I-1)}$$

Here ε_k, $\varepsilon_{k'}$, are the energies of the two electrons, measured

from the Fermi level, ω_q is an average phonon cut-off frequency, generally taken to be the Debye frequency of the lattice and $\hbar$, Planck's constant. The nett interaction results from the screened Coulomb repulsion and the phonon-mediated attractive interaction. Its strength is characterised by the magnitude of the interaction parameter V which is positive for a superconductor in the convention we adopt.

BCS showed that the lowest energy state was obtained for pairing between electrons of equal and opposite wave--vectors and spins i.e. $\underline{k}\uparrow$ and $-\underline{k}\downarrow$, which form the so called Cooper pairs. The temperature T_c below which the electron condensation is energetically favorable is related to the interaction parameter by the following expression

$$k_B T_c = 1.14 \hbar\omega_q \exp(-1/N(0)V) \qquad \text{(I-2)}$$

N(0) is the density of states at the Fermi level for electrons of one spin and k_B the Boltzmann constant. The theory also showed that below T_c, a gap of magnitude $\Delta(T)$, the forbidden band, appears in the density of states of the excitations. This gap separates the excited states from the condensate. $2\Delta(T)$ is the binding energy of a pair, its value at 0^oK being given by

$$2\Delta(0) = 3.52 k_B T_c \qquad \text{(I-3)}$$

The predicted temperature variation of the gap can be expressed in the following simplified form (4)

$$T_c > T \gtrsim 0{\cdot}7T_c\,,\ \Delta(T) \simeq 3{\cdot}2k_B T_c(1-T/T_c)^{1/2}$$

$$T < 0{\cdot}5T_c\,,\ \Delta(T) \simeq \Delta(0) \qquad \text{(I-4)}$$

The binding energy per pair is seen to be of the order of 10^{-3} eV. This explained the well-known observation (5,6) that even a small amount of a magnetic impurity that produced localised moments in a superconductor caused a drastic lowering of T_c or destruction of superconductivity altogether. It arises because of the much larger (~ 0.5 eV) exchange energy that the Cooper pair constituents of anti-parallel spins would have in the presence of a magnetic moment.

1.4 Interaction Parameter of a Normal Metal

The absence of superconductivity in magnetic metals thus accounted for, the important question remained of whether every non-magnetic metal would become superconducting at sufficiently low temperatures or whether there were intrinsically 'normal' metals where the interaction parameter was zero or negative. Precise theoretical calculations of V have proved to be rather difficult and have had varying degrees of success. As an example, one may refer to the calculation of T_c for the metals Zn, Cd, Be and Mg by Allen and Cohen (7). For the first three of these metals which are known superconductors their results are in very good agreement with experiment. They predict a T_c of $0.012^{\circ}K$ for

Mg. An earlier calculation by Morel and Anderson (8) many of whose results were also in satisfactory agreement with experiment, however, predicted $(T_c)_{Mg}$ of 2.3°K. Recent measurements by Mota et al. (70) on very pure Mg (resistance ratio 20,000) have failed to indicate a superconducting transition down to T = .0025°K. However, by extrapolation of the transition temperatures of Cd-Mg alloys of different compositions, they predict a $(T_c)_{Mg}$ of 0.5 mK.

An examination of Eqn. (I-2) shows that because of the exponential dependence of T_c on N(0)V, the critical temperature goes down very rapidly with N(0)V for N(0)V < 0.1. In view of this, the agreement between the calculated $(T_c)_{Mg}$ (7) and the indirect experimental determination would appear good. Eqn. (I-2) also makes it apparent that any hope of a direct observation of superconductivity in metals with N(0)V < 0.1 has to be abandoned and indirect means of determining the interaction parameter in such cases explored.

As indicated above, the transition temperature of certain alloys shows a systematic variation with concentration. This experimental fact has been used to predict T_{cN} by extrapolation. The method is essentially an empirical one and its use limited to metals that form good solid solutions and show a systematic variation of T_c over a wide range of concentrations.

By far the most popular method for the indirect determination of V in a normal metal has been the study of the proximity effect. We mentioned earlier the important role

that the lattice is believed to play in producing the attractive interaction between electrons. Unlike the alloying experiment, the lattice under investigation in the proximity effect is left essentially unchanged and only an exchange of electrons allowed between it and the superconductor. This makes the problem a lot less complex to analyse theoretically. The good qualitative, and often quantitative, agreement between theory and early experiments has prompted further investigation. Moreover, this appears to be the only class of experiments at present available for studying the interaction in metals like Cu, Ag and Au (10).

1.5 Post-BCS Proximity Experiments

The experiments of H. Meissner (11) in the years 1958 to 1960 heralded renewed interest in the proximity effect. He carried out a systematic study of the contact resistance between crossed wires of superconductors plated with normal metals, and vice versa, as a function of the current, temperature and thickness of the plated metal. He found that a supercurrent could be passed between superconducting wires and through the plated normal metal provided its thickness did not exceed a certain critical value. The critical thickness for films of Au, Cu and Ag on Sn wires was of the order of 2000 to 3000 $\mathring{A}$, whereas for films of magnetic materials, Fe, Co and Ni it was ~ 100 $\mathring{A}$. These results were explained in terms of Pippard's concept of the coherence length ξ. According to this, rapid changes in the number density n_s of the superconducting electrons are energetically unfavourable.

Therefore n_s would gradually tail off to zero over a distance ξ in the normal metal which would thus sustain a supercurrent if its thickness was less than ξ. The much smaller critical thickness in the case of the magnetic metals was understood in terms of the greater scattering of the superconducting electrons by the magnetic atoms.

These experiments firmly established the superconducting proximity effect and provided an estimate of its range. They stimulated interest into the search for other experimentally observable effects of the induced superconductivity in the normal metal and the counter-effects, if any, on the superconductor.

We mention below a few of the representative experiments with the aim of showing their wide variety and their interpretation Comprehensive reviews of experiments in certain classes, e.g. transition temperature measurements, exist and will be referred to in what follows. Certain aspects of theory will be touched upon insofar as they help in the interpretation of the results.

EXPERIMENTS IN ZERO FIELD

1.6 Transition Temperature of NS Layers

Transition temperature determination, on account of being the simplest kind of measurement, was the most popular of the early proximity experiments. Clarke's review article (12) contains an extensive bibliography of such experiments. We discuss these with reference to Hilsch (9) in whose careful experiments special effort was made to minimise the effects due to intermetallic diffusion. His was also the first such experiment to include data on mean free paths in the normal films, a quantity

that proved to be important for comparison with theory when this came about.

As will be seen in Chapter II, most proximity experiments have been done in the "dirty" limit so that spurious effects due to not having the ideal sharp, well-defined boundary on account of inevitable structural defects and interdiffusion, may not dominate. The criterion for the dirty limit is that the mean free path ℓ of the electrons be much smaller than the coherence length $\xi(T)$. For a normal metal $\xi(T)$ is defined by Eqn. (I-5) and the above criterion then becomes (12)

$$\xi = \left(\frac{\hbar v_F \ell}{6\pi k_B T}\right)^{1/2} \gg \ell \qquad \text{(I-5)}$$

where V_F is the Fermi velocity. The vapour quenching technique that Hilsch used for the deposition of Pb/Cu films onto cooled substrates generally gives a defect-rich structure and short ℓ and all his films were therefore in the dirty limit. The films, deposited onto substrates at $10^{\circ}K$, were not warmed up or exposed to oxygen until after the measurement.

He found the following empirical relation to fit his data:

$$T_{cS} - T_{cNS} = (T_{cS} - \theta)(1 - \exp(-d_N/a))$$

where T_{cS} and T_{cNS} are the transition temperatures of the isolated S and of NS films respectively, d_N the copper film thickness, θ the limiting value of T_{cNS} as $d_N \to \infty$, for a given Pb thickness d_s. 'a' is an adjustable parameter which turned out to be proportional to $\ell^{\frac{1}{2}}$. For a more rigorous analysis, de Gennes and Guyon (13) formulated a theory of the proximity effect which used the linea-

rised form of Gor'kov's self-consistency integral for the gap parameter $\Delta(\underline{r})$ in the normal metal

$$\Delta(\underline{r}) = \int \Delta(\underline{r}') K(\underline{r},\underline{r}') \, d^3\underline{r}' \qquad \text{(I-6)}$$

$\Delta(\underline{r})$, the analogue of the BCS energy gap Δ for a homogeneous system, is now a function of position and has to be small compared to $k_B T$ for the linearised relation to be valid. They obtained an analytical solution for the kernel $K(\underline{r},\underline{r}',T)$ and the boundary conditions it obeys in the "dirty" limit. The transition temperature T_{CNS} is then the highest temperature for which Eqn. (I-6) has a non-trivial solution.

Werthamer (15) used the de Gennes-Guyon expression for $K(\underline{r},\underline{r}')$ in N together with an equivalent one for S to obtain the following relations between T_{CS}, T_{CN} and T_{CNS}:

$$\chi(\xi_S^2 k_S^2) = \ln(T_{CS}/T_{CNS}) \qquad \text{(I-7A)}$$

$$\chi(-\xi_N^2 k_N^2) = \ln(T_{CN}/T_{CNS}) \qquad \text{(I-7B)}$$

where

$$\chi(z) = \psi(1/2 + z/2) - \psi(1/2) \qquad \text{(I-8)}$$

and $\psi(z) = -\sum_{n \geq 0} \frac{1}{(n+z)}$ is the digamma function. k_N^{-1} and k_S^{-1} are lengths which define the range of variation of $\Delta(\underline{r})$ at $T = T_{CNS}$ in N and S respectively, and ξ for each metal is defined by Eqn. (I-5).

Fig. 1 shows the comparison between the de Gennes-Werthamer theory and Hilsch's experimental results which is seen to be fairly good.

To test the theory in a case where $(NV)_N$ and T_{CN} were known, Hauser and Theuerer (16) carried out similar measurements on the Pb/Al system with Al being regarded as a 'normal' metal above its transition temperature $T_{CN} = 1.2^oK$. Their results for T_{CNS} as a function of Pb thickness d_S for fixed d_N are shown in fig. 2. There is seen to be a good agreement between theory (solid curve) and experiment. However as the dotted curve, calculated with $T_{CN} = 0^oK$, illustrates, T_{CNS} is sensitive to the exact value of $(NV)_N$ only at temperatures fairly close to T_{CN}. This underlines the inaccuracy involved in using such a method to estimate $(NV)_N$ or T_{CN} in cases where these may be very small or zero.

De Gennes (14), in fact, used Hilsch's results to estimate $(NV)_{Cu}$ as +0.05 with possible limits -0.06 and +0.10.

Later theoretical studies by Moorman (17), not restricted to dirty films, and by Jacobs (18) for dirty films served to emphasize the difficulty in quantitatively interpreting T_{CNS} data for cases where $T_{CN} << T_{CS}$.

1.7 T_{CNS} for Magnetic 'Normal' Films

As mentioned in §1.3 a small number of localised moments can produce a drastic lowering of the critical temperature of a superconductor. For the same reason a magnetic normal film in the proximity of a superconducting film would be expected to produce profound effects on the properties of the latter.

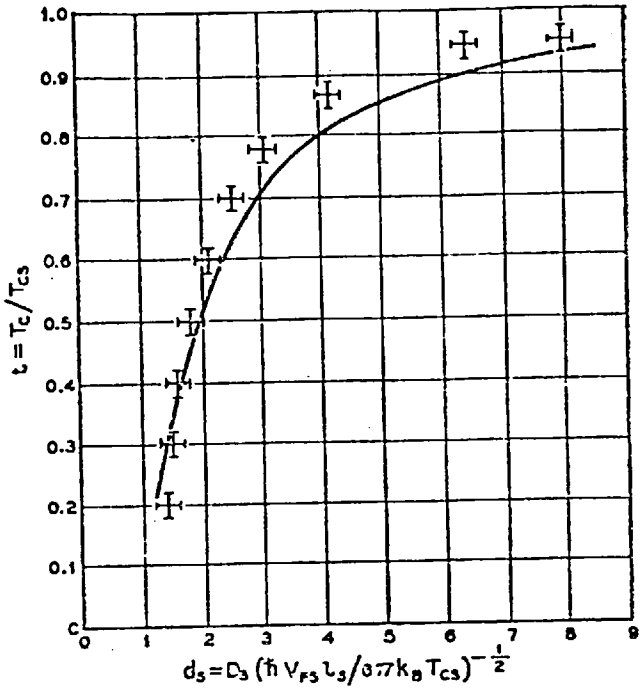

Figure 1-Reduced transition temperature (t) of Pb/Cu sandwiches as a function of reduced lead thickness (d_S) as predicted by the Werthamer theory (solid curve). Data points are from Hilsch's data (9).
(Reproduced from Werthamer (15))

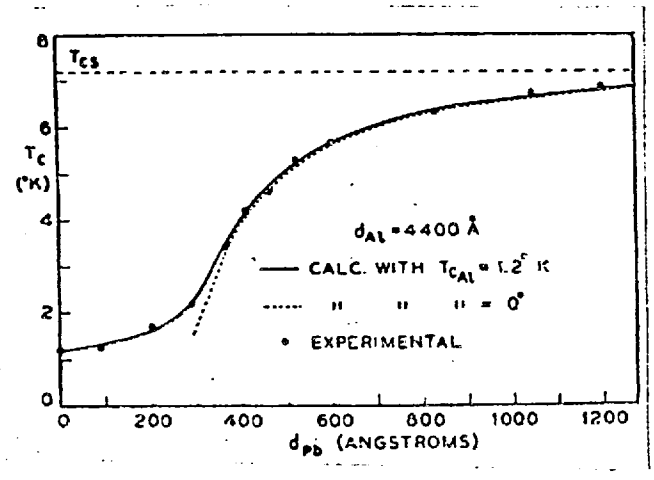

Figure 2 - Transition temperature (T_c) of Pb/Aℓ sandwiches for a constant Aℓ thickness of 4 400 Å as a function of the Pb film thickness (d_{Pb}).
(Reproduced from Hauser and Theuerer (16))

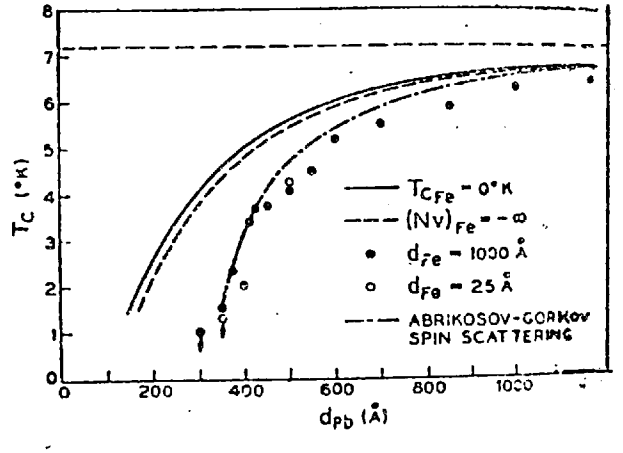

Figure 3 - Transition temperature (T_c) of Pb/Fe sandwiches as a function of Pb thickness (d_{Pb}).
(Reproduced from Hauser et al. (21, 22))

Abrikosov and Gorkov (19), and later de Gennes and Sarma (20), considered the pair-breaking effect of a low concentration of magnetic impurities on the transition temperature T_{CS} of a superconductor. They obtained the following expression for T'_{CS}, the transition temperature in the presence of the impurity:

$$\ln(T_c/T'_{cs}) = \chi(\hbar/2\pi\tau_s k_B T'_{cs}) \qquad \text{(I-9)}$$

τ_S is the life-time of a Bloch state at the Fermi surface due to the interaction between conduction electrons and the impurities and the function χ is defined as in Eqn. (I-8).

There is a close analogy between the expressions for T_{CNS} in the proximity problem and T'_{CS} for the case of magnetic doping. Hauser et al. (21, 22) combined these two results in order to describe the proximity effect between S and a magnetic N film for which they obtain:

$$\ln(T_{CN}/T_{CNS}) = \chi(-\xi_N^2 k_N^2 + \hbar/2\pi\tau_s k_B T_{CNS}) \qquad \text{(I-10)}$$

They studied experimentally situations where the normal film was ferromagnetic, antiferromagnetic or a dilute magnetic alloy. Fig. 3 shows their results for T_{CNS} of different thicknesses of Pb films deposited at 77°K onto a 1000 Å film of iron. It is seen that the theoretical curves obtained simply by using (i) $T_{CN} = 0$, $(NV)_{Fe} = 0$, (solid curve) and (ii) $(NV)_{Fe} = -\infty$ (broken curve) in the unmodified Eqn. (I-7) are in poor agreement with experiment. By using $T_{CN} = 0$ and $\tau_S = 10^{-14}$ s, estimated by fitting Eqn. (I-10) to one experimental point, they obtain a

curve (dot-dash) which is seen to be in fair agreement with their data.

From Eqn. (I-10) they estimated the pair penetration distance into Fe, k_N^{-1}, to be about 6 Å. Thus $\Delta(\underline{r})$ goes virtually to zero at the superconductor's boundary with a magnetic film. This important conclusion was experimentally verified by Groff and Parks (23) and confirmed by the calculation of Fulde and Maki (24).

For the important case of very dilute magnetic alloys with randomly orientated spins that we are interested in, and to which the Abrikosov-Gor'kov theory is strictly applicable, Eqn. (I-10) gave a good fit to the data of (22). For an N film of Pb Gd (2.9 at %), τ_S was also estimated by an independent measurement of the transition temperature T'_{CS} of an isolated alloy film and agreed well with the value obtained from Eqn. (I-10) and T_{CNS}.

More recently, Hauser et al. (46), in an interesting set of experiments, have used T_{CNS} measurements in conjunction with the theory outlined above as a means of investigating the Kondo effect in films of dilute Cu Mn, Cu Fe and Cu Co alloys in the proximity of Pb films.

1.8 Specific Heat Measurements

The first reported measurement of specific heat in this context was that of Shiffman et al. (25) on a layered two-phase structure of Pb-Sn eutectic alloy. Photomicrographs of alloy specimens showed them to consist of uniformly spaced alternate lamellae of Pb-rich and Sn-rich phases, of average thickness 0.75 μ and 1.8 μ respectively. The heat capacities C_S and C_N

of this material in the superconducting and normal states were measured as a function of temperature, the normal state being obtained by applying a magnetic field. The quantity $\Delta C(T) = C_N(T) - C_S(T)$ was compared with its expected value in a situation where the two phases were independent and non-interacting. The large discrepancies between the two were attributed to the proximity effect between adjoining layers.

Fulde and Moorman (26) subsequently advanced a theory based on the generalised Ginzburg-Landau equations to account for the thermodynamic properties, especially the magnitude of the specific heat jump at the transition temperature of a thick superconductor in the proximity of a normal metal. Their results were in reasonably good agreement with Shiffman's experiments. An important conclusion of Fulde's work was to show that the magnitude of the specific heat discontinuity was a far more sensitive measure of the proximity effect than the shift in the transition temperature, in the limit of thick superconductor. He showed, for example, that for an S layer of thickness $d_S \simeq 100\xi_S$ in contact with a paramagnetic film, the specific heat jump at T_{CNS} is 15% smaller than that expected in the absence of a proximity effect whereas the transition temperature is depressed only by about 0.05%. Recently Shiffman et al. (27) have made more measurements on the Pb-Sn two phase system, with varying thicknesses of the lamellae, to check Fulde's prediction for the magnitude of the discontinuity. In the absence of exact numerical solutions of his equations, they have made an approximate calculation based on these and find satisfactory agreement.

Manuel and Veyssie (28) report specific heat measurements on a 2600 Å Ag film sandwiched between two 6000 Å Pb films. The measurements are, however done in the ^{3}He range and therefore far from T_{CS}. They claim an overall resolution equivalent to 5×10^{-3} of the heat capacity of a 1μ thick Pb film. Although their results convincingly demonstrate induced superconductivity in the Ag, the large background heat capacity due to substrates, etc. places limitations on quantitative interpretation of their data.

1.9 Critical Current of SNS Sandwiches

Meissner's experiments (11), mentioned in §1.5, demonstrated the ability of sufficiently thin normal metal layers sandwiched between superconductors to support a supercurrent. The I-V characteristic of such a junction shows the existence of a critical current I_C above which the junction displays resistance. Qualitatively, this can be understood in terms of the kinetic energy of the superelectrons exceeding the minimum value of the induced energy gap $\Delta(\underline{r})$ in the normal film. De Gennes (4, 14) has shown that in the neighbourhood of T_{CNS}, the critical current of such a junction is given by

$$I_c = A k_s^2 k_N^{-1} \Delta_s^2(T) \exp(-2k_N d_N) \qquad \text{(I-11)}$$

where A is a constant and $\Delta_S(T)$ the energy gap in S far from the interface. In the 'one-frequency' approximation used by de Gennes, k_N and k_S are defined as in Eqns. (I-7A & B) with only the terms corresponding to n = 0 retained. Then it is

easily shown that $k_N \propto \ell_N^{-\frac{1}{2}}\left(1 + \frac{2}{\ell n\ (T/T_{CN})}\right)^{-\frac{1}{2}}$ and that, near T_{CNS}, $k_S \propto (T_{CS}-T)^{\frac{1}{2}}$. As both $\Delta_S(T)$ and k_S vary as $(1-t)^{\frac{1}{2}}$ near $t = T/T_{CS} \simeq 1$, Eqn. (I-11) predicts $I_C \propto (1-t)^2$.

The above temperature and thickness dependence of the critical current was verified by Clarke (30) who made measurements on Pb/Cu/Pb with dirty Cu Aℓ films of varying thicknesses and with d_S fixed.

In a separate series of experiments, Clarke (12) also verified that $I_C \propto \exp(-\text{const.} \times \ell^{-\frac{1}{2}})$ as predicted by Eqn. (I-11). From the thickness dependence of I_C, he estimated $k_N(T)$ and hence an upper limit of 0.11 for $(NV)_{Cu}$.

1.10 Resistance of SNS Junctions

More recently, Clarke et al. (31) have carried out sensitive measurements of the resistance of SNS sandwiches, with very thick N layers, as a function of temperature. To interpret their results for Pb/Ir/Pb ($d_N \sim 53\ \mu$, $d_S \sim 1\ \mu$), whose resistance was measured in the temperature range 50 mK < T < 7°K, they construct a simple model. They assume the following results of de Genne's theory (14), valid in the dirty limit:

$$\frac{\Delta_N(0)}{V_N N_N} = \frac{\Delta_S(0)}{V_S N_S}$$

$$\Delta_N(X) = \Delta_N(0)\exp(-k_N X) \qquad \text{(I-12)}$$

with

$$k_N^{-1} = \left[\frac{\hbar V_F \ell}{6\pi k_B (T-T_{CN})}\right]^{1/2}$$

It is also assumed that an electron of energy $k_B T$ in the normal metal travelling towards an interface would be Andreev scattered at $x = x_o$ where x_o is determined by the condition $\Delta_N(x_o) = k_B T$ (fig. 4a & b). The electron would then pair up with another one from the Fermi sea to form a Cooper pair (overall momentum and charge being conserved by the creation of a hole, as shown) and hence not be scattered during the remainder of its journey in N.

For electrons, all of energy $k_B T$ incident at the interface from the normal metal, the measured resistance will be

$$R(T) = R_o(a - x_o)/a \qquad \text{(I-13)}$$

where 2a is the thickness of N and R_o the bulk resistance of the Ir slab.

From Eqns. (I-12) and (I-13) and using $(NV)_{Ir} = 0.11$, $(NV)_{Pb} = 0.45$, they obtain

$$R(T) = R_o\left(1 - \frac{k_N^{-1}}{a} \ln\left(\frac{1.9}{T}\right)\right) \qquad \text{(I-14)}$$

The comparison between their experiment and theory is shown in fig. 4c and the agreement is seen to be good.

On the basis of this simple model, they show that the sensitivity of the technique for measuring $(NV)_N$ improves with decreasing T and estimate that at T = 20 mK, $(NV)_N$ of about 10^{-3} should be detectable. Measurements on Cu and Ag are understood to be currently in progress (32).

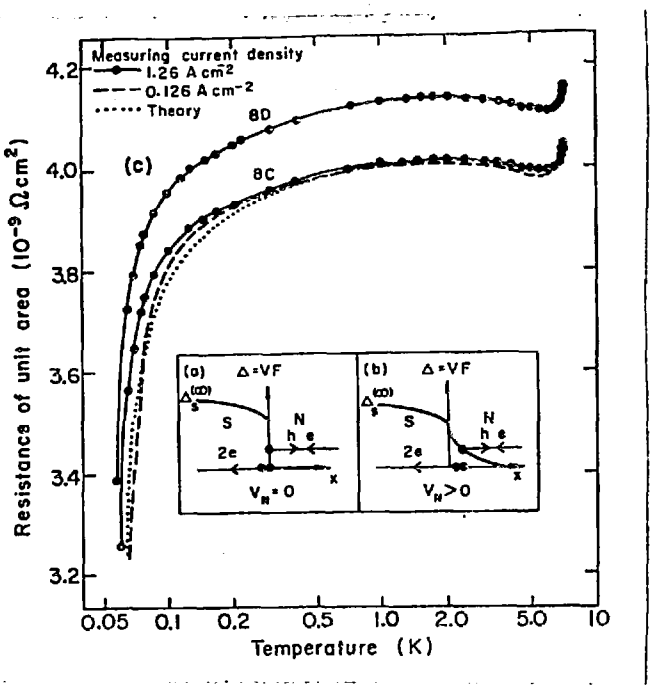

Figure 4 - (a) Variation of pair potential Δ across SN interface for $V_N = 0$. Incident electron is reflected at the SN interface. (b) Variation of pair potential across SN interface for $V_N > 0$. Incident electron is reflected inside N. (c) Variation of resistance with temperature for two Pb-Ir-Pb samples. Thickness of Ir in 8C was 53 ± 1μ, and in 8D 54 ± 1μ. The theoretical curve is for 8C. (Reproduced from Clarke et al. (31))

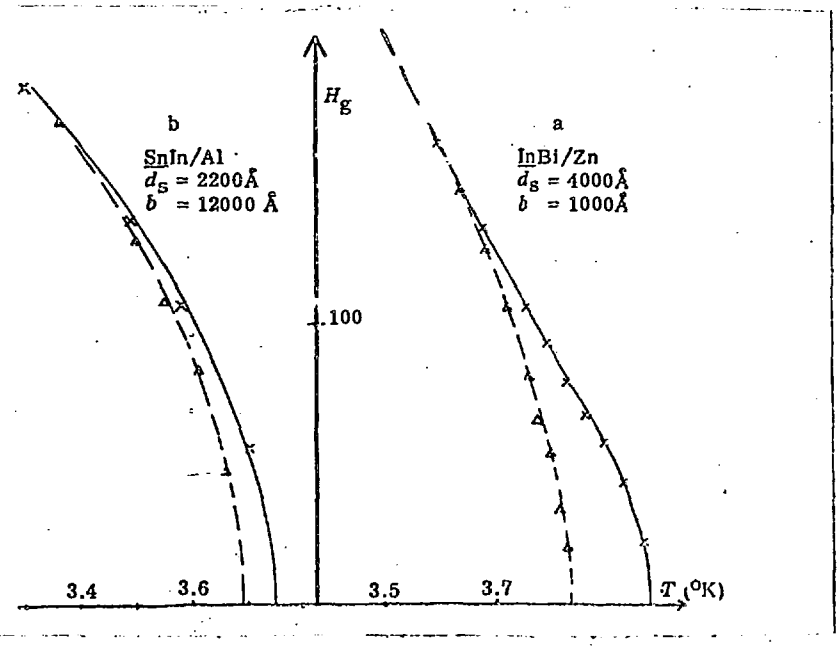

Figure 5 - Critical fields for: (1) an isolated superconducting film S of thickness d_S (full curve); (2) a film S of same thickness covered on one side with a normal metal layer N (dotted curve). (Reproduced from ref. (55))

1.11 Tunnelling Experiments on NS Layers

Unlike all the experiments described so far, tunnelling measurements make possible, at least in theory, a direct determination of the energy gap and the excitation spectrum of a superconductor. The experiments involve measuring the current, produced by one-electron tunnelling through a thin (~ 20 Å) insulating barrier separating two conductors, as a function of an applied voltage. This general description encompasses a wide variety of experiments depending on different combinations of electrodes, i.e. normal, superconducting, NS double layers, magnetic materials etc. for different physical investigations.

This technique was first used for the study of superconductors by Giaever (33) who measured the I-V characteristics of an $Al/Al_2O_3/Pb$ i.e. (Al - Pb) junction. His work was followed by a large number of experimental and theoretical studies. Among the latter, the work of Harrison (34) and Bermon (36) typified the general approach to the study of N-S and S-S sandwiches. This was to start with a realistic model for the excitation spectrum and from that to calculate the I-V characteristics for comparison with experiment. To proceed in the opposite direction, i.e. to calculate the density of states starting from the experimental I-V characteristics involves deconvoluting an integral equation and introduces large errors (12).

Bermon (36) used the BCS density of states in his calculations, namely,

$$N(E) = \frac{|E|}{(E^2-\Delta^2)^{1/2}} \quad , E \geq \Delta$$

$$= 0 \quad , E < \Delta \qquad \text{(I-15)}$$

where E is the excitation energy and Δ the energy gap. Comparison of his results with the experiments of Giaever (37) has shown that the BCS-based model does indeed provide a good agreement in most cases.

For an N-S junction the conductance is determined by the density of states and the energy gap at the surface of S next to the insulator. In theory then, $\Delta(\underline{r})$ and the density of states $N(E,r)$ on either side of an NS layer that replaces the S electrode may be determined by this technique.

The first experiment of this kind was done by Smith et al. (38) on Pb - Ag/Pb sandwiches. For Ag and Pb thicknesses of 5700 Å and 1500 Å respectively they found an induced gap of 0.16 meV in Ag. From the large number of experiments using this technique that followed, two facts soon became apparent. Firstly, the BCS-like excitation density of states worked out from Eqn. (I-15) by putting in Δ estimated from the measured value of the differential conductance $(\frac{dI}{dV})_{V=0}$ showed poor agreement with experiment. Secondly, it appeared that the energy gap seen by the tunnelling excitations was not necessarily that at the surface but the smallest gap Δ_m anywhere in a not too thick NS sandwich.

Of the subsequent theoretical calculations of the excitation spectrum of NS layers, the following two have proved to be in reasonably good agreement with experiments:

(i) McMillan's (39) for thin ($d \ll \xi$) clean films at $T \ll T_{CNS}$.

(ii) Fulde and Mooreman's (43) for thick, dirty films at $T \sim T_{CNS}$.

PROXIMITY EFFECT IN THE PRESENCE OF A MAGNETIC FIELD

In experiments in this category, an externally applied field is used as a means of producing superconducting to normal state transitions in proximity specimens. By this means not only can useful information be obtained about the critical fields of the N and S layers but the "degree" of induced superconductivity of N may also be measured from the magnitude of the change in some such property as ultrasonic attenuation or thermal conductivity in the course of a state transition. This last point is illustrated by the experiments reviewed in §1.13 and §1.15.

1.12 Determination of Parallel Upper Critical Field of NS

In an isolated superconductor nucleation in decreasing fields takes place on the surface parallel to the applied field at a field H_{C_3} given by the relation (67)

$$H_{c3} = 1.695 \times \sqrt{2}\,\kappa H_c = 2.4\kappa H_c \qquad \text{(I-16)}$$

where κ is the Ginzburg-Landau parameter and H_C the thermodynamic critical field of S. It is seen that $H_{C_3} > H_C$ for $\kappa > 0.42$. The surface critical field, however, is lowered by the proximity of a normal material. Fig. 5 shows the results reported by the Orsay Group (55) for Sn In/Aℓ and In Bi/Zn films, the upper critical field $H_{||}$ being determined from the a.c. permeability

of films deposited on hollow cylinders. When $d_S >> \xi_S(T)$, a condition that in the above experiments is attained by lowering the temperature, nucleation can take place on the free (uncoated) S surface regardless of the presence of N and $H_{||}$ then approaches H_{C_3}. It is important to realise that when the specimen is sufficiently thick for nucleation on either surface to be independent of the presence of the other, the specimen will have two surface critical fields; H_{C_3} at the free S surface and H_{if} at the NS interface.

A theoretical study of H_{if} has been done by Hurault (47, 48) whose main conclusion is that for a type II superconductor, (i.e. when $\kappa > 1/\sqrt{2}$ so that $H_C < H_{C_2} < H_{C_3}$ where $H_{C_2} = \sqrt{2}\,\kappa\, H_C$ is the bulk critical field) H_{if} is equal to H_{C_2} when $\sigma_N > \sigma_S$, where σ_N and σ_S are the normal state conductivities of N and S. When $\sigma_N < \sigma_S$, he shows that $H_{C_2} < H_{if} < H_{C_3}$.

However, measurements of H_{if} have not been used explicitly as a means of estimating very small $(NV)_N$, presumably on account of their being sensitive to material properties only in the very close vicinity of the interface, where spurious effects due to crystal imperfections and metallic interdiffusion dominate, and also because of additional approximations necessary to allow for strong field effects on the order parameter and on the boundary conditions when attempting a theoretical analysis. Moreover, like T_{CNS} determination, they measure the effect produced on S by the proximity of N and are therefore intrinsically far less sensitive to the interaction parameter in N than those experiments (e.g. of breakdown fields (§1.14) or of the screening distance (§1.15)) which directly measure the induced supercon-

ductivity of N, and which have therefore been more popular in the investigation of $(NV)_N$.

The upper critical field $H_{||}$ has been studied theoretically and experimentally by several workers (49, 50, 51). These experiments too have not been widely used as a means of estimating very small $(NV)_N$. The Orsay group (55), report agreement between the values of the extrapolation length b, obtained both by $H_{||}$ and T_{CNS} measurements. The extrapolation length b is defined by the following relation

$$\left(\frac{d\Delta}{dX}\right)_{X=0^-} = -\frac{\Delta(0^-)}{b} \qquad \text{(I-17)}$$

where X = 0 defines the NS boundary, the superconductor occupying the space $-d_S < x \leq 0$. The quantity b can be related to k_N and hence to $(NV)_N$ (see §2.5).

1.13 Thermal Conductivity Measurements

At very low temperatures, the electronic contribution to the thermal conductivity of a crystal is the dominant one. In a superconductor, the Cooper pairs are no longer able to transport thermal energy across the crystal, this task being left to the 'normal' fluid. The magnitude of the thermal conductivity is, therefore, a measure of the fraction of electrons in the normal state.

Wolf et al. (52) have made measurements on Pb Bi/Ag (double) and Pb Bi/Ag/Pb Bi (triple) layers in the ^3He range of temperatures. The thermal conductances were measured in a direction parallel to the interface, both in zero field and in applied fields sufficient to quench the superconductivity of the

Ag layer, but not that of the Pb alloy. Their results for a clean triple layer are shown in fig. 6 (a) and (b), T_i denoting the temperature for which $\frac{K_S}{K_N} = 0$, where K_S and K_N are the conductivities of Ag in the superconducting and normal states.

They use the theoretical results $T_i = 0.27\ T_C$, and $\Delta(0) = 1.76\ k_B T_C$, both valid for homogeneous BCS superconductors, to obtain the induced energy gap in Ag. From this they estimate $(NV)_{Ag}$ to be ~ 0.1.

In the course of the above experiments, the authors also found (53, 68) that the phase transition in Ag became a first order transition below a temperature T^*, the transition field being then identifiable with the normal film breakdown field H_b (see §1.14). They observed that the supercooling field connected with H_b, decreased linearly with decreasing T, until a temperature T_S was reached. Below T_S, the supercooling field remained constant and they attribute this to the phenomenon of "saturation" in the Ag (see Chapter II). They use the value of T_S to obtain an independent estimate of $(NV)_{Ag}$ also of about 0.1.

These results and those of Valette (see §1.16) on the observation of "saturation" will be discussed more fully in Chapter VI after the required theoretical background has been presented.

1.14 Critical Field of N: 'Breakdown' Field H_b

In the course of r.f. permeability and tunnelling measurements on In Bi/Zn layers in the presence of a field, Burger et al. (54, 55) observed that when the applied field was weak it was effectively screened by N and little change was observed. How-

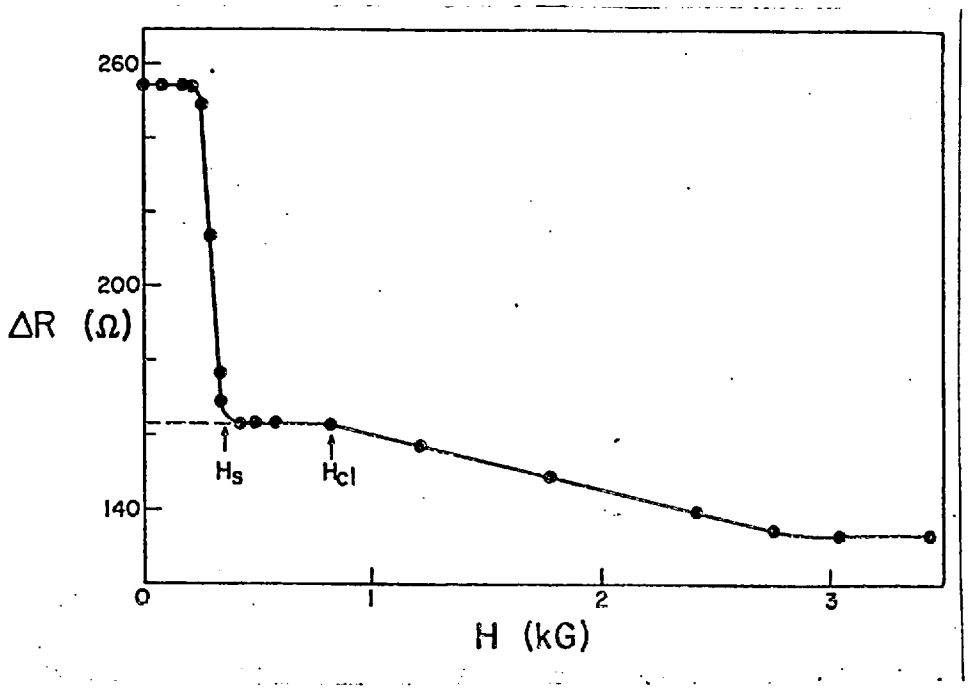

Figure 6(a) - Difference ΔR between the two specimen thermometers as a function of magnetic field. At H_S the silver layer becomes normal. The lead-alloy layer remains superconducting until H_{c1}. The dashed line shows the curve for a lead-alloy layer without silver.

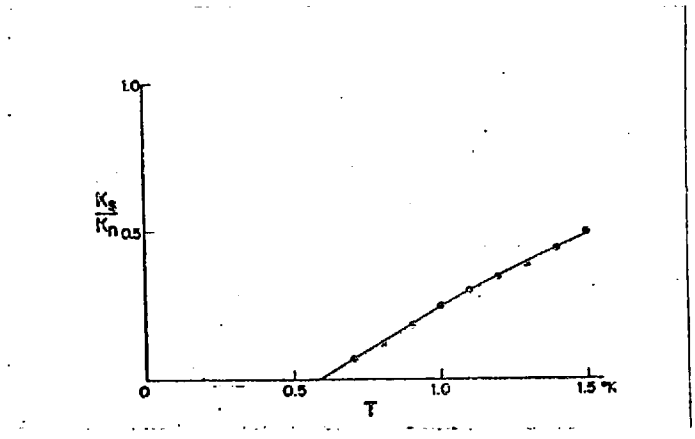

Figure 6(b) - The ratio of the thermal conductivities in the superconducting state (K_s) and in the normal state (K_n) for the silver layer of the specimen for which d_n = 1500Å. (Reproduced from Deutscher et al. (53, 68)).

ever, when the field reached a value H_b a sudden penetration of flux occurred. This was associated with a phase transition in N which was found to be first order. This effect could be observed for a certain range of values of d_N and of the temperature. In particular, for a given thickness d_N, no breakdown effects could be observed above a limiting temperature T^*. That the transition was of the first order was shown by the presence of field hysteresis and by the suddenness of the transition (fig. 7). The presence of a sharp peak in the r.f. permeability as seen in the figure is characteristic of a first order transition, as explained in Chapter V.

The Orsay Group (54, 55) have made calculations of H_b, and, in particular have compared the theoretical and experimental values of T^* as a function of d_N (56). Theoretically, they showed that the maximum value of T^*, denoted by T^*_m, for any d_N is obtained from the following implicit relation

$$\lambda_N(X=0, T_m^*).k_N(T_m^*) = 0.44 \qquad \text{(I-18)}$$

where k_N^{-1} is the coherence length in N defined by Eqn. (I-7B). λ_N, the penetration depth in N at the interface, is defined by the following equation, derived by Maki (57) from the generalised G-L equations:

$$\frac{1}{\lambda_N^2(X=0,T)} = \frac{4\sigma_N \Delta^2(X=0)}{\hbar c^2 k_B T}\ \psi_2\left(\tfrac{1}{2} - \frac{\hbar D k_N^2}{4\pi k_B T}\right) \qquad \text{(I-19)}$$

$D = \frac{1}{3} v_F \ell$ is the diffusion coefficient and ψ_2 is the first derivative of the digamma function i.e. $\psi_2(z) = \sum_{n \geq 0} \frac{1}{(n+z)^2}$.

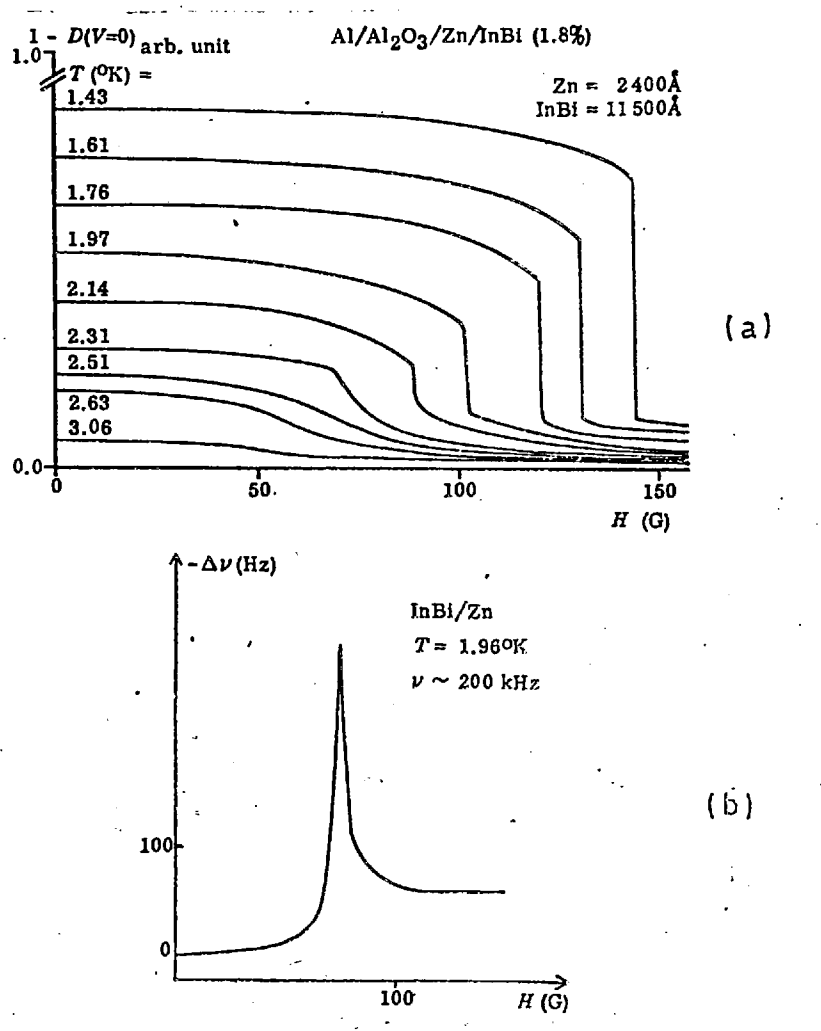

Figure 7 - (a) Initial conductance D(V = 0) for a InBi/Zn/$A\ell_2O_3$/Aℓ system, as a function of the applied (parallel) field H, and for various values of the temperature T (the T values are above the transition point of Zn). Notice the very sharp breakdown at H = H_b when T is low.

Figure 7 - (b) R.F. permeability of an InBi/Zn sandwich as a function of static field. T = 1.96°K, ν = 200 kHz. Notice the peak in permeability when H = H_b. (From ref. (56)).

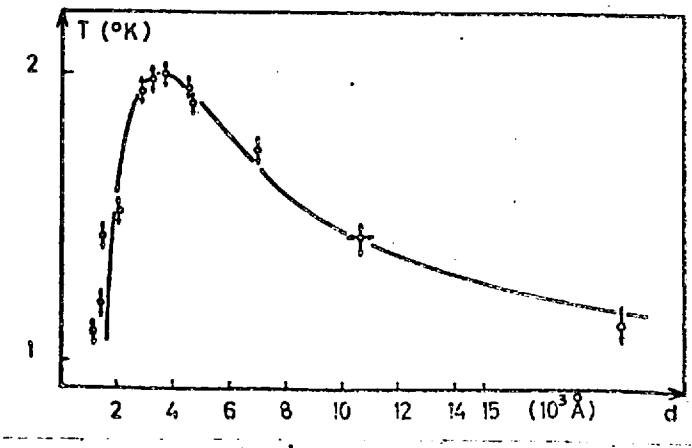

Figure 8 - The temperature T^* as a function of the normal layer thickness d_N. The full curve is theoretical. (Reproduced from ref. (56))

Agreement between the prediction of Eqn. (I-18) and experiment was poor. For In Bi/Zn, T_m^* theoretical was ~ 3^o K whereas its experimental value was ~ 2^o K. The authors concluded that Maki's expression (I-19) for λ_N which did not take into account non-local effects, needed correcting. The "correction factor" for λ_N which was required for agreement between theoretical and experimental T_m^* was about 1.8. The theoretical curve $T^*(d_N)$ calculated with the "corrected" value of λ_N was in good agreement with experiment (fig. 8). That their theory was basically correct was shown by the good agreement, without any adjustable parameters, that it gave with experiments on Pb/Sn. These were carried out in the vicinity of T_{CN}, which enabled the use of the conventional G-L equations in N.

The above results for H_b on In Bi/Zn, coupled with screening distance measurements on the same system by Deutscher and Hurault (58), confirmed the inadequacy of Maki's expression for calculating λ_N in the non-homogeneous situations encountered in proximity experiments. The same group (59) subsequently made a more refined calculation of λ_N, taking into account non-local effects, and in particular the contribution of the superconductor to values of λ_N (x = 0). This is more fully described in Chapter II.

Krätzig and Schreiber (10) have recently reported measurements of H_b in Pb/Ag, Pb/Cu and Pb/Aℓ specimens in the ^{3}He range. They use the Orsay group's theory together with the modified expression for λ, to obtain $k_N(T)$, from which they estimate $(NV)_{Ag}$ as ~ 0.07.

1.15 'Meissner' Screening in N

As seen in the last section, the normal part of an NS double layer may, under suitable conditions, screen weak applied magnetic fields, both r.f. and d.c.. If, however, d_N is large so that $\Delta(d_N)$, the order parameter in N at the free N surface, is virtually zero, then the field is screened by a part and not the whole of the N film. Under these conditions, increasing the applied field produces a smooth and continuous, second order transition in N. A measurement of the screening distance 'δ' (fig. 9), i.e. the distance from the interface to the position of the 'flux front' in zero field, may be made by an r.f. permeability technique as was demonstrated by Deutscher et al. (58, 59) and the Orsay Group (61). Theoretical calculation of δ on the basis of applying the generalised G-L equations in N, with the inclusion of non-local corrections (§1.14) has been made by Deutscher (62). In the dirty limit in which the theory is strictly valid, Valette (63, 64) finds it in good agreement with his measurements on Pb/Ag alloys and Pb/Cu alloys. Valette also observes "saturation" effects below $T_S \simeq 2.1^\circ$ K for Ag and $T_S \simeq 2.3^\circ$ K for Cu alloys, this effect apparently being manifested by the quantity $T^{\frac{1}{2}}\delta$, which normally increases rapidly with decreasing T, acquiring a constant value independent of temperature, for $T < T_S$ (fig. 10). Deutscher and Valette (66) have recently put forward a theory of this effect which is claimed to permit a determination of $(NV)_N$.

The measurement of δ as a means of studying the interaction parameter of N is particularly attractive for several reasons. R.f. permeability measurements are simple and the usual technique

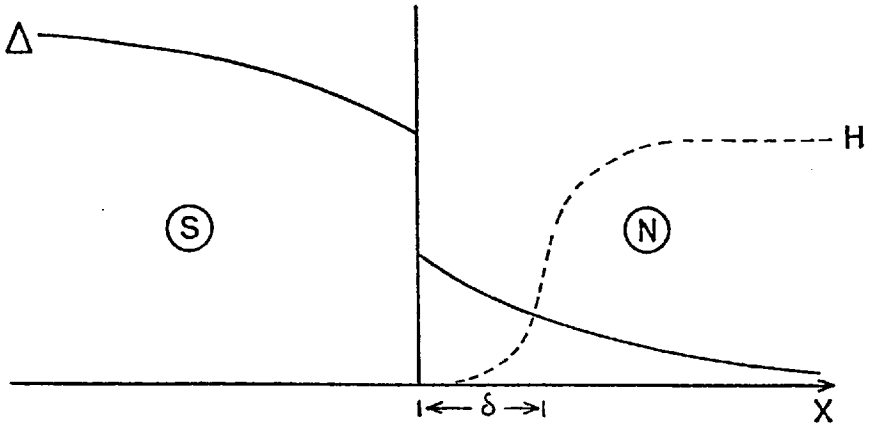

Figure 9 - Schematic representation of the screening distance δ in a weak applied field.

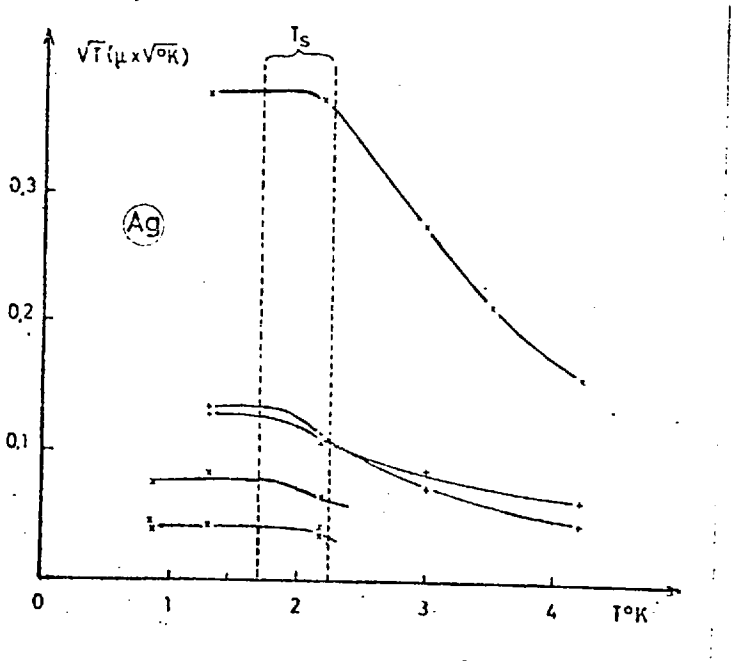

Figure 10 - The results reported by Valette (64) for the quantity $T^{\frac{1}{2}}\delta$ as a function of the temperature for the Pb/Ag system.

employed for this, viz., the measurement of the resonance frequency, can be very accurate and sensitive. Deutscher's (62) calculations show (fig. 17) the screening distance to be a sensitive funciton of $(NV)_N$. This is to be contrasted particularly with T_{CNS} measurements, far from T_{CN} where very small errors in measurement can lead to much larger ones in estimating $(NV)_N$. Moreover, a bad electrical contact between N and S can lead to an overestimation of $(NV)_N$ by T_{CNS} measurement whereas a similar condition leads to a smaller value of δ and hence of $(NV)_N$. This is because T_{CNS} is a measure of the effect on the properties of S produced by N whereas δ is a direct measure of the induced superconductivity in N. Additional advantage arises from the fact that thick S and N films are used which have well-defined crystal structures, more representative of the bulk. Finally, one need not know d_N accurately for quantitative interpretation of the data, the only requirement being that $d_N >> k_N^{-1}$ so that breakdown effects are avoided when the field-induced phase transition occurs.

1.16 The Present Work

We have done screening distance measurements by the Schawlow-Devlin technique (65) on flat NS double layers, with pure Pb constituting the S film. The N film variously consisted of pure Ag, dilute magnetic and non-magnetic Ag alloys, Cd and its dilute alloys and pure Zn.

Initially we had intended to compare Deutscher's theory with experiments on metallic systems for which screening distance measurements had not yet been made. However, during our pre-

liminary investigation on the Pb/Ag system, we found a reasonable agreement with Valette's (62, 63) results for high $T \geq 2.5^{\circ}$ K but unlike him did not observe saturation effects down to the lowest temperatures attainable, $T \sim 1.45^{\circ}$ K. Moreover, the screening distances that we measured were somewhat smaller than Valette's. These reasons prompted an investigation of the Ag alloy system he had studied. It was felt that Cd and Zn. systems, as known superconductors, should provide a test for the theory of screening distances and should also show up "saturation" effects, if present, more readily on account of their comparatively high transition temperatures.

CHAPTER II

THEORY

2.1 Introduction

As mentioned in the last chapter, the proximity effect came to be studied in detail, both experimentally and theoretically, after the advent of the successful BCS microscopic theory. However, the theory, as originally formulated, confined itself to the problem of an infinite, homogeneous medium where the interaction potential V was regarded as a spatially uniform, point interaction. The energy gap parameter Δ_{BCS} for such a medium had also to be assumed in the original theory to be spatially uniform. However, in practice, one often meets situations where Δ is position dependent. The scale of spatial variations of Δ viz. $\xi(T)$ is found to be ~ 1000 Å. (Since Anderson and Morel (8) have shown that the range of V is about k_F^{-1} i.e. ~ 10 Å, k_F being the wave vector of an electron on the Fermi surface, V can still be considered a point interaction.) To tackle the problems of spatially varying Δ and those presented by non-homogeneous systems encountered in the proximity situation where V, too, is spatially varying, it was necessary to formulate extensions of the original theory.

2.2 Gor'kov's Formulation of the Microscopic Theory

Soon after the publication of the microscopic theory, Gor'kov (71a) successfully recast the original BCS variational wave function approach into the Green's function formalism. This was an important advance as it not only made the BCS theory

easier to manipulate mathematically, but also allowed for spatial variations of Δ and V (1b). Gor'kov showed that the energy gap parameter Δ of the homogeneous superconductor was identifiable with the pair potential $\Delta(\underline{r})$, defined by Eqn. (II-2), which satisfied the following non-linear, self-consistent integral equation

$$\Delta(\underline{r}) = \int d^3\underline{r}' K(\underline{r},\underline{r}')\Delta(\underline{r}') \qquad + \text{higher order terms} \tag{II-1}$$

where

$$\Delta(\underline{r}) = V(\underline{r})F(\underline{r}) \tag{II-2}$$

$F(\underline{r})$ is the Cooper pair condensation amplitude i.e. $F(\underline{r}) = \langle \psi_\uparrow(\underline{r})\ \psi_\downarrow(\underline{r}) \rangle$, the probability of finding a Cooper pair at the point $\underline{r}$ being $|F(\underline{r})|^2$. The range of the kernel $K(\underline{r},\underline{r}')$ is of the order of $\xi(0)$ the Ginzburg-Landau (temperature-dependent) coherence length evaluated at $T = 0^oK$ (see §2.7) and the integral equation thus incorporates the BCS concept of long range order at the same time as allowing for spatial variations in $\Delta(\underline{r})$.

Gor'kov's formalism has been the basis of the derivation by Gor'kov (71b) of the original Ginzburg-Landau equations, valid for $T \sim T_c$, from the BCS theory; of the derivation by Maki (57) and de Gennes et al. (72) of the generalised G-L equations, valid, in dirty superconductors, at all temperatures as long as H is close to H_{c2} so that $\Delta << k_B T_{cs}$; and of all the studies made of the boundary conditions at the NS interface in the proximity situation (e.g. 14, 17, 76).

2.3 Variation of $\Delta(\underline{r})$ in a Normal Metal for $T \lesssim T_{CNS}$

The spatial variation of the pair potential in a normal metal in the proximity of a superconductor may be predicted theoretically when $\Delta(\underline{r})$ in both the metals is small enough for the linearised form of Eqn. (II-1) to be used. This condition occurs when the system is close to a second order transition, which is the case when $T \sim T_{CNS}$ in zero field. For the one-dimensional geometry of semi-infinite N and S metals occupying the half spaces $X > 0$ and $X < 0$ respectively (fig. 11), the linearised Gor'kov equation can be written (14)

$$\Delta(X) = V(X) k_B T \sum_{\omega} \int K_{\omega}(X,X') \Delta(X') dX' \qquad \text{(II-3)}$$

where $K_{\omega}(X,X')$ is the Fourier transform of the kernel $K(X,X')$ of Eqn. (II-1), i.e.

$$K_{\omega}(X,X') = \int_{-\infty}^{\infty} K(X,X') \exp(-i\omega q)\, dq$$

with $$\hbar\omega = (2n+1)\pi k_B T \qquad \text{(II-4)}$$

The sum over ω extends over all ω in Eqn. (II-4), with n taking all (positive, negative and zero) values. The interaction parameter takes the values

$$V(X) = V_S \qquad X < 0$$
$$= V_N \qquad X > 0$$

In accordance with the original BCS prescription (§1.3) the

retarded nature of the interaction is taken into account by supposing that the interaction is cut-off i.e. equal to zero, in each metal, for $|\omega|$ greater than the Debye frequency of that metal.

Approximate analytical solutions of Eqn. (II-3) have been obtained in special cases as follows:

(a) $V_N = 0$, Normal Metal 'Clean'

In the clean limit, i.e. $\ell > \xi_N$ (cf. Eqn. I-5), the probability amplitude F(X) has a finite tail in the N region, although $\Delta(X) = V(X)\,F(X)$ will be zero. F(X) in zero field is obtained as the integral, over S only, of Eqn. (II-3). On making use of the standard form of Green's function for a pure metal, Silvert and Cooper (73) show that the decay of F(X) in N is of the form

$$F(X) \propto \frac{1}{X} \exp(-k_N X) \qquad \text{(II-5)}$$

where $k_N^{-1} = \frac{\hbar v_N}{2\pi k_B T}$. The above result holds far from the interface, i.e. for $X >> k_N^{-1}$ since only the leading term, corresponding to $|\hbar\omega| = \pi k_B T$, has been retained in the summation over discrete values of ω (assuming finite T).

$\sum_{\omega}$ is replaced by an integral as $T \to 0$, in which limit Falk (35) has shown that in both clean and dirty limits

$$F(X) \propto \frac{1}{X + X_1} \qquad \text{(II-6)}$$

where X_1 is a constant.

(b) $V_N = 0$, Normal Metal 'Dirty'

When N is dirty the leakage of Cooper pairs from S into

N is controlled by a diffusion process and the Green's function kernel may be written down explicitly (1a). The spatial variation of F(X), far from the interface, is then found to be

$$F(X) = F(0)\exp(-k_N X) \qquad \text{(II-7)}$$

with $k_N^{-1} = (\frac{\hbar D}{2\pi k_B T})^{\frac{1}{2}}$ where the diffusion coefficient $D = \frac{1}{3} v_N \ell_N$. The factor $(\frac{\hbar D}{2\pi k_B T})^{\frac{1}{2}}$ is denoted by q_o^{-1} in many expressions that follow (cf. Eqn.II-66B)

(c) $V_N > 0$, Normal Metal 'Dirty'

For finite V_N (> 0), the interaction cut-off at $|\omega| = \omega_{DN}$, the Debye frequency of N, has to be introduced in the summation in Eqn. (II-3). De Gennes and Guyon (13) then find a solution to Eqn. (II-3), in the normal metal, of the form

$$\Delta(X) = \sum_i c_i \exp(-k_i X) \qquad \text{(II-8)}$$

where k_i are the positive roots of the equation

$$\frac{1}{NV} - \ln \frac{1.14\hbar\omega_{DN}}{k_B T} = \psi(1/2) - \psi(1/2 - k_i^2/2q_o^2) \qquad \text{(II-9A)}$$

$\psi(Z)$ is the digamma function. The BCS result of Eqn. (I-2) namely $^1/_{NV} = \ell n \frac{1.14\hbar\,\omega_{DN}}{k_B\, T_C}$ is seen to be a special case of Eqn. (II-9A) for $k_i \equiv 0$ i.e. Δ spatially constant. Using this relation for a normal metal ($T_C = T_{CN}$) Eqn. (II-9A) may be written

$$\ln(T/T_{CN}) = \psi(1/2) - \psi(1/2 - k_i^2/2q_o^2) \qquad \text{(II-9B)}$$

It should be noted that the above result follows directly from

the generalised linear G-L equations, Eqns. (II-24 & 26), §2.7, upon assuming their validity in a dirty superconductor above its critical temperature.

It is seen from fig. 12 that $\psi(Z)$ is a periodic function of Z for $Z < 0$. Eqn. (II-9B) therefore has an infinite number of solutions when $T_{CN} < T$. Far from the interface, i.e. for $X > q_0^{-1}$, the solution with the longest range (smallest root $k_i = k_N$, region I, fig. 12) dominates and the pair potential is given by

$$\Delta(X) = \Delta(0^+) \exp(-k_N X) \qquad \text{(II-10)}$$

We note that k_N is always smaller than q_0. However, for $T_{CN} << T$, $k_N \sim q_0$. Only when $T \sim T_{CN}$ do k_N and q_0 differ significantly.

For $V_N = 0$ i.e. $T_{CN} = 0$, and N dirty, one recovers from Eqns. (II-8 & -9) the result of §2.3(b) (Eqn. II-7) upon (i) noting that for $Z \to 0$, $\psi(Z) \to -\infty$ and (ii) retaining the smallest root k_N.

(d) $V_N < 0$, Normal Metal Dirty

Neither theoretical studies (4,47) nor experimental evidence rule out the possibility of V_N being small and negative for the 'normal' metals like Cu and Ag. Hurault (47) has discussed this case and shows that a direct application of the generalised G-L equations cannot provide a physically meaningful prediction of the behavior of such a metal in the proximity situation.

Consider the solution of the generalised G-L Eqn. (II-24) valid for X far from the interface:

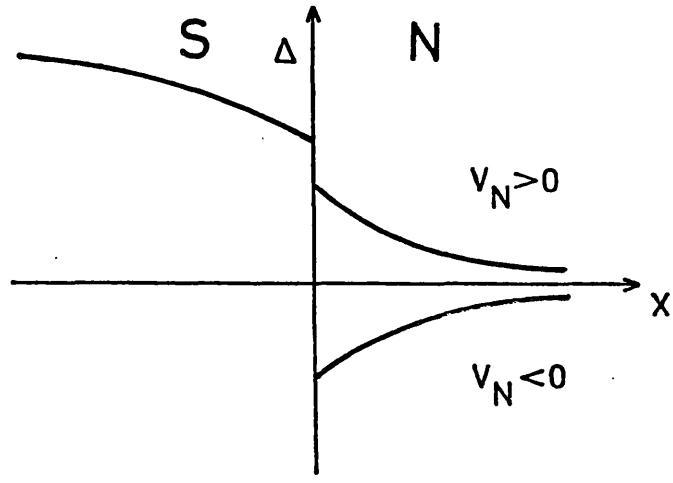

Figure 11- Schematic variation of the pair potential Δ across an NS interface.

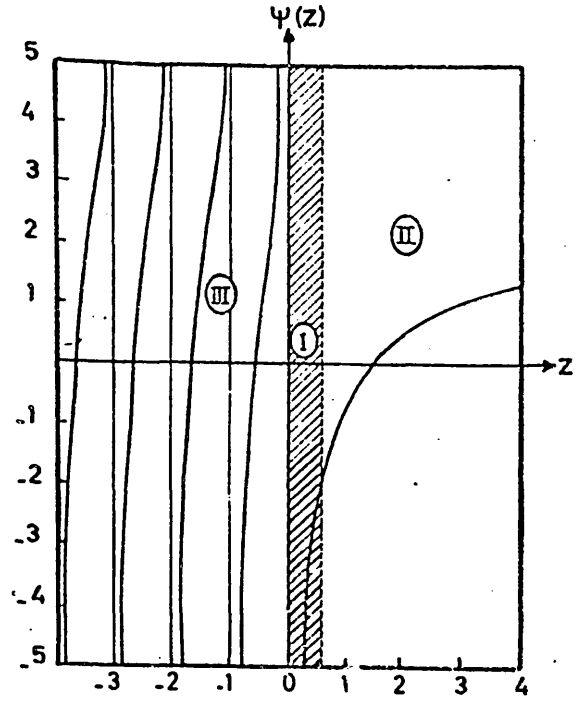

Figure 12- The digamma function Ψ(Z).

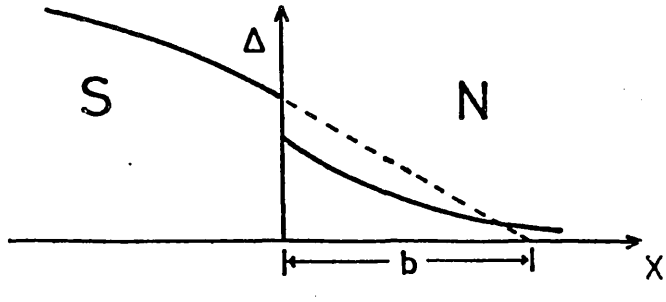

Figure 13- Geometric meaning of the extrapolation length b.

$$\Delta(X) = \Delta(0^+) \exp(-k_N X) \qquad \text{(II-11)}$$

k_N is the smallest positive root of Eqn. (II-26) which is identical to Eqn. (II-9B). However, now that V_N is small and negative (and T_{CN} therefore undefined) we rewrite (II-26) in the same form as Eqn. (II-9A)

$$\psi(1/2 - k_i^2/2q_o^2) - \psi(1/2) = \ln\left(\frac{1.14\hbar\omega_{DN}}{k_B T}\right) - 1/N_N V_N \qquad \text{(II-12)}$$

The first term on the right hand side of Eqn. (II-12) is $\sim \ln T_D/T$ where $T_D = \frac{\hbar\,\omega_{DN}}{k_B}$ is the Debye temperature of the metal. At the temperatures of interest this term is large and positive and so is the term $-1/N_N V_N$. The r.h.s. of (II-12) is therefore large and positive and an inspection of fig. 12 shows that under these conditions all the roots k_i of the equation are real and that the smallest of these, viz. k_N is such that $k_N^2 > q_o^2$. This condition can be shown to make the leading term in Gor'kov's integral, Eqn. (II-3) (which is proportional to $\int \exp(k_N X - q_o|X|)\,dX$) diverge in the limit $X >> q_o^{-1}$. We recall that for the case $V_N > 0$, the Werthamer approximation greatly simplified the problem by the retention of the smallest root k_N for describing Δ in a thick normal film, $d_N >> q_o^{-1}$. In order that a similar approach may be used for $V_N < 0$, Hurault (47) postulates a solution of the form (II-11). He uses this solution to evaluate the kernel in Gor'kov's equation in terms of k_N and q_n. So as to circumvent the problem of the leading term di-

verging, he sets the coefficient of this term equal to zero and uses this condition to evaluate k_N in terms of q_0. He finds that k_N is then given by

$$k_N = q_0(1 - 1/2\alpha) \qquad \text{(II-13)}$$

where $\alpha = \frac{V_S}{V_N}$ and is large (>> 1) and negative in this case.

It is shown in ref. 47 that a necessary condition for the validity of the above approach is that the temperature be high enough for Gor'kov's integral to be expanded in powers of Δ not only in N but also in S. Although the above solution for the case $V_N < 0$ has not been rigorously derived, it is nonetheless consistent with the results for $V_N > 0$ and $V_N = 0$ insofar as the three solutions imply a continuous variation of the ratio k_N/q_0 as V_N changes sign (i.e. $k_N/q_0 < 1$ for $V_N > 0$, $k_N/q_0 = 1$ for $V_N = 0$). When $V_N < 0$, $\Delta(0^+)$ in Eqn. (II-11) will also be negative (see Eqn. (II-16) below) and $\Delta(X)$ in N will be of the form shown in fig. 11.

2.4 Boundary Conditions on $\Delta(X)$

Having considered the spatial variation of the pair potential in an infinite N medium, we now examine how it varies across the SN interface and at the free surfaces of S and N of thicknesses d_S and d_N respectively.

For the case of dirty metals near T_{CNS} when the linearised Eqn. (II-3) may be used, de Gennes (14) derives the following boundary conditions that the pair potential must satisfy, assuming specular reflection of electrons at plane boundaries:

(a) On the free surfaces of S and N, i.e. at $X = -d_S$ and at $X = d_N$

$$\left(\frac{d\Delta}{dX}\right)_{X=-d_s} = 0 \qquad \text{(II-14)}$$

$$\left(\frac{d\Delta}{dX}\right)_{X=d_N} = 0 \qquad \text{(II-15)}$$

(b) At the SN interface,

$$\frac{\Delta_S(0^-)}{N_S V_S} = \frac{\Delta_N(0^+)}{N_N V_N} \qquad \text{(II-16)}$$

and

$$\frac{D_S}{V_S}\frac{d\Delta_S(0^-)}{dX} = \frac{D_N}{V_N}\frac{d\Delta_N(0^+)}{dX} \qquad \text{(II-17)}$$

We note that the above conditions are derived in the absence of a magnetic field. The example below illustrates the use of these boundary conditions in a practical case.

2.5 Werthamer Approximation for Evaluating T_{CNS}

This approximation was referred to in §1.6. Werthamer (15) retained only the smallest root $k_i = k_N$ of Eqn. (II-9) and assumed a general solution of the form $\Delta(X) = a \exp(k_N X) + b \exp(-k_N X)$ to be valid <u>throughout</u> N ($0 < X < d_N$). The solution satisfying the B.C. of Eqn. (II-14) is

$$\Delta_N(X) = \frac{\Delta(0^+)\cosh k_N(X-d_N)}{\cosh(k_N d_N)} \qquad \text{(II-18)}$$

In S, near its critical temperature, Δ is given by the G-L equation (II-24), and one finds

$$\Delta_S(X) = \frac{\Delta(0^-)\cos[k_s(X+d_s)]}{\cos(k_s d_s)} \qquad \text{(II-19)}$$

where, for $T < T_{CS}$, k_S is the positive root of

$$\ln(T/T_{cs}) = \psi(1/2) - \psi(1/2 + k_s^2/2q_o^2) \qquad \text{(II-20)}$$

(region II of fig. 12).

Applying the boundary conditions of Eqns. (II-16 and -17) to the above solutions one gets

$$k_N D_N N_N \tanh(k_N d_N) = k_S D_S N_S \tan(k_S d_S) \qquad \text{(II-21)}$$

Both k_S and k_N are functions of temperature and Eqn. (II-21) is an implicit relation for T_{CNS}.

Werthamer's approximation also brings out in an instructive manner the physical significance of the extrapolation length b and its dependence on the nature of N and S. b is defined by the relation

$$\frac{d\Delta_S(0^-)}{dX} = -\frac{\Delta_S(0^-)}{b} \qquad \text{(fig. 13)}$$

Using Eqns. (II-19 & 21) we find that b at $T = T_{CNS}$ is given by

$$b = \frac{N_S D_S}{N_N D_N} \frac{\coth(k_N d_N)}{k_N} \qquad \text{(II-22A)}$$

From fig. 13, it is seen that the magnitude of b is a measure of the effect of N on the order parameter in S. When $b >> k_S^{-1}$, Δ_S at the interface is practically unperturbed and equal to its equilibrium value in isolated S. This occurs when, for instance, $D_S >> D_N$, that is, when the N material is a very poor conductor or an insulator. When $b << k_S^{-1}$, $\Delta_S(0^-)$ is practically zero, indicating a strong proximity effect.

For semi-infinite N and S with $N_N = N_S$, $D_N = D_S$, the extrapolation length at $T = T_{CNS} = T_{CS}$, is given by

$$b = k_N^{-1} \qquad \text{(II-22B)}$$

in the Werthamer approximation.

The theory outlined so far has been for temperatures just below T_{CNS}. Before going on to the theoretical description at lower temperatures, we digress a little to consider the electrodynamics of superconductors and to introduce the generalised Ginzburg-Landau equations.

2.6 Electrodynamics of Superconductors

About twenty years after the discovery of superconductivity, which was at first thought of simply as a zero resistance state, the second fundamental property of superconductors was established. This was the 'Meissner' effect, that is, the expulsion by a macroscopic superconductor of magnetic flux from all of its interior except for a region at the surface (whose thickness is of the order 1000 Å) called the penetration depth.

The most successful of the early phenomenological models to describe this effect was due to the Londons, fully discussed

in many textbooks (4,5). We simply recall that their theory arrived at a 'local' or point relation between the currents $\underline{j}(\underline{r})$ which screened the field, and the vector potential $\underline{A}(\underline{r})$ defined by Curl $\underline{A}(\underline{r}) = \underline{H}(\underline{r})$. The range of spatial decay of $\underline{j}$ and $\underline{A}$ into the superconductor was λ, the penetration depth. However, on the basis of experimental evidence in disagreement with a local relation between $\underline{j}$ and $\underline{A}$, Pippard (29) introduced the concept of non-local electrodynamics. He suggested that in a pure superconductor, the screening current $\underline{j}(\underline{r})$ at the point $\underline{r}$ in response to an applied field $\underline{H}(\underline{r})$ depends on the value of the vector potential $A(\underline{r}')$ at all neighbouring points $\underline{r}'$ for which $|\underline{r} - \underline{r}'| < \xi_p$. ξ_p was a characteristic distance, the coherence length of a superconductor. The current $\underline{j}$ is then determined by an integral of $\underline{A}$ over the range ξ_p. Pippard's concept of non-locality was later confirmed by the BCS theory. Their expression for ξ_p in a pure superconductor, denoted by ξ_o is (4)

$$\xi_o = \frac{\hbar v_F}{\pi \Delta(0)} = \frac{0.18 \hbar v_F}{k_B T_{cs}} \qquad \text{(II-23)}$$

and is very close to Pippard's estimate. In a dirty material the range $|\underline{r} - \underline{r}'|$ over which the integral for $\underline{j}(\underline{r})$ has to be evaluated is $\sim \xi_d$ given by $\frac{1}{\xi_d} = \frac{1}{\xi_o} + \frac{1}{\ell}$. For $\ell << \xi_o$, $\xi_d \sim \ell$. When $\underline{j}$ and $\underline{A}$ vary slowly over the Pippard coherence length i.e. when $\xi_p << \lambda$, Pippard's integral equation may be approximated by a differential, and hence local, relation.

The above description of the superconductor's electrodynamics applies in a homogeneous medium where the "degree of

superconductivity", now identified with Gor'kov's pair potential $\Delta(\underline{r})$, is spatially uniform. This, however, is not the case in many practical situations of interest, e.g. type II superconductors in the mixed state where partial penetration of flux into the body of the superconductor takes place so that normal and superconducting regions co-exist. Such spatial variations of $\Delta(\underline{r})$ are taken into account in the phenomenological Ginzburg-Landau theory (1b). This too provides a local relation between $j(\underline{r})$, $A(\underline{r})$ and $\Delta(\underline{r})$. For the validity of their electrodynamic equation, one obviously requires that $\underline{j}$ and $\underline{A}$ vary slowly over ξ_p i.e. the condition $\lambda >> \xi_p$ has to be fulfilled for these equations to be valid. Except in very dirty superconductors, this condition is normally only satisfied when $T \sim T_{CS}$. This is so because, in this limit, $\lambda \sim (T_C - T)^{-\frac{1}{2}}$. This restriction on the temperature for the validity of the G-L equations was their major limitation, as indeed it was for the G-L equations that Gor'kov had derived from the microscopic theory.

2.7 Generalised Ginzburg-Landau Equations

In order to overcome this limitation, considerable effort went into developing from the microscopic theory differential equations like those of G-L that would be valid at lower and preferably at all temperatures. A complete generalisation without any restriction on the temperature, the pair potential or its spatial gradient $\nabla\Delta(\underline{r})$ has proved to be impossible to formulate On the other hand, extensions to lower temperatures by imposing restrictions on either Δ or on $\nabla\Delta(\underline{r})$ have been obtained. The conditions and ranges of validity of such generalisations are

themselves the subject of extensive study (1b).

Of these various extensions, the G-L like equations derived independently by Maki (57) and de Gennes (72), hereafter referred to as the generalised G-L equations, are of particular interest in the present study. Their derivation imposes no restriction on the rate of spatial variations of $\Delta(\underline{r})$, but requires $\Delta(\underline{r})$ itself to be small compared to its equilibrium BCS value which is of the order of $\frac{\pi}{2} k_B T_{CS}$ for all $T < 0.7\ T_{CS}$ (§1.3). In addition, local electrodynamics ($\lambda(T) >> \xi_p$) and short mean free paths ($\ell << \xi(0)$) have to be assumed. $\xi(T)$ ($\sim \xi(0)(\frac{T_{CS}}{T_{CS} - T})^{\frac{1}{2}}$) is the G-L (temperature-dependent) coherence length which determines the scale of variation of $\Delta(T)$ in the G-L temperature regime. ($\xi(T)$ is thus identical to the length $k_s^{-1}(T)$ of Eqn. (II-20) for $T \lesssim T_{CS}$, when $k_s^{-1}(T) \simeq (\frac{\hbar v_F \ell}{2\pi k_B T_{CS}})^{\frac{1}{2}} (\frac{T_{CS}}{T_{CS} - T})^{\frac{1}{2}}$). The generalised equations have been successfully used in describing the behavior at all temperatures of dirty type II superconductors close to a second order transition i.e. applied field $H \sim H_{C2}$. They have also been applied to the problem of induced superconductivity in dirty N materials (55).

(a) Linearised equations in one dimension

We state below the linearised version of the generalised G-L equations for a homogeneous superconductor, confining ourselves to a plane one-dimensional geometry with the superconductor occupying the half space $X > 0$, and the applied field H in the Z-direction. Then the pair potential Δ, the screening currents j and the vector potential $\underline{A}$ will all be functions of X only. As in the case of the 'conventional' G-L equations, the gauge of $\underline{A}(X)$ can be chosen for $\Delta(X)$ to be real. The

generalised equations can then be written

$$-\frac{d^2\Delta}{dX^2} + \left(\frac{2eA}{\hbar c}\right)^2 \Delta = k_s^2 \Delta \qquad \text{(II-24)}$$

and

$$\underline{j}(X) = \frac{-\sigma}{\pi k_B T \hbar c} \psi_2\left(\tfrac{1}{2} + \tfrac{1}{2} k_s^2 q_o^{-2}\right) \Delta^2(X) A(X) \qquad \text{(II-25)}$$

where σ is the normal state conductivity of the metal and $\psi_2(Z)$ is the first derivative of the digamma function. k_s^2 is the solution of

$$\ln(T/T_{cs}) = \psi(\tfrac{1}{2}) - \psi\left(\tfrac{1}{2} + \tfrac{1}{2} k_s^2 q_o^{-2}\right) \qquad \text{(II-26)}$$

$k_s^2 > 0$ for a superconductor below its critical temperature. $k_s^{-1}(T)$ is the temperature-dependent coherence length. As $T \to T_{CS}$, k_s^{-1} diverges and at $T = T_{CS}$, the term $k_s^2 \Delta$ on the R.H.S. of Eqn. (II-24) is zero. This is the familiar result of the phenomenological theory.

Eqn. (II-25), first derived by Maki(57), is usually written in the more familiar form

$$\underline{j} = \frac{-c}{4\pi\lambda^2} \underline{A}(x) \qquad \text{(II-27)}$$

with the weak field penetration depth λ given by

$$\frac{1}{\lambda^2} = \frac{4\sigma\Delta^2(X)}{\hbar c^2 k_B T} \psi_2\left(\tfrac{1}{2} + \tfrac{1}{2} k_s^2 q_o^{-2}\right) \qquad \text{(II-28)}$$

generally referred to as Maki's expression for λ. The dimension-

less G-L parameter κ is defined as

$$\kappa = \frac{\lambda(T)}{k_s^{-1}(T)} \qquad \text{(II-29)}$$

Near T_{CS}, κ can be shown to be almost temperature independent and equal to the value obtained from the phenomenological theory. In a dirty superconductor, this limiting value, κ_{GG}, first derived by Gor'kov from the microscopic theory and approximated by Goodman, is given by (4)

$$\kappa_{GG} = \kappa_0 + 7.5\times10^{-3}\gamma^{\frac{1}{2}}\sigma^{-1} \qquad \text{(II-30)}$$

Here $\kappa_0 = 0.96\,\frac{\lambda_L(0)}{\xi(0)}$, $\lambda_L(0)$ being the London penetration depth at $T = 0$, γ is the coefficient of the electronic specific heat in ergs/cm^3 x $^oK^2$ and σ the normal state conductivity in micro-ohm cm.

(b) Non-linear G-L equations

With the inclusion of the next higher order term, namely, the Δ^3 term, the generalised G-L equation for Δ in zero field becomes (75)

$$\sum_{n\geq 0}\left(\frac{1}{n+\frac{1}{2}+P/2} - \frac{1}{n+\frac{1}{2}} - \ln t\right)\Delta(\underline{r}) - \frac{1}{8\pi^2T^2}\sum_{n\geq 0}(n+\tfrac{1}{2}+P/2)\left|\Delta(\underline{r})\right|^2\times\left[\frac{1}{(n+\frac{1}{2}+P/2)^4}\right]\Delta(\underline{r}) = 0 \qquad \text{(II-31)}$$

where P is the operator

$$P = -\frac{\hbar D\nabla^2}{2\pi k_B T}$$

and D the diffusion coefficient ($D = \frac{1}{3}v_F\ell$ in the dirty limit).

The coefficient of the Δ^3 term is in general a function of temperature. However, near $T = T_{CS}$, it is temperature-independent. Then, the non-linear equation may be written in the following form (4)

$$C\Delta'' = A\Delta + B\Delta^3 \qquad \text{(II-32)}$$

with the coefficients given by

$$A(T) = \frac{N(0)(T-T_{cs})}{T_{cs}} \qquad B = \frac{0{\cdot}098\,N(0)}{(k_B T_{cs})^2} \qquad \text{(II-33)}$$

$$C \simeq \frac{\pi}{24}\,\frac{N(0)\hbar v_F l}{k_B T_{cs}}$$

2.8 Description of Δ at Lower Temperatures

We have already described the spatial variations of $\Delta(X)$ in N and the boundary conditions it obeys when the temperature is close enough to T_{CNS} for the linearised Gor'kov equation to be used. In experiments such as the determination of T_{CNS} or of the specific heat discontinuity, the temperature requirement $T \lesssim T_{CNS}$ is fulfilled. However, for the study of the induced superconductivity in N by, for example, screening distance or breakdown field measurements, one is interested in operating at temperatures much lower than T_{CNS}. We then have to consider two things: (i) down to what temperature are the results obtained above stillvalid and (ii) what possible corrections can be made when above results cease to be valid.

To facilitate our discussion we may define three temperature regimes as follows:

(1) high temperatures, for which the non-linear terms in Gor'kov's self-consistency relation for Δ in the normal material, Eqn. (II-1) are small compared to the linear term. As we shall see, this condition may hold down to $T << T_{CNS}$.

(2) Intermediate temperatures for which the non-linear terms in Gor'kov's expansion are no longer negligible although a power series is still convergent.

(3) Very low temperatures $T < T_e$, for which the expansion of the gap equation in powers of Δ is non-convergent.

Silvert (74) has shown that for a homogeneous superconductor the expansion is convergent as long as $T > T_e = \frac{\Delta_{BCS}(T)}{\pi k_B}$. Hurault (47) applies this convergence condition to normal metals replacing Δ_{BCS} by $\Delta(\underline{r})$ in the normal metal. This has a maximum value at the NS interface where the condition must be tested.

$\Delta(\underline{r})$ at the interface may be easily estimated in a practical case using the boundary condition of Eqn. (II-16). For a normal metal of $(NV)_N \sim 0.1$, in the proximity of Pb for which $T_C = 7.2^oK$ and $(NV)_{Pb} \sim 0.4$, $\Delta_N(0^+) \simeq 2k_BT$ at $T = 2^oK$. For normal metals like Cu and Ag, $(NV)_N$ has an estimated value of $\lesssim 0.1$ ($T_e \lesssim 1.2^oK$) and the condition $\Delta_N < \pi k_BT$ is well-satisfied, especially in the bulk of N, at temperatures of interest to us i.e. $T > 1.5^oK$.

For N metals like Zn , and Cd (NV ~ 0.2), in contact with Pb, $\Delta_N \gtrsim \pi k_BT$ at $T = 2^oK$ and the convergence condition is not then fulfilled at the interface. However, considering that Δ undergoes a rapid decrease within the range of the kernel ($\sim q_o^{-1}$) of integration the above condition may always be assumed to hold

in N except near the interface, in the temperature region of interest.

In the discussion of induced superconductivity so far published, it has always been assumed the power series expansion (II-1) is convergent.

(a) Δ in dirty N at $T \gtrsim T_{CN}$

When the temperature is sufficiently close to T_{CN}, Δ may be large in the neighborhood of the interface. Then the term in Δ^3 in the generalised G-L equation (II-31) may be comparable with or larger than the linear term. $\Delta(X)$ is then the solution of

$$-\frac{d^2\Delta}{dX^2} + E\Delta^3 = -k_N^2\Delta \qquad \text{(II-34)}$$

To picture the spatial variation of Δ in a simple manner we note that at $T = T_{CN}$, the linear term in the above equation is zero, and the pair potential given by

$$\Delta(X) = \frac{\Delta(0^+)X_0}{X_0 + X} \qquad \text{(II-35)}$$

where

$$X_0^2 = \frac{2}{E\Delta^2(0^+)}$$

Compare $\frac{1}{X}$ decrease of $F(X)$, predicted by Falk (35) for the case $V_N = 0$ when $T \to 0$ (§2.3(a)). When T is just above T_{CN}, the non-linear term will still dominate near the interface and Δ displays the $1/X$ decay as in eqn. (II-35) but beyond some point X_c, $E\Delta^3 << k_N^2\Delta$ and Δ will then decay exponentially with X.

How close to T_{CNS} must we be for the Δ^3 term in the G-L equation to be comparable to the linear term, near the interface?

The answer will depend not only on the properties of the N material, but also on the S metal in contact with it. Hurault (47) estimates the temperature $T = T_{CN} + \delta T$, above which the non-linear term may be neglected, by considering the relative magnitudes of the terms in the generalised G-L equation. He obtains the following result for T when $\frac{\delta T}{T_{CN}}$ is small

$$\ln\left(\frac{T_{CN}+\delta T}{T_{CN}}\right) = \frac{\delta T}{T_{CN}} = \frac{\Delta^2(0^+)}{(\pi k_B T)^2} \cdot \frac{1}{1+\frac{4}{3}\frac{\Delta^2(0^+)}{(\pi k_B T)^2}} \qquad \text{(II-36)}$$

For the above estimate to be valid, $\Delta(0^+)$ must be less than $\pi k_B T$, so that the generalised G-L equations can apply throughout N. This, and the assumption of small $\frac{\delta T}{T_{CN}}$ (i.e. $T \sim T_{CN}$) make such an estimation applicable only when $\Delta(0^+) < \pi k_B T_{CN}$. Thus, one may use it for Pb/Sn, ($(NV)_{Sn} \sim 0.25$, $T_{CN} \simeq 3.8^\circ K$) and for In Bi/Zn ($(NV)_S \sim 0.3$, $T_{CS} \simeq 4.4^\circ K$, $T_{CN} \simeq 0.9^\circ K$) to obtain $\frac{\delta T}{T_{CN}} \sim 0.3$ to 0.4. Experimentally, the Orsay Group (56) have found $\frac{\delta T}{T_{CN}} \sim 0.1$ for both the above systems.

For Pb/Zn, however, $\Delta(0^+) \simeq 8k_B T_{CN}$ and the above procedure becomes inapplicable. The same difficulty would be encountered for any N metal with $T_{CN} < 1^\circ K$ (e.g. Cd, Ag, Cu) in contact with Pb. That this will be so can be seen by noticing that whereas $\Delta(0^+)$ decreases linearly with $(NV)_N$, T_{CN} decreases logarithmically. T_{CN} is, of course, also proportional to the Debye temperature of the N metal (see Eqn. I-2) but this varies by less than a factor of 3 among any of the normal materials we consider in this thesis.

In short, when $T_{CN} << T_{CS}$, the power series expansion (II-1) may not remain convergent (and generalised G-L equations cease to

be a valid description of the induced superconductivity in N) at a temperature much higher than T_{CN}. However, Deutscher et al. (59) comment that their calculation of the non-local penetration depth $\lambda(\Delta)$ (see §2.11) agrees reasonably well with experiments on Pb/Cd down to $T = 1^{o}K$ in spite of the fact that $T < T_{c}$ of $2.1^{o}K$.

(b) Boundary conditions at interface when $T \ll T_{CNS}$

By taking into account the Δ^3 term in Gor'kov's self-consistency relation (II-1), Hurault (47) has shown that when $T \ll T_{CNS}$ Δ obeys the following boundary conditions at the interface of two metals that differ only in respect of V (i.e. for which $D_N = D_S$, $N_N = N_S$):

$$\frac{\Delta}{V} \ , \ \frac{1}{V}\frac{d\Delta}{dX} \qquad \text{continuous} \qquad \text{(II-37)}$$

It is seen that the above boundary conditions are identical to those for $T \lesssim T_{CNS}$, i.e. Eqns. (II-16 & 17) for the case $D_N = D_S$, $N_N = N_S$. Nevertheless Hurault demonstrates that it cannot be shown in a simple manner that the two sets of boundary conditions will be identical when $D_N \neq D_S$, $N_N \neq N_S$. However, theoretical and experimental studies (17,76) indicate that the continuity of $\frac{\Delta}{NV}$ is probably a good approximation to the truth even when it cannot be demonstrated rigorously (particularly when Δ is large).

The authors of the theories presented in the following sections always make one of two simplifying assumptions as indicated regarding the diffusion coefficients in the metals. Then, in the two cases, the following boundary conditions apply:

(i) when $D_S = D_N$,

$$\frac{\Delta}{NV}\ ,\ \frac{1}{V}\frac{d\Delta}{dX} \qquad \text{continuous} \qquad \text{(II-39)}$$

(ii) when $D_S >> D_N$,

$$\frac{\Delta}{NV} \qquad \text{continuous,} \quad \Delta_s(0^-) \simeq \Delta_{BCS}(T) \qquad \text{(II-40)}$$

PROXIMITY EFFECTS IN MAGNETIC FIELDS

In Chapter I we saw that a large number of proximity experiments are done in the presence of a magnetic field. Of these, the ones concerned with the electromagnetic properties of the specimen can be divided into two classes. These are the study of

(a) effects on the S side such as the lowering of the critical fields of S(55, 48) and the change in the weak-field penetration depth of S (77)..

(b) effects on the N side like the screening of r.f. and d.c. fields and field-induced phase transitions in N(56, 59).

In the following we shall confine ourselves to the electromagnetic properties of the N side.

2.9 Magnetic Effects on N Side

To describe the response of the normal layer to an applied magnetic field, the Orsay Group (55) use the generalised linear G-L equations (II-24, & 26). The material is assumed to be dirty and $\Delta_N(\underline{r})$ small everywhere in N. In the one-dimensional geometry as specified in §2.7(a), with the applied field in the

z-direction and the gauge chosen for Δ to be real, the equations are

$$\frac{d^2\Delta}{dX^2} - \left(\frac{2e}{\hbar c}\right)^2 A^2\Delta = k_N^2\Delta \tag{II-41}$$

$$j = \frac{-c}{4\pi\lambda^2} A \tag{II-42}$$

where $$\frac{1}{\lambda^2} = \frac{4\sigma\Delta^2}{\hbar c^2 k_B T}\ \psi_2(1/2 - k_N^2/2q_o^2) \tag{II-43}$$

In the Werthamer approximation (§2.5) which we use, k_N is the smallest root of

$$Ln(T/T_{cN}) = \psi(1/2) - \psi(1/2 - 1/2\, k_i^2 q_o^{-2}) \tag{II-44}$$

From now on we drop the subscript and denote the smallest root by k. We make two important observations about the penetration depth $\lambda(\Delta)$ in the normal metal (55, 1a). Firstly, when $V_N \to 0$ (i.e. $\Delta \to 0$ since $\Delta = V_N F$), it would appear from Eqn. (II-43) that $\lambda \to \infty$. However, the function ψ_2 diverges in the limit $V_N \to 0$, and λ remains finite.

$$\lim_{V_N \to 0} \lambda = \frac{\hbar c N_N}{2F}\left(\frac{k_B T}{\hbar\sigma}\right)^{1/2} \tag{II-45}$$

Physically, the above result means that electromagnetic screening in N may be observed even when $V_N = 0$. Eqn. (II-43), also implies that $\lambda \to 0$ as $T \to 0$, which is unphysical. In this limit, however, the Cooper pair amplitude does not decay exponentially anymore but goes as $\frac{1}{X}$ (see Eqn. (II-6)). The derivation of Eqn. (II-43) is not then valid.

2.10 G-L Parameter in N

We can now define a G-L parameter in N, analogous to that in a homogeneous superconductor, in terms of λ and the coherence length k^{-1}. As λ is strongly position-dependent, we define κ_N with reference to the point $X = 0^+$ at the interface,

$$\kappa_N = \kappa_N(0^+) = \lambda(0^+)\, k \qquad \text{(II-46)}$$

We know that $\lambda(X) \sim \Delta^{-1}(X) \sim \exp(kX)$ for small values of Δ in Eqn. (II-41). Hence

$$\kappa_N(X) = \kappa_N \exp(kX) \qquad \text{(II-47)}$$

κ_N is also a strong function of temperature. For $T \sim T_{CS}$, Δ is small in N and λ therefore large while k is finite. Thus

$$\lim_{T \to T_{CS}} \kappa_N = \infty$$

When the temperature is lowered λ decreases while k^{-1} increases and diverges in the limit $T = T_{CN}$. Therefore

$$\lim_{T \to T_{CN}} \kappa_N = 0 \qquad \text{(II-48)}$$

Wolf et al. (53) and Hurault (47) postulate, however, that once κ_N reaches the value κ_{GG}, the 'intrinsic' G-L value for the metal, it remains constant and does not decrease any more as the temperature is lowered towards T_{CN}. We shall discuss this further in §2.14.

Far from the interface into N, the local values of $\lambda(X)$ and $\kappa_N(X)$ are both large and an applied field can penetrate

freely. As we move closer to the interface $\lambda(X)$ and $\kappa_N(X)$ decrease rapidly and the field is more and more strongly screened. A reasonable estimate of the screening distance δ measured from the interface to the 'flux front' (fig. 14a) may be made by putting $\kappa_N(\delta) \simeq 1$ (a more precise definition of δ is given in the next section). Using Eqn. (II-47) we obtain

$$\delta = \frac{1}{k} \ln\left(\frac{1}{\kappa_N}\right) \qquad \text{(II-49)}$$

A significant amount of screening i.e. $\delta > k^{-1}$ is obtained when $\kappa_N << 1$.

2.11 Screening Distance δ in Thick N Layer: $\kappa_N << 1$

We now outline a more rigorous calculation of δ due to the Orsay Group (55, 47). We start with the linearised G-L equations which in the Werthamer approximation write

$$\frac{d^2\Delta}{dX^2} - \left(\frac{2e}{\hbar c}\right)^2 A^2 \Delta = k^2 \Delta \qquad \text{(II-51)}$$

$$\frac{d^2A}{dX^2} = \frac{A}{\lambda_N^2}\left(\frac{\Delta}{\Delta_N}\right)^2 \qquad \text{(II-52)}$$

where λ_N and Δ_N are the zero field values of these quantities at the interface, $X = 0^+$. In obtaining (II-52) use has been made of Maxwell's equation $\frac{4\pi}{c}\underline{j} = \text{Curl } \underline{H}$. We now make the simplifying assumption that if the applied field is weak, we may use the zero field solution for Δ, viz. $\Delta = \Delta_N \exp(-kX)$. This actually constitutes two assumptions. Firstly that in Eqn. (II-51), $\left(\frac{2e}{\hbar c}\right)^2 A^2 << k^2$ at distances $\sim\delta$ from the interface.

Taking $\delta \sim k^{-1}$, we require $H_o \lesssim \frac{\phi_o k^2}{2\pi}$ where $\phi_o = \frac{hc}{2e}$. Secondly, we have made the implicit assumption that $\Delta(0^+) = \Delta_N$ (the zero field value). This amounts to supposing that the field is weak enough for the order parameter in S to remain unaffected and for the continuity of $\Delta/_{NV}$ at the interface to be a valid boundary condition. Eqn. (II-52) can then be solved analytically, to yield

$$A = H_o k^{-1} K_o\left(\frac{\exp(-kX)}{K_N}\right) \qquad \text{(II-53)}$$

where K_o is the zero order Modified Bessel function of imaginary argument. The solution can be shown to satisfy the boundary conditions:

$$\text{for } X \to 0,\ A \to 0$$

$$\text{and for } X \text{ large}, (\gg k^{-1}) \quad A \to H_o(X-\delta) \qquad \text{(II-54)}$$

where

$$\delta = k^{-1}\left(\ln\left(\frac{1}{K_N}\right) - 0.116\right) \qquad \text{(II-55)}$$

The behavior of A for large and small x as described by Eqns. (II-54) is depicted in fig. 14b which shows how δ, as calculated above, is geometrically related to the asymptotic form of A at large X. As a drastic simplification, useful for some discussions, we may think of δ as denoting the position of a magnetic 'flux front' so that H increases from a near zero value for $X < \delta$ to H_o for $X \geq \delta$.

How does the flux front move as the field is raised? The distortion of the order parameter by the field can no longer be ignored. Suppose now that the field is increased so that

$\frac{\phi_o k^2}{2\pi \kappa_N} > H_o > \frac{\phi_o k^2}{2\pi}$. Let $L \equiv \delta(H_o)$ now denote the distance of the flux front from the interface. Then in the region $L > X > 0$, Δ is nearly zero and the normalised solution for Δ is

$$\Delta = \frac{\Delta_N \sinh[k(L-X)]}{\sinh(kL)} \qquad \text{(II-56)}$$

For $X > L$, Δ will be very nearly zero and the field constant and equal to H_o. To relate L and H, we multiply (II-51) by $\Delta' \equiv \frac{d\Delta}{dX}$ and integrate with respect to X:

$$(\Delta')^2 - \Delta^2\left[\left(\frac{2e}{\hbar c}\right)^2 A^2 + k^2\right] + \left(\frac{2e}{\hbar c}\right)^2 (A')^2 (\Delta_N \lambda_N)^2 = \text{Const} \qquad \text{(II-57)}$$

Here $A' = \frac{dA}{dX}$ and we have used $\frac{d^2A}{dX^2} = \left(\frac{\Delta}{\Delta_N}\right)^2 \frac{A}{\lambda_N^2}$ (Eqn. II-52). Using the boundary conditions that $\Delta \simeq 0$ and $A' = H_o$ for $X \to \infty$, we find that the constant in (II-57) is $\left(\frac{2e}{\hbar c}\right)^2 (\Delta_N \lambda_N)^2 H_o^2$. For $X = 0$, we have $A = 0$, $A' = 0$, $\Delta = \Delta_N$ and $\Delta' = \Delta_N k \frac{\cosh kL}{\sinh kL}$. Substituting these into Eqn. (II-57) and simplifying yields

$$H_o \sinh(kL) = \frac{\hbar c k}{2e\lambda_N} = \frac{\phi_o k^2}{2\pi \kappa_N} \qquad \text{(II-58)}$$

To summarise, Eqn. (II-55) gives an approximate analytic expression for δ in the limit of weak fields ($H_o < \frac{\phi_o k^2}{2\pi}$) whereas (II-58) describes the variation of $L \equiv \delta(H_o)$ with H_o for $\frac{\phi_o k^2}{2\pi \kappa_N} > H_o > \frac{\phi_o k^2}{2\pi}$, when $\kappa_N << 1$.

2.12 $\kappa_N << 1$, Normal Layer Thin: Breakdown Effect

Upto now we have considered very thick N layers so that far from the interface, an applied field could freely penetrate

N and only begin to decay at distances ~ δ from the interface. In other words, a well defined flux front already existed in N even at very small fields and this moved inwards (towards the interface) smoothly as H_o was increased. What happens when the normal layer has a thickness $d_N \lesssim \delta$? In §1.14 we saw that this leads to the phenomenon of 'breakdown'. Qualitatively, we can understand the phenomenon as follows. For a thin film, Δ will have a finite value $\Delta(d_N)$ at the free sufrace of N. A small applied field H_o will decay strongly as soon as it enters N whereas Δ remains unperturbed. No 'flux front' exists inside N. As H_o is increased it continues to be screened strongly by N until it reaches a value H_b. Then a sudden penetration of flux occurs; that is, a flux wall enters N. This non-continuous transition is of the first order. We may crudely estimate H_b by setting $d_N \sim L$ in Eqn. (II-58). For reasons that will become apparent soon we shall denote this field by H_W. Hence,

$$H_W \sinh(kd_N) = \frac{\varphi_o k^2}{2\pi K_N} \qquad \text{(II-60)}$$

In Fig. 15 the two penetration 'modes' for $H_o < H_b$ and $H_o > H_b$ are shown schematically.

This effect has been studied theoretically and experimentally by the Orsay Group (55, 56). Their experiments on In Bi/Zn & Pb/Sn and the recent ones by Kratzig (10) on Pb/Ag were reviewed in §1.14.

In the theory proposed by the Orsay Group (56), they calculated the Gibb's free energy of N as a function of H_o for

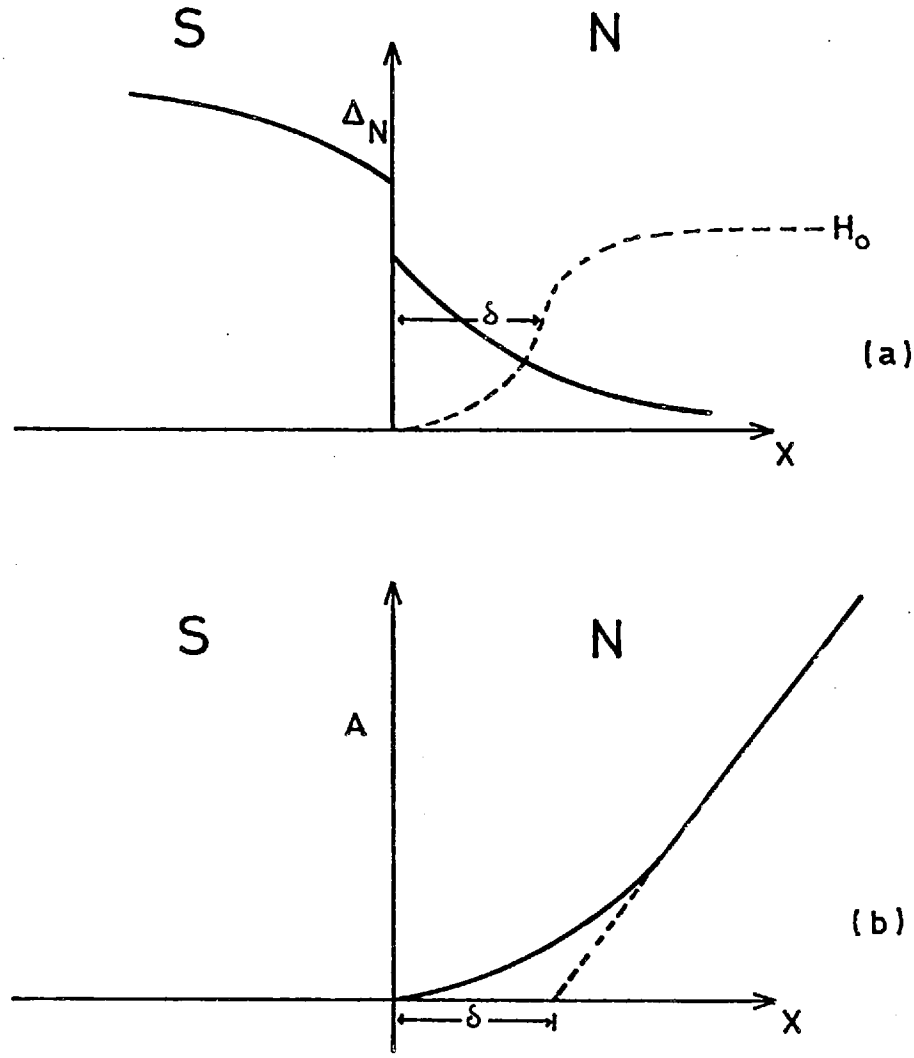

Figure 14 - Spatial variation of (a) $\Delta(X)$ and H_o and (b) $A(X)$ for the case of a thick normal layer with $\kappa_N \ll 1$.

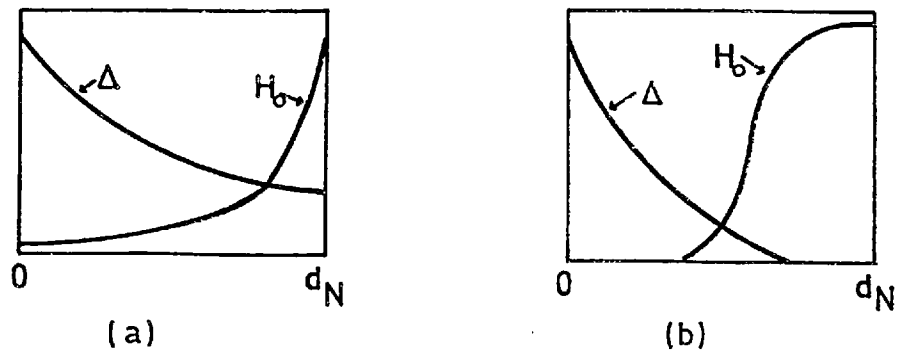

Figure 15 - Spatial variation of $\Delta(X)$ and H for a thin normal layer with $\kappa_N \ll 1$ when (a) $H_o < H_b$ (b) $H_o > H_b$.

the two penetration modes, using the integrals of G-L equations to evaluate it for the 'superconducting' regions. They showed that under certain conditions (of temperature and thickness d_N, described below), one or the other of the two modes was the stable one (of lower free energy) depending on the value of H_o. They showed that in very thick films, flux would penetrate continuously as H_o is increased and hence no breakdown observed (penetration mode of fig. 15b being the stable one for all H_o). In the thickness region where H_b does exist, it increases rapidly (Eqn. (II-60)) as d_N is reduced. For very thin films then, the second penetration mode may not become energetically favourable before the critical field of S is reached. Thus d_N must lie in a certain range of thickness for breakdown to be observed.

For a given thickness d_N, k^{-1} and hence $\Delta(d_N)$ is a strong function of temperature. Above a certain temperature T^*, $\Delta(d_N)$ will be too small for the field to be effectively screened. Flux will then penetrate continuously with increasing H_o. For a given d_N, T^* is found to be given (in terms of $k = k(T)$) by

$$k(T^*)d_N/K_N = \frac{3}{2}\cosh[k(T^*)d_N] \qquad \text{(II-63)}$$

The authors solve this equation graphically and show that T^*_{max}, the maximum T^* for any d_N occurs when $\kappa_N = 0.44$.

We recall that in type I superconductors (4,5) a first-order phase transition occurs when $H_o = H_c$, the thermodynamic critical field of the superconductor. H_c and H_b can thus be considered analogous. As in other field induced first-order

transisions, the breakdown effect shows supercooling and superheating. By supercooling we mean the existence of a metastable 'normal' (supercooled) state in decreasing fields at fields $H_o < H_b$. In the breakdown field context supercooled state means the second penetration mode, with a flux wall inside N. We can now see that in Eqn. (II-60) we actually obtained the field for the exit of the wall in decreasing fields. H_W is, therefore, the supercooling field. The superheating field H_s can be shown to be given by (55)

$$H_s = \frac{\varphi_o k^2}{2\pi \kappa_N}\left(\frac{8}{27\kappa_N \sinh(kd_N)}\right)^{1/2} \qquad \text{(II-61)}$$

The expression obtained by equating the Gibb's energies of the two modes has, in general, to be solved numerically to obtain H_b. However when $\exp(kd_N) > 1$ and $\kappa_N \exp(kd_N) << 1$, which can occur if $\kappa_N << 1$, the Orsay Group (55) obtain

$$H_b = 1.9 H_w = 3.8 \frac{\varphi_o k^2}{2\pi \kappa_N} \exp(-kd_N) \qquad \text{(II-62)}$$

In §1.14 we described how strong disagreement between experiment and theoretical predictions of the breakdown and screening phenomena as outlined above led Deutscher et al. (56, 59) to trace this to the inadequacy of Maki's expression for $1/\lambda^2(\Delta)$, Eqn. (II-28). We recall that Maki's result, derived for a homogeneous medium, relates λ to the local value of Δ. However, Δ changes abruptly across the interface and Deutscher et al. (59) argue that $\lambda_N(\Delta)$ close to the interface

should include a strong non-local contribution from Δ in S. They attempted an improved calculation of $\lambda_N(\Delta)$ the results of which we briefly sketch below.

2.13(a) Improved calculation of $\lambda(\Delta)$

In their calculation the authors make the following simplifying assumption about the form of Δ in S and N:

$$\text{S: } X < 0 \qquad \Delta(X) = \Delta_{BCS}(T) = \text{Const.}$$

$$\text{N: } X > 0 \qquad \Delta(X) = \frac{1}{\alpha}\,\Delta_{BCS}(T)\,\exp(-kX) \tag{II-64}$$

where $\alpha = \frac{(NV)_S}{(NV)_N}$. To obtain an analytical solution they also have to take $D_N = D_S$ and $N_N = N_S$. Then, in the one-dimensional geometry they obtain the following electrodynamic equation

$$j(X) = -Q(X)A(X) \tag{II-65}$$

with

$$Q(X) = \frac{4\pi\sigma T k_B \Delta^2(X)}{D^2 c} \sum_{n\geq 0} \left[\frac{2q_n}{q_n^2 - k^2} + e^{(k-q_n)X}\left(\frac{\alpha}{q_n} + \frac{1}{k-q_n}\right)\right]^2 \frac{1}{q_n^2} \tag{II-66}$$

and

$$q_n^2 = \left(n + \tfrac{1}{2}\right)\left(\frac{4\pi k_B T}{\hbar D}\right) \tag{II-66B}$$

Eqn. (II-66) without the second term in the bracket can be shown to lead exactly to Maki's expression for λ. An examination of this term shows that it is important for $X \lesssim \frac{1}{|k-q_o|}$, provided that k is smaller than the smallest q_n i.e. q_o. In §2.3 we saw that $k \lesssim q_o$ for V_N small and positive (T_{CN} finite) and that $k \to q_o$ when $T_{CN} \to 0$. Hence, the distance $\frac{1}{|k-q_o|}$, over which a correction has to be made to λ, grows

longer as $V_N \to 0$. Alternatively, the correction is much more important for $T >> T_{CN}(k \to q_o)$ than it is for $T \sim T_{CN}$. For the latter case, the author's suggest that Maki's expression may safely be used.

When V_N is small and negative, they assume k to to be given by (see § 2.3)

$$kq_o^{-1} = (1 - \frac{1}{2\alpha}) \qquad \text{(II-13)}$$

Either case (of V_N negative or positive) follows the same analysis. Then, by the use of an approximation to evaluate the summation in Eqn (II-66), the following result is obtained for $|V_N|$ small

$$\frac{1}{\lambda^2(X)} = \frac{\sigma}{\hbar c^2 T k_B}\left(\alpha + 0.5\right)^2 \Psi_2(\tfrac{1}{2})\,\Delta^2(X) \qquad \text{(II-67)}$$

Eqn (II-67) shows that when $T >> T_{CN}$, λ is a much more sensitive function of α than k is. For the simplified form of pair potential used i.e. $\Delta_N(0) = \frac{1}{\alpha}\,\Delta_{BCS}(T)$, we can obtain the dependence of κ_N and hence of δ on α (see Eqns (II-46 & 49))

$$\kappa_N \propto k(1-0.5/\alpha)$$

Thus, in any measurement of κ_N, a precision better than $0.5/\alpha$ would be required to establish the sign of α. For a metal like Ag in contact with Pb, $|\alpha| \sim 5$, and the required accuracy ~10%.

(b) Deutscher's numerical calculation of δ

Deutscher (62) has made a numerical calculation of Q(X) from Eqn. (II-66). Fig. 16 shows his results for Q(X) as a function of X for different values of the parameters $\alpha = \frac{V_S}{V_N}$ and k/q_o. For $V_N > 0$, k/q_o is determined by Eqn (II-44) and is a function of temperature. However, for $T >> T_{CN}$, $k/q_o \simeq 1$ and practically independent of T. When V_N is small and negative,

$k/q_o = (1 - \frac{1}{2\alpha})$ (Eqn (II-13)) and once again $k/q_o \simeq 1$.

The calculated values of Q(X) together with Eqn. (II-65) are then used to evaluate the vector potential A(X). Upon expressing this in the asymptotic form $A(X) = H(X-\delta)$ far from the interface the author obtains the screening distance δ. Fig. 17 shows the dimensionless quantity $q_o\delta$ plotted as a function of $q_o\ \lambda_N(X = 0, \alpha^{-1} = 0) \equiv q_o\ \lambda_{oo}$ for different values of α with kq_o^{-1} taken as unity. λ_{oo} is calculated from Eqn. (II-67) where we use $\Delta_N(0^+) = \frac{\Delta_{BCS}}{\alpha}$, to give

$$\frac{1}{\lambda_{oo}^2} = \frac{\sigma}{\hbar c^2 k_B T}\ \Psi_2(1/2)\,\Delta_{BCS}^2 \qquad \text{(II-68)}$$

The comparison of the above numerical calculations with the experiments of Valette (63, 64) is presented in Chapter VI.

(c) Discussion of the validity of the model

Three main assumptions were made in the above calculations of $\lambda(\Delta)$ by Deutscher et al. (59) and of δ by Deutscher (62) which we now examine.

(i) A crucial step in the derivation of Eqn. (II-66) is the supposition that Q(X) may be expanded in powers of $\Delta(T)$ both in N and S. For such an expansion to be convergent, $T > T_e$ where T_e is given by $T_e = \frac{\Delta_{BCS}(T)}{\pi k_B}$ (74), see § 2.8

(ii) The densities of states at the Fermi level and the diffusion coefficients were taken to be the same for both metals. The authors remark however that a calculation with $N_N \neq N_S$ and $D_N \neq D_S$ leads to the same result for $\lambda(0)$ and very nearly the same for $\lambda(X)$.

(iii) A simple form of variation, Eqn. (II-64), has been assumed for $\Delta(X)$. The approximation $\Delta(0^-) = \Delta_{BCS}$ is valid if

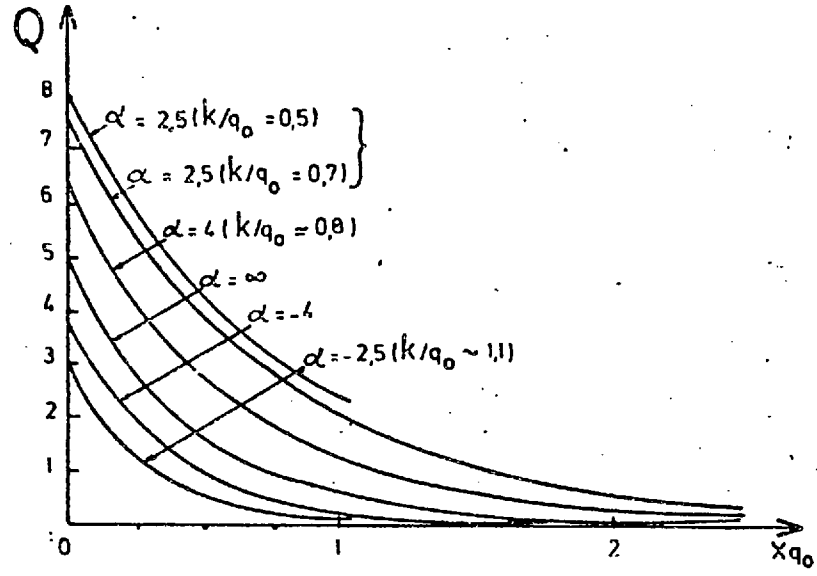

Figure 16 - Q(X) as a function of Xq_o for different values of α and of k/q_o as calculated by Deutscher (62).

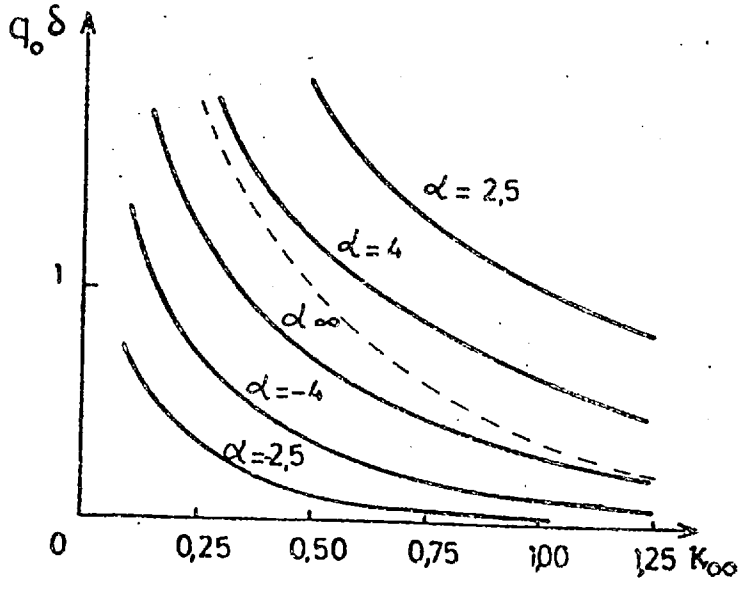

Figure 17 - The quantity $q_o\delta$ as a function of $\kappa_{oo} = q_o\lambda_{oo}$ (see text) for different values of α (Reproduced from Deutscher (62)).

$D_N << D_S$ (see §2.5). When this is not so, the only modification to the calculations is to replace Δ_{BCS} by the actual value $\Delta_S(0^-)$.

2.14 'Saturation' Effects

(a) Introduction

In §2.8a we obtained the theoretical result that at $T = T_{CN}$, $\Delta(X) \propto \frac{X_o}{X+X_o}$. We saw that this asymptotic behavior of Δ could, under suitable circumstances, be dominant at $T \gtrsim T_{CN}$ close to the interface. It is claimed (66) that some of the results obtained on the assumption of an exponential decay are remarkably altered when this $\frac{1}{X}$ decay of Δ comes into play. The term 'saturation' effects has been used by the Orsay Group to describe this phenomenon. Likewise, the temperature below which the effect may be observed is called the saturation temperature, T_S.

At first sight it would appear that T_S would be quite close to T_{CN}. However, Deutscher and Valette (66) report observing much higher saturation temperatures; for example, they observe $T_S \sim 2.1^oK$ for Ag, the transition temperature of which, from their theory of the saturation effect, they deduce to be $\sim 10^{-5}\ ^oK$. The only other reported observation of saturation effects is by Deutscher, Lindenfeld and Wolf (53, 68), arising from thermal conductivity measurements on Pb Bi/Ag layers. They use the Orsay model to explain some of their results which we shall refer to in due course. We present below a description of the Orsay model. So that the reader does not lose track of

the underlying physics in the ensuing mathematical detail we summarise here the kernel of their argument. This is that $\kappa_N(X=0, T)$ which decreases as T is lowered, cannot decrease below κ_{GG}, the intrinsic value of this parameter for the particular N metal. According to their model, the temperature T_S, defined as the highest temperature for which $\kappa_N(X=0, T_S) = \kappa_{GG}$, coincides with the onset of saturation i.e. the Δ^3 term of the G-L equation becoming dominant in comparison with the linear term. Lowering T below T_S would extend the saturation region into N (say upto $X=X_C(T)$) so that for $X < X_C$, $\kappa_N = \kappa_{GG}$ and for $X > X_C$, $\kappa_N = \kappa_{GG} \exp k(X-X_C)$.

(b) <u>The Orsay model of 'saturation'</u>

In §2.11 an earlier calculation of δ was outlined (yielding Eqn. (II-55)) based on two principal assumptions (i) that λ in N could be considered a local function of Δ which allowed the use of Maki's expression for $\lambda(\Delta)$ and (ii) that a linearised G-L like equation could be used to describe $\Delta(X)$. Deutscher and Valette (66) argue that a 'local' calculation of λ, neglecting the contribution of S to the screening current in N, is valid only when the field in N is screened off sufficiently far from the interface i.e. $\delta(T) > k^{-1}(T)$. To satisfy this condition, the temperature has to be low ($T << T_{CNS}$) but then the order parameter will be large and non-linear effects important. They conclude that the assumptions of locality and linearity are mutually exclusive and suggest that at high temperatures, when the assumption of linearity is valid, non-local corrections like those of Deutscher et al. (59) (see §2.13) are essential. At low temperatures, the dominant effects arise

from the non-linear term in the G-L equation and λ may quite adequately be considered a local function of Δ.

To take into account the non-linear effects Valette (64) assumes that $\Delta(X)$ in N may be described by the non-linear G-L equation in zero field

$$C\Delta'' = A\Delta + B\Delta^3 \tag{II-69}$$

Implicit in the derivation is the assumption that even at $T >> T_c$ the coefficients A, B and C are still given by the expressions (II-33) which, strictly speaking, are valid for T just below T_c. We recall that these coefficients are

$$A = N(0)\frac{T-T_c}{T_c}\ , \quad B = \frac{0{\cdot}098\,N(0)}{(k_B T_c)^2}\ , \quad C = \frac{\pi}{24}\frac{N(0)\hbar v_F l}{k_B T_c} \tag{II-33}$$

When Δ is large, the Δ^3 term will be dominant close to the interface and the solution is

$$\Delta(X) = \Delta(0)\frac{X_0}{X+X_0} \tag{II-70}$$

with

$$X_0 = \frac{1}{\Delta(0)}\left(\frac{2C}{B}\right)^{1/2} \tag{II-71}$$

Far from the interface, where the linear term is the more important, one has

$$\Delta(X) = \Delta_c \exp(-kX) \tag{II-72}$$

where

$$k^{-1} = \left(\frac{C}{A}\right)^{1/2} \tag{II-73}$$

A simplification is introduced by taking for $\Delta(X)$ the expression (II-70) for $0 < X \leq X_c$ and (II-72) for $X \geq X_c$, with

the two solutions and their first derivatives matched at $X = X_c$. On doing this, one obtains the following relations

$$\Delta_c = \frac{\Delta(0) X_o \exp(k X_c)}{k^{-1}} \qquad \text{(II-74)}$$

$$X_c = k^{-1} - X_o \qquad \text{(II-75)}$$

Note that (II-76)

$$\Delta(X_c) \equiv \Delta_p = \frac{\Delta(0) X_o}{k^{-1}}$$

The condition for a 'saturation' regime to exist is $X_c > 0$ i.e. $X_o < k^{-1}$.

In the 'saturation' region ($X \leq X_c$) the authors use the following definition of a position-dependent coherence length, due to Hurault (47)

$$X < X_c \,, \quad k^2(X) = \Delta'' \cdot \frac{1}{\Delta} = \frac{B}{C} \Delta^2(X) \qquad \text{(II-77)}$$

We note that in the region $X > X_c$, the above definition leads to the familiar result of Eqn. (II-73), with $k \neq k(X)$. With the use of $k(X)$ and k of (II-73) a G-L parameter is defined for each of the two regions in N in terms of a local penetration depth $\lambda(X)$

$$X < X_c \,, \quad \kappa_N(X) = \frac{\lambda(X)}{k^{-1}(X)} = \lambda(X)\Delta(X)\left(\frac{B}{C}\right)^{1/2} \qquad \text{(II-78)}$$

$$X > X_c \,, \quad \kappa_N(X) = \frac{\lambda(X)}{k^{-1}} = \frac{\lambda(X_c)}{k^{-1}} \times \frac{\Delta_p}{\Delta(X)}$$

$$= \frac{\lambda(X_c)}{k^{-1}} \exp k(X - X_c) \qquad \text{(II-79)}$$

Using the G-L equilibrium relation between λ and Δ which holds in a superconductor when $T < T_C$ and when Δ is spatially constant (4), namely,

$$\lambda(T) = \frac{\hbar c}{4e} \frac{1}{(2\pi C)^{1/2}} \frac{1}{\Delta(T)} \qquad \text{(II-80)}$$

the authors obtain, <u>for $X < X_C$</u>,

$$\kappa_N = \frac{\hbar c}{4eC} \left(\frac{B}{2\pi}\right)^{1/2} \equiv \kappa_{GG} \qquad \text{(II-81)}$$

The identity used for κ_{GG} in the last equation is a familiar result from the G-L theory (e.g. ref. 4), valid in a superconductor at $T \lesssim T_{CS}$. By requiring $\kappa_N(X)$ to be continuous at $X=X_C$ they write for <u>$X > X_C$</u>,

$$\kappa_N(X) = \kappa_{GG} \exp[k(X-X_c)] \qquad \text{(II-82)}$$

Fig. 18a, reproduced from ref. 64, shows the spatial variations of Δ and κ as calculated above.

The above derivation may be criticised on several counts as outlined later, in section (d). At this point, however, we examine how the model has been used to interpret some experimental observations.

(c) <u>Evaluation of δ and its temperature dependence</u>

To evaluate δ in the 'saturation' regime of their model, Deutscher and Valette (66) use Eqn. (II-55) with the value of $\kappa_N(0)$ replaced by $\kappa_N'(0)$ which is the value obtained by extrapolating Eqn. (II-82) to X = 0 i.e. $\kappa_N'(0) = \kappa_{GG} \exp(-kX_C)$. δ is then given by

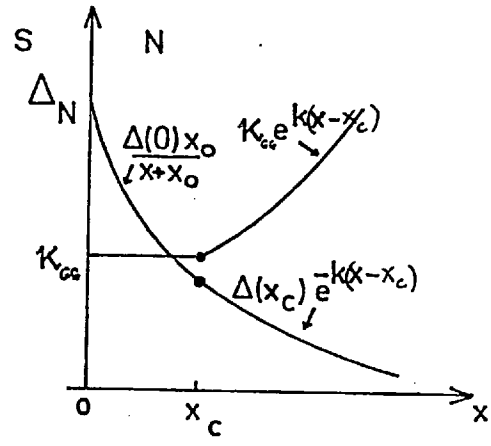

Figure 18(a) - The spatial variation of κ_N and $\Delta(X)$ in the Orsay model of 'saturation' (reproduced from ref.(64)).

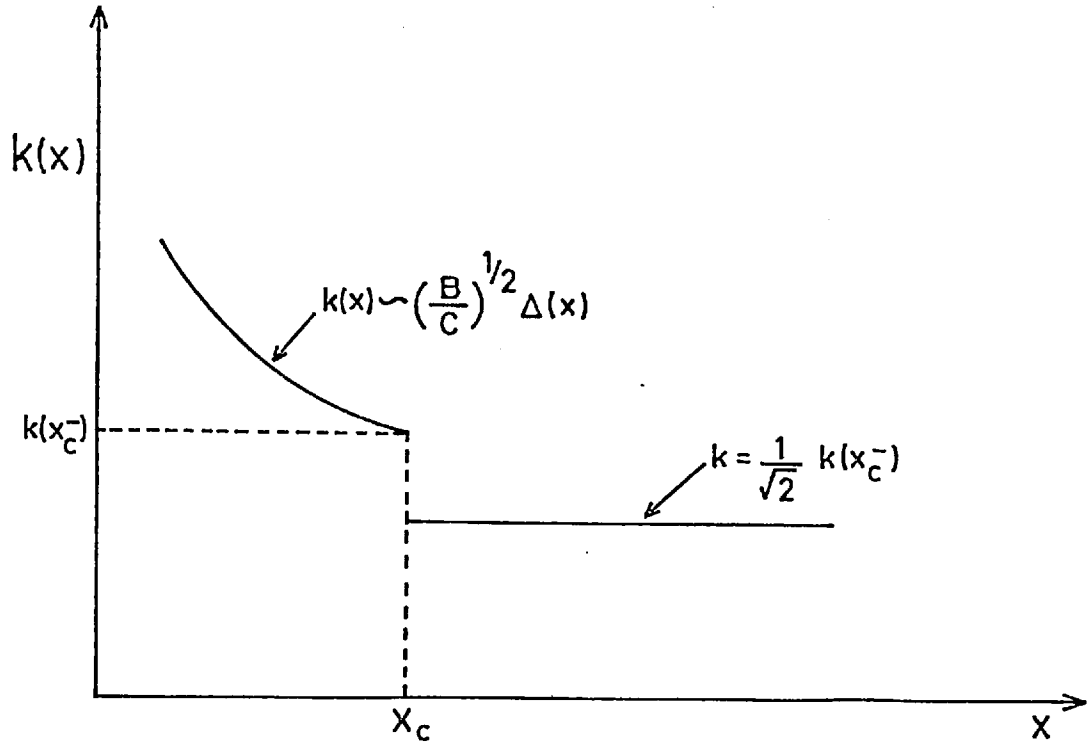

Figure (18(b) - The spatial variation of k(x) for the above model.

$$\delta = \frac{1}{k}\left[\ln\left(\frac{\exp k X_c}{K_{VGG}} \right) - 0.116 \right] \qquad \text{(II-84)(A)}$$

$$= X_c + \frac{1}{k}\left[\ln\left(\frac{1}{K_{VGG}} \right) - 0.116 \right] \qquad \text{(B)}$$

As Eqn. (B) above shows, the procedure is equivalent to taking $\delta = X_C + \delta_1$ and calculating δ_1 as if the interface had been at X_C.

Assuming the validity of Eqn. (II-84) the variation of $k\delta$ with temperature may be predicted from the knowledge of the temperature-dependence of $X_C = k^{-1} - X_o$. The procedure for evaluating $\frac{dX}{dT}C$ adopted by the authors which is now described is also shown to be open to criticism.

Valette (64) states that the use of the boundary condition (II-17), i.e. the continuity of $\frac{D\Delta'}{V}$ across the interface leads to

$$X_o = k^{-1} \qquad \text{(II-85)}$$

On closer examination we find that the condition (II-17) in the present case ($D_N = D_S$, $N_N = N_S$) leads to the result $X_o = b$, the extrapolation length. To obtain (II-85) one has then to suppose that $b = k^{-1}$, which we recall is only true in the Werthamer approximation i.e.when the temperature is close to the transition temperature T_{CNS} and $\Delta_N(X)$ decays exponentially <u>throughout</u> N i.e. $\Delta_N(X) = \Delta_N(0^+)\exp(-kX)$ (cf.§2.5, Eqn. II-22B). If, however, we take $b = k^{-1}$, then Eqns.(II-84 and II-85) lead to the result obtained by the Orsay Group, viz.

$$k\delta = \left[\ln\left(\frac{1}{K_{VGG}} \right) - 0.116 \right] = \text{Const.} \qquad \text{(II-86)}$$

From this they conclude that the quantity $k\delta$ (which for metals like Ag with very small V_N is proportional to $T^{\frac{1}{2}}\delta$) remains constant as a function of temperature for all $T < T_S$ where the 'saturation' temperature T_S is defined by the relation $\kappa_N(X = 0, T_S) = \kappa_{GG}$.

We note that the above argument implies that X_C remains equal to zero even when the temperature is lowered below T_S. In other words the 'saturation' region does not grow with a decrease in temperature which appears rather strange, at first sight. This result is a consequence of putting $X_0 = k^{-1}$, Eqn. (II-85). However, on examining the original definition of X_0, Eqn. (II-71) which gives $X_0 = \frac{1}{\Delta(0)}(\frac{2C}{B})^{\frac{1}{2}}$ one would expect all the quantities that define X_0 to be practically constant with respect to temperature. The coefficients B and C as defined in (II-33) are constant and well below T_{CS}, $\Delta_S(0)$ and hence $\Delta(0)$ (in N) are also temperature-independent. This leads to the result

$$\frac{dX_c}{dT} = \frac{d(k^{-1})}{dT} \qquad \text{(II-87)}$$

which implies that the slope of the curve $k\delta$ vs T does not become zero as T is lowered below T_S, even on the basis of the Orsay model. In fact, the slope would be predicted to change from $\sim -\frac{1}{T}$ for $T > T_S$ to $\sim -\frac{2}{T^{\frac{1}{2}}}$ for $T < T_S$. The contention that X_0 remains constant with respect to temperature and that the temperature variation of X_C is given by (II-87) is supported by Deutscher, Lindenfeld, Hsieh, Wolf (68). Indeed, they use Eqn. (II-87) to interpret their observation of 'saturation'

in Ag with the help of the Orsay model. Since they measured the thermal conductivities of N/S sandwiches, the detailed analysis of their results is different from ours and we shall not introduce it here for reasons of space. Their results will be discussed in Chapter VI.

(d) Discussion of the Orsay model

A close examination of the Orsay model raises several questions. The model uses the coefficients A, B and C (as evaluated at $T \lesssim T_{CN}$) to compute λ and k and it is therefore not surprising that κ turns out to equal κ_{GG}. What the model does not justify is firstly the use, at a temperature several orders of magnitude greater than T_c of these coefficients A, B, C. Secondly the G-L expression (II-80) for λ in terms of Δ only applies in a situation where Δ is spatially constant. In view of the above two points, it would appear more logical to evaluate κ from the directly calculable quantities λ and k. In fact, the G-L relations (II-80) and (II-73) are, in practice, used to evaluate experimentally the coefficients C and A (4) in terms of the directly measurable λ and k. It is not difficult to determine how the values of the coefficients so defined compare with those used, in the model. C, for instance would be given by

$$C = \frac{\hbar v_F l N(0)}{12\pi k_B T} \psi_2(1/2 \pm 1/2 k^2 q_0^{-2}) \qquad \text{(II-88)}$$

Eqn. (II-88) has been obtained by comparison between the G-L equation

$$j = -\frac{8e^2 C \Delta^2}{c\hbar^2} A(r) \qquad \text{(II-89)}$$

and the corresponding relations (II-27/8) derived by Maki. As expected, we recover from (II-88) the value of C as given by (II-33) when we use the fact that $k/q_o \to 0$ as $T \to T_C$ and that $\psi_2(\frac{1}{2}) = \pi^2/2$. However, for temperatures of interest in the present context $T_{CN}/T \sim 10^{-5}$ for which (II-44) yields $k/q_o \simeq 0.92$ and $\psi_2(\frac{1}{2} - k^2/2q_o^2) \simeq 170$. Then C as given by (II-88) will be smaller than its value at T_C by a factor of $\sim 25 \times 10^2$. In other words λ (which is proportional to $C^{-\frac{1}{2}}$) as calculated by Maki's expression will be ~ 50 times larger than that computed in this model, if Δ remained the same. For a normal metal with NV ~ 0.1, $T_{CN} \sim 10^{-5}$ and $\sigma^{-1} \sim 1\mu\Omega cm$, Maki's expression yields the value of ~300 Å for λ at 2^oK which is of the right order of magnitude. It would therefore appear that calculating λ from Maki's expression, k from (II-44) and using these to define κ is a more reliable procedure than the one adopted in this model.

The Orsay model also appears to lack internal consistency. Consider the coherence length as defined by (II-73 and 77) for the regions $X < X_C$ and $X > X_C$ respectively. In fig. 18(b) we have plotted k(X) vs X. There is a discontinuity (by a factor of $\frac{1}{\sqrt{2}}$) in the value of k at X_C. But $\Delta(X)$ is continuous and it therefore follows, in view of our comments in the last paragraph that λ as calculated by the usual prescription in the 'non-saturation' region is discontinuous by a factor of ~50 at X_C. This makes the continuity of κ_N at $X = X_C$ impossible. In fact, for the continuity of κ to be maintained one has to have $\lambda(X_C^+) = \sqrt{2}\ \lambda(X_C^-)$.

Finally, we examine one of the stated hypotheses of the model which does not appear to have been used in the derivation

of any of the results except by implication. This is that κ_N has a lower limit of κ_{GG} below which it cannot decrease. To start with, we establish a relation between κ_N and κ_{GG} as defined for $T > T_c$ and $T \lesssim T_c$ respectively. The theory so far outlined provides a unified description of superconductivity in the two temperature regions below and above T_c with $\Delta(X)$ being given by

$$\Delta(X) = \sum_n A_n \exp(ik_n X) \tag{II-90}$$

where k_n are the roots of

$$\ln\left(\frac{T}{T_c}\right) = \psi(1/2) - \psi(1/2 + 1/2 k_n^2 q_o^{-2}) \tag{II-91}$$

For $T > T_c$ there exist an infinite number of imaginary roots k_n whereas for $T < T_c$, there is only one pair of real roots $\pm k_s$. It is easy to show that if the mathematical definition of κ_{GL} was carried over to $T > T_c$, the resulting 'kappa' would be an imaginary quantity equal to $i\kappa_N$. Therefore the temperature variation of a 'kappa' (call it κ_A) that is defined in the same way both above and below T_c (see II-93 below) is as follows: as T is lowered from well above T_c, the <u>modulus</u> of κ_A decreases, κ_A remaining imaginary until T_c is reached. Using Maki's Eqn. (II-28) for λ and solving (II-91) for $T \sim T_c$, we obtain the following relations

$$k^{-1} = \left[\frac{\pi \hbar v_F \ell}{24 k_B T_c} \frac{T_c}{T_c - T}\right]^{1/2} \tag{II-92}$$

$$\kappa_{rA} = \frac{3ck_B T_c}{e\pi v_F \ell}\left(\frac{2}{\pi N(0)}\right)^{1/2}\frac{1}{\Delta} \times \left[\frac{T_c - T}{T_c}\right]^{1/2} = \kappa_{rGG} \times \frac{\pi k_B T_c}{\Delta}\left[\frac{T_c - T}{T_c}\right]^{1/2} \tag{II-93}$$

According to the above, the modulus of κ_A decreases to zero as T is lowered to T_C. κ_{GG} is the temperature independent real limit that κ_A approaches when the metal itself turns superconducting as T is lowered below T_C and an energy gap $\Delta(\simeq 3.2\ k_B\ T_C(\frac{T_C-T}{T_C})^{\frac{1}{2}})$ is produced within the material rather than induced externally by proximity. Why should this limiting value of κ_A (which is a result of the form of Δ just below T_C) have any special significance as far as the modulus of κ_A above T_C is concerned, is far from obvious.

Fig. 10 shows the Orsay Group's results of screening distance measurements in Pb/Ag. In view of our observations regarding the Orsay model itself and regarding the calculation from it of the slope of $T^{\frac{1}{2}}\delta$ vs T, the agreement between theory and experiment is somewhat surprising and, in our view, calls for some alternative explanation.

CHAPTER III

SPECIMEN PREPARATION

In this chapter we describe the preparation of the specimen films and of the alloy pellets from which the films were made by vacuum evaporation. The evaporation procedure is dealt with in some detail and practical considerations determining the order of evaporation of N and S materials are discussed. Film trimming and the thickness measurement technique are also described. We begin by considering the criteria that dictate the choice of materials in the preparation of the superimposed metal films.

3.1 Choice of Materials

In all the double layer systems studied in this series of experiments, high purity lead formed the S material. The N metal variously consisted of Ag, Ag Aℓ alloys of composition ranging from 0.25 to 1.5 at %, very dilute Ag Mn alloys, Zn, Cd and a Cd Mg alloy. The choice of materials was primarily governed by the need to minimise the deletereous effects due to alloying or compound formation between the N and S materials in the vicinity of the interface. This imposes the rather stringent requirement that the two metals should not form any intermetallic compounds and should ideally have zero (or very low) mutual solid solubility. None of the above N materials forms an intermetallic with Pb with which they all have very low mutual solubility. Typical values are (106)

Ag in Pb ~ 0.04 at. % at 100°C

Pb in Ag ~ 0.35 at. % at 250°C

Pb in Zn $<$ 6×10^{-5} at .%

Mg in Pb $\sim$ 3.0 at .% at 250°C (least favourable)

The other considerations in the above choice of materials were -

(a) the high transition temperature of Pb (7.2° K), which is desirable for our experiments, and

(b) their capability of being deposited by vacuum evaporation.

3.2 The Evaporator

Fig. 20 shows the plan of the evaporator. The evacuation was by means of a 4 in. oil diffusion pump (C.V.C. type PMC-4B) with a nominal pumping speed of 690 litres/sec.. This, no doubt, was considerably reduced at the chamber itself because of the impedance due to interconnecting gate valve and chevron baffle liquid nitrogen trap. The backing line and chamber pressures were measured using Pirani and Ionisation gauges respectively which were connected to a "Speedivac" control unit (model 1).

The stainless steel base-plate of the vacuum chamber had three sets of electrodes for the joule heating of evaporation sources (fig. 20). Externally, the electrodes were connected to low tension power supplies. The base plate also had insulated electrical inputs, used for a film thickness monitor, and two mechanical inputs, one for operating the pellet dropper and the other for positioning an aluminium screen. The screen was only a few millimetres away from the substrates and it could be manoeuvred in the course of evaporation of NS double layers so as to obtain separate N and S strips as well.

The pellet dropper consisted of two 3 in. dia. aluminium discs, held horizontally one on top of the other. The lower one was fixed rigidly to the base-plate while the top disc which had about 150 small holes drilled around its periphery (fig. 20) could be rotated from outside. This enabled pellets to be dropped, one at a time, into a quartz shute which led to a boat.

Separate boats, made from 0.005 in thick Mo sheet, were used for Pb(S) and the alloy (N). A tungsten wire heater was connected to the third set of electrodes. It was positioned so as to be ~4 cm below the horizontally held substrates but not in the direct path from either boat to the substrates.

3.3 Substrate Cleaning Procedure

The films were evaporated onto room temperature substrates which were soda lime glass microscope coverslips (20 x 8 mm). These were always freshly cleaned and a standardised cleaning procedure was adopted as part of an effort to maintain as far as possible, a uniformity of the entire preparation procedure for all the specimens. The substrates were cleaned

(1) in a dilute solution of "Decon" (a commercial detergent) in an ultrasonic bath for about one hour, followed by

(2) immersion in conc.nitric acid for several minutes and finally by

(3) immersion in hydrogen peroxide.

Each of the above steps was followed by a rinse in de-ionised water. The coverslips were dried in a jet of N_2 gas before being mounted on the substrate holder.

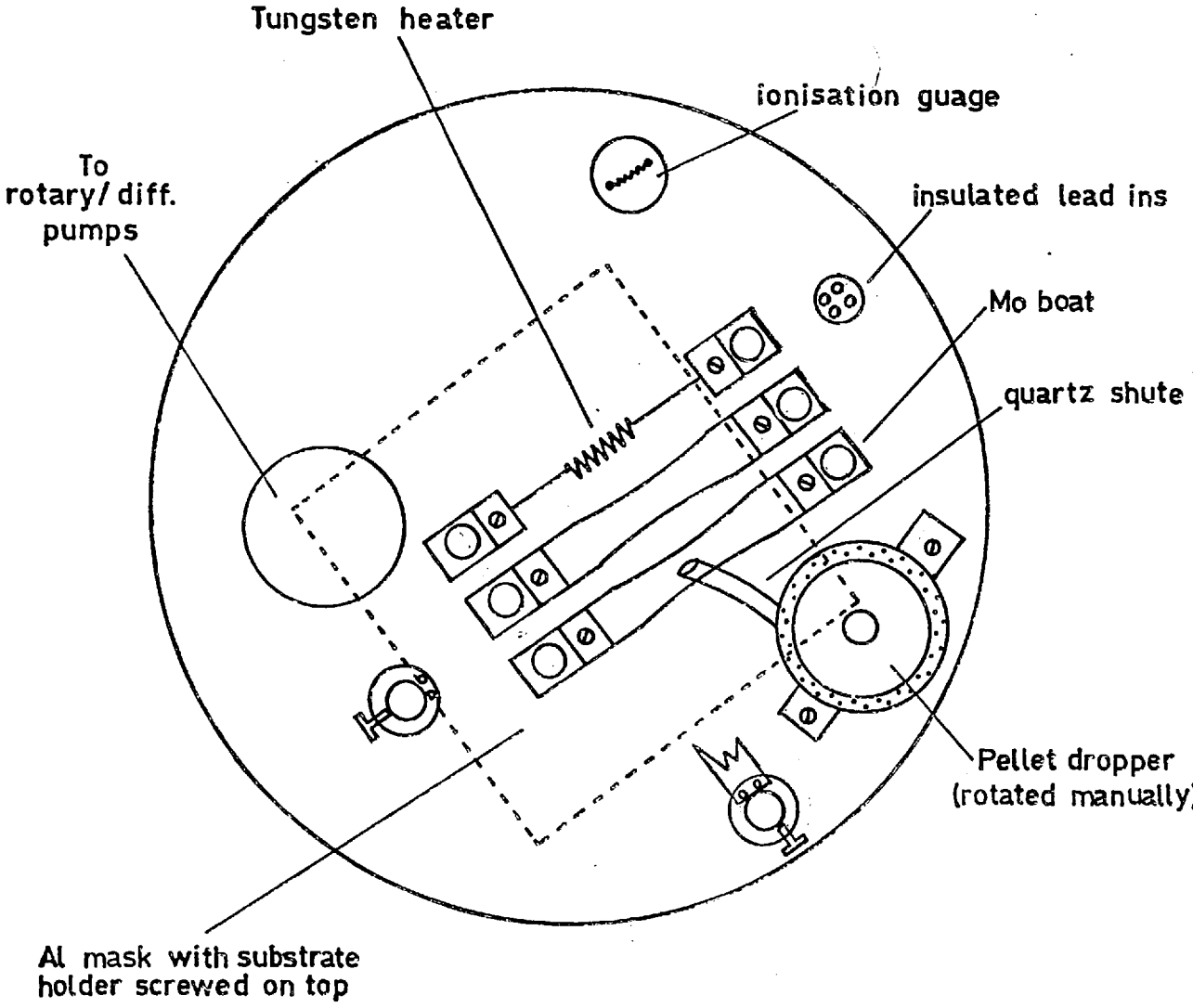

Figure 20 - Plan of the evaporator.

3.4 Film Geometry and Trimming

The coverslips fitted into milled depressions in the aluminium block that formed the substrate holder. Onto this was screwed a close-fitting mask made from an aluminium sheet. This enabled rectangular strips (6.2 x 18 mm) to be deposited on each substrate. Penumbra effects could not be eliminated by this simple technique. However, the need to trim the film edges all-round had been envisaged from the onset. This followed from the observation by Hinde (79) who found evidence for thickness gradients near the film edges of Pb based alloys in spite of using a stainless steel mask specially lapped to attain a high degree of flatness. This effect is thought to arise from the high surface mobility of Pb atoms (80).

The film edges were trimmed by means of a stainless steel surgical blade held in a fixed position and pressed down onto the film by means of a phosphor-bronze spring. The coverslip which for this operation was stuck on a microscope slide by an adhesive (Durofix), was then moved along the cutting edge by means of a microscope cross-slide. A vernier scale on the cross-slide enabled the dimensions of the film and the substrate to be measured.

All except six specimens had the N layer next to the glass and for all these, it was found that after trimming, the edge strips (~ ½mm. wide) peeled off rather neatly. Only very near the edges where the films were thinning out did portions remain stuck to the glass and had to be scrapped off with a blade. The adhesion of these 4 to 5 micron thick films to the

substrates was, however, good enough to withstand numerous recyclings between 4° K and room temperature. For the specimens where Pb was put down first, strong adhesion to glass was observed and the edges had to be scrapped off after trimming.

3.5 Preparation of Alloys

The alloys used in these experiments were very dilute Ag Mn (~ 50 to 200 ppm) Ag Aℓ (~ 0.25 to 1.5 at .%), Ag Aℓ Mn (0.6 at .% Aℓ, 100ppm Mn) and Cd Mg (~ 2 at .%). The nominal purity of materials used was as follows:

Ag 5N (supplied by Koch-Light Lab. Ltd.)

Zn 6N (K-L)

Mn 4N5+ (K-L)

Mg 3N8 (K-L)

Aℓ 5N (K-L)

Cd Spectrographically pure (Johnson Matthey)

The dilute Ag Mn alloys were prepared in an arc furnace starting from a 1% master alloy. The Ag Aℓ alloys, on the other hand were made by melting appropriate weights of the metals in evacuated (~ 2×10^{-5} torr), sealed quartz tubes in a vertical furnace. This allowed mechanical mixing of the metals, by shaking the tube. This procedure had also to be used for the Cd Mg alloy on account of the fact that both metals sublime.

The following etching reagents were used for removing any surface contamination from the metals before and after alloy preparation.

For Ag: A mixture of H_2 O_2 and NH_4 OH in equal parts by volume.

Cd, Mg, Zn: Dil. HCℓ (cold/warm)

Aℓ: Conc. NaOH solution

Mn: Conc. HNO_3

3.5 Preparation of Pellets

Special care was taken when handling the alloys not to introduce any ferromagnetic contamination as this would have a drastic influence on the proximity effect. Copper-Beryllium tools were used at all times. Pellets were prepared by first rolling the alloys into ~ 1 mm dia. wire which was then chopped up into bits ~ 3 mm long. To avoid any iron contamination from the steel rolling mill, the alloys were rolled with a 0.005" thick Cu sheet wrapped round them which was subsequently peeled off.

3.6 Necessity for Use of Pellets

For a quantitative study of the screening distance δ (which is directly dependent upon the mean free path ℓ) the homogeneity of alloy films is of paramount importance. However, it has been shown by Holland (81) that neither Ag Aℓ nor Ag Mn is an ideal "constant evaporation rate" alloy, that is, one in which there is no tendency for the composition of the vapour phase to be different from that of the base material due to different volatility of the constituent metals. Moreover, for the large thicknesses of film required for our investigation, 1.5 to 2 g of an alloy would have to be evaporated. If an attempt were made to evaporate the whole mass at once from a small boat, the resulting slow rate of evaporation would further encourage the separation of the constituents. The possibility

of homogenising the films by high temperature annealing subsequent to deposition is ruled out by the need to prevent or, at any rate, minimise interdiffusion at the NS boundary.

The above considerations limit one's options to the two main techniques for vacuum evaporation of alloys. These are (a) simultaneous condensation of the constituents from separate sources (b) the flash evaporation of small particles from a preheated source. We have used technique (b) which is the more convenient one from the experimental point of view. However, instead of very fine alloy particles, we used pellets of up to 40 mg. which took between 3 to 5 secs. to evaporate. This method has been used quite successfully for alloys the vapour pressures of whose constituents are not vastly different (81) which is the case with Ag Aℓ and Ag Mn alloys.

Not surprisingly however, the technique did not work for a Zn Ag (3 at .%) alloy that we tried to evaporate. The vapour pressure data for the two metals is:

Zn v.p. = 10 microns Hg at 343° C

Ag v.p. = 10 microns Hg at 1047° C

The evaporation of the alloy pellets could be seen to proceed in distinct stages. Zn which does not wet Mo evaporated instantly leaving behind tiny beads of Ag sticking to the boat. The attempt to study Zn alloys was abandoned as no metal could simultaneously satisfy the three requirements of solubility in Zn, a vapour pressure of comparable magnitude and very low solubility in Pb.

The problem of the repulsion of the pellets by the heated boat was also encountered to varying degrees for all alloys.

This resulted in the pellets 'jumping' out of the boat upon arrival. It could, however, be overcome by adapting the boat shape and positioning the shute correctly.

3.7 Evaporation Procedure

After setting up the evaporator and accessories, the chamber was flushed out with dry nitrogen before being pumped down with the diffusion pump for at least 5 to 6 hours. During this time the Pb charge was outgassed by melting and the empty boat for the evaporation of the alloy was also heated up to around its final operating temperature. The tungsten wire heater was switched on for about an hour during the pump down. Its primary function was to heat the substrates to ~ 150° C to expel any remaining traces of moisture. The substrates were allowed to cool for about half an hour before beginning the evaporation.

Evaporation was begun at pressures of ~ 5×10^{-6} torr which rose typically to around 3×10^{-5} torr during the Pb or Ag evaporation and to ~ 10^{-4} torr during that of Zn and Cd. For all except one Pb/Ag specimen, the N film was evaporated first (Zn and Cd are discussed in §3.9). Large pellets of ~ 40 mg (≡ 400 Å Ag) were used to put down all but ~ 3000 Å near the interface for which smaller pellets of ~ 15 mg were used. The large pellets took on an average ~ 5 sec. to evaporate. A pellet was allowed to evaporate to completion before dropping another. During the normal metal evaporation the Pb was kept just below its melting point so as to minimise the interval between the N and S metal evaporations. On average, this interval was kept down to ~ 15 secs. The mean rate of deposition

of Pb was ~ 150 Å/sec.. The thickness d_S of the Pb film was about 2μ while d_N varied from ~ 1 to 3μ for Ag alloys and over 3 microns for Zn and Cd. The measured thicknesses for all specimens are listed in Table VI-1. Normally four NS specimens and two strips each of N and S were prepared at a time.

A thickness monitor crystal was used during evaporations. However, it was found to overload and stop oscillating for film thicknesses $\gtrsim$ 2.5μ even after the aperture was reduced to a quarter of the size recommended for a linear variation of frequency with thickness of deposition. It could not therefore be reliably used for thickness measurement but served as a useful estimate of initial evaporation rates. A sensitive film thickness control during evaporation was not necessary for our experiments. Thicknesses to the required degree of accuracy, i.e. to within ~ 3000 Å to 5000 Å were satisfactorily obtained from an empirical relationship with the evaporant mass. For the Pb films, a pre-weighed Pb charge was evaporated to completion whereas the mass of the N alloy evaporated was estimated from the number of pellets.

Once deposited, however, the thickness d_S of the Pb film of each specimen had to be known accurately for calibration purposes. Measurement of the electrical resistance of the films was used to determine d_S.

3.8 Film Thickness Measurement

The film strips prepared for resistance measurements were cut in the shape shown in fig. 21a on the film trimming device and their resistance determined using a four-terminal technique.

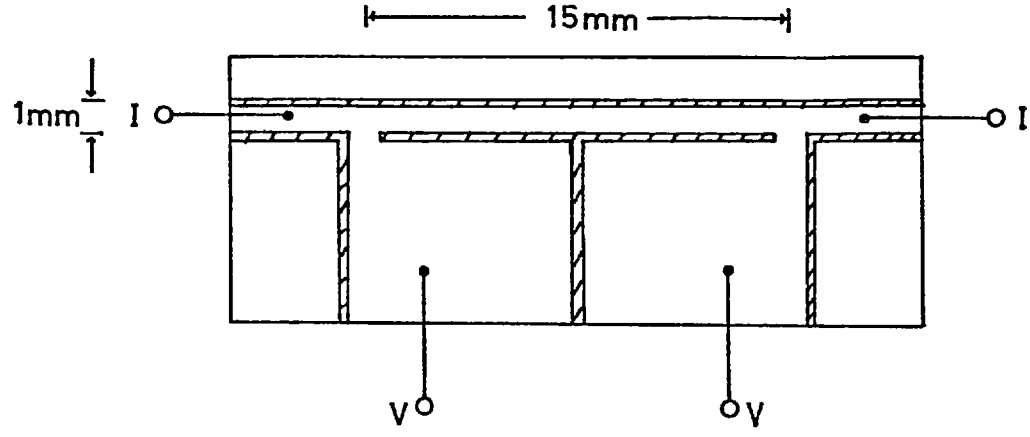

Figure 21(a) - Geometry of film section cut out for resistance measurement.

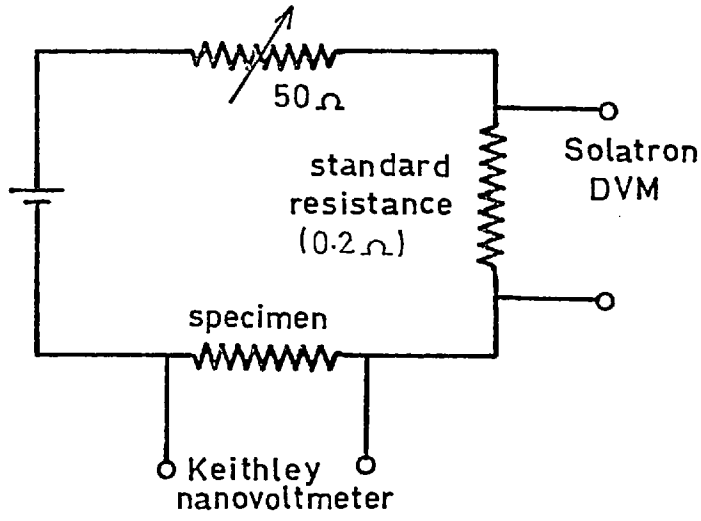

Figure 21(b) - Circuit used for film resistance measurement.

The dimensions of the strips (nominally 15 x 1 mm) could be measured on the Vernier scale to 0.1 mm. When greater accuracy was required the width of a strip was measured on a travelling microscope at two or three points along its length. 50 s.w.g. copper leads were connected to the film at points I, V as shown on the diagram by means of conducting silver paint. The free ends of the leads were soldered on to electrical pins held firmly in a tufnol block.

The thicknesses were calculated from measured room-temperature resistance, using bulk resistivity of Pb.

The basic underlying assumption in the use of electrical methods for thickness measurement is that the film has the same electrical properties as the bulk. Consequently, factors like the grain structure, crystalline state including crystal orientations and the film thickness all have an important bearing on the accuracy of the result. Ittner (82) has analysed this method in detail and concludes that in a favourable case, the electrical methods are actually to be preferred to optical ones for applications to superconductivity. A favourable case in this context is one where (1) the film obeys Matthiessen's rule so that its room temperature resistivity is the sum of a temperature-dependent lattice contribution ρ_L and temperature-independent residual contributions. These latter would include ρ_i arising from impurity and defect scattering and ρ_S from surface scattering, important in thin films. Strictly, ρ_S depends on the m.f.p. and hence on the temperature according to Fuch's (83) theory but both ρ_S and $\frac{d\rho}{dT}S$ are very small except when $d \lesssim \ell$. (2) ρ_L in the film is the same as the lattice contribution in

the bulk material.

As noted by several investigators (e.g.ref.84, 85)Pb evaporates compactly onto room temperature glass substrates, giving an even, polycrystalline deposit of low defect density. This is shown by the high resistance ratios (> 100, corresponding to ℓ > 1 micron at liquid He temperatures) they observe for a few microns thick Pb films, as indeed do we. In fact, in the course of an investigation into the magnetic transitions in Pb films and foils as a function of thickness, Cody and Miller (86) found that Pb film thicknesses determined by the electrical method agreed well with the optical measurements, for thick films like ours, $d_S \gtrsim 1$ micron. Freake (32) has made a similar observation for somewhat thinner films.

We also determined the thicknesses of three of the Pb films by surface density (mass/unit area) measurement. For this, carefully degreased and dried substrates were weighed on a microbalance both before and after dissolving away the films in conc. HNO_3. The results are shown below:

Sp. No.	d_S electrical (μ)	d_S from weight (μ)
10	1.63	1.57
11	1.77	1.92
13	2.13	2.28

The error in each individual determination of d_S above was ~ 5%. However, the measurements by the two techniques were done on films on separate substrates. Considering that the substrate holder was ~ 4 cm. sq. and that it was held ~ 20 cm. from the boats during evaporation, a simple calculation (81)

shows that thickness variations of ~ 2% over the length of a substrate and of ~ 10% between substrates held 4 cm. apart can be expected. Therefore, the above results represent good agreement between the two techniques.

All the above evidence suggests that the use of the electricalmethod for Pb thickness measurements is well justified.

The thicknesses of the N films, some of which consisted of alloys, were determined from the film resistance at room temperature and at 4.2°K. Application of Matthiessen's rule and assuming the lattice contribution to the resistivity of dilute alloy films to be the same as in the pure bulk metal enabled the residual resistivity and also the film thickness d_N to be determined.

However, as long as the necessary requirement for screening distance measurements, namely, that the N films be in the thick limit (i.e. $d_N >> \delta$) is satisfied, their exact thicknesses are of no quantitative significance to the analysis of our data. To this extent the electrical method is quite satisfactory also for determining d_N.

3.9 Order of Evaporation

In most previous measurements of the screening distance (58, 59, 63), films deposited on cylindrical formers were used. The cylindrical S films shielded the interior from any applied fields. For a proximity study involving applied fields (d.c/r.f) therefore, the N film necessarily had to be on the outside. In other words, it had to be deposited after the S material. It is well known that the nucleation and crystallisation of metal

films is dependent upon the nature of the substrate and therefore the N film of an NS specimen prepared in this way is likely to be different from the test N strip. Valette (64), for instance, attributes to this effect his observation of systematically higher resistristies of Cu films deposited on Pb as compared to those on glass.

It will be remembered that ℓ, the electron m.f.p. in N, is a very important parameter in the theory. An indirect determination of it is possible from a measurement on the separate N strip. So as to have both the test N strip and the specimen N layer crystallise on identical surfaces, it was considered preferable to deposit the N films first. However, this order of deposition could not always be followed (see Zn, Cd systems below).

Ag/Pb

Additional advantages resulting from the above order of evaporation for the Ag/Pb specimens include the fact that thick Ag films, in contrast to Pb films, had optically smooth (shiny) surfaces. Evaporating the Ag film first would thus result into a smooth interface boundary. Again because of the comparative ease with which Pb oxidises, the likelihood of oxide barrier formation at the interface would be enhanced if the Pb were deposited first.

In a control experiment, a specimen of Pb/Ag was also prepared with the order of evaporation reversed. The results are presented in Chapter VI.

Zn/Pb and Cd/Pb

As Holland (81) observes, the very low melting points of Zn and Cd and the extremely weak adhesive forces between the vapour atoms and room-temperature glass substrates, necessitate very high vapour intensities in order to initiate nucleation. This results in a high degree of vapour scattering by inter-atomic collisions and re-evaporation from the walls of the vacuum chamber. On the two occasions that we evaporated Cd first, it was found to be impossible to prevent the contamination of the Pb source. This was shown up by the resistance ratios of the test Pb strips being more than an order of magnitude lower than the average value of ~ 200 and the critical fields about 30% higher than for pure Pb. After an evaporation of Zn or Cd, every accessible part of the chamber, regardless of whether or not in 'direct' geometric path of the source, would be found covered in a film of the material. For this reason, the Pb was deposited first for subsequent specimens. It has been observed (40) that the nucleation of these metals is facilitated by pre-coating the substrate with a 'base' film and that this results in a less granular texture. We certainly found this to be the case. The separate Zn strips showed a much coarser grain than the double layers under an optical microscope. The Cd strips too had slightly dull, matt surfaces indicative of agglomerated growth but were much less granular than the Zn strips.

3.10 Storage of Specimens

On average, it took less than four days to complete all the measurements on a specimen, including all the auxiliary

resistance measurements. In some cases, specimens were re-measured over periods of up to three weeks, primarily to study if their properties changed with time. Throughout this period, the specimens were stored in a dessicator in an atmosphere of N_2.

CHAPTER IV

APPARATUS

4.1 Introduction

The technique employed for measuring the screening distance is the one due to Schawlow and Devlin (65) who originally used it for measuring the penetration depth of superconductors. It is an a.c. technique and basically involves the measurement of changes produced in the inductance of the coil of a parallel-tuned oscillator circuit by monitoring its resonance frequency. The coil contains the superconducting specimen and the inductance changes may be brought about by varying the temperature or, as in our case, the applied field. An inherent practical limitation to achieving high sensitivity in the original technique arose from the use of a valve oscillator with the 'active' circuit necessarily at room temperature and connected to the specimen coil by a co-axial lead running down the cryostat, the lead thus forming a part of the 'tank' circuit. This problem can however be avoided by the use of oscillators with low-power solid state components for the active circuit, capable of performing at liquid helium temperatures. Both tunnel-diode and MOSFET oscillators have been used successfully and we have used a version of the former first reported in the literature by Boghosian et al. (87).

A detailed description of our apparatus including the back-diode oscillator (BDO) is given in the sections that follow.

4.2 The Cryostat

A two glass-dewar, Helium^4 cryostat of conventional design was used. Details of cryostat construction, precooling and transfer procedure have been given by Wipf (88) and we simply mention that with the cryostat insert in position, the helium dewar held about one litre of the liquid. When the specimen heater was not used, this lasted for about 4½ hours. However, the heater had to be used after every sweep of the field to drive out trapped flux (see §5.3). Then, in the course of a normal run it was found necessary to transfer more liquid in order to cover the whole of the temperature range attainable with our equipment viz., 4.2°K to 1.45°K.

4.3 Temperature Control and Measurement

The temperature of the helium bath was lowered by pumping on the helium vapour. A rubber diaphragm manostat (88) was used to set the temperatures and hold them constant to within a few millidegrees over periods of up to 30 minutes.

The temperature of the bath was determined from the helium vapour pressure using the 1958 He^4 temperature scale (89). The pressure was measured using a vertically mounted mercury manometer, made of 10 mm. bore glass tubing, with an attached steel scale standard at 20°C. For helium pressures below 40 mm. of Hg a similar oil manometer with an attached glass scale was used. Mirror strips fixed behind the manometer tubes helped eliminate parallax errors when the column heights were read.

The 1958 He^4 temperature scale is tabulated in terms of pressure measured in height of Hg at 0°C and standard gravity.

Errors that arise when directly measured (uncorrected) pressure values are used can be shown to be generally small. The required temperature correction to Hg density is of order 0.4% and the gravitational acceleration one ~0.05%; the former figure corresponds to a correction of ~ 0.15 mm. to the height of the Hg column at the λ point and is then of the order of accuracy to which the scale is read, which is ± 0.2 mm. (corresponding to ± 2 mK at 2°K). The correction due to the hydrostatic head of the liquid can be much bigger and just above the λ point a 10 cm. height of the liquid necessitates a correction of 10 mK. When using the oil side of the manometer frequent checks were made against a glow discharge to ensure that the vacuum in the reference arm was satisfactory (< .05 mm. Hg) as even the smallest leaks would be capable of producing large errors at low temperatures.

After making the necessary corrections the maximum error in the temperature of the bath is estimated to be ± 5 mK at 1.5°K.

4.4 Cryostat Insert

The cryostat insert consisted of a 0.5 inch diameter stainless steel tube soldered to a brass flange at one end and to an exchange gas can at the other. The can (fig. 22), o.d. 1.5", was made of duralumin and had a stainless steel (s/s) top plate sealed to it by 'Loctite'. This top plate was soldered to the s/s tube with a cadmium-zinc solder. A demountable copper base plate was fitted to the can by a cone joint arrangement. The joint was made by applying silicone vacuum grease to both the surfaces, and heating them with a hot air blower after assembly.

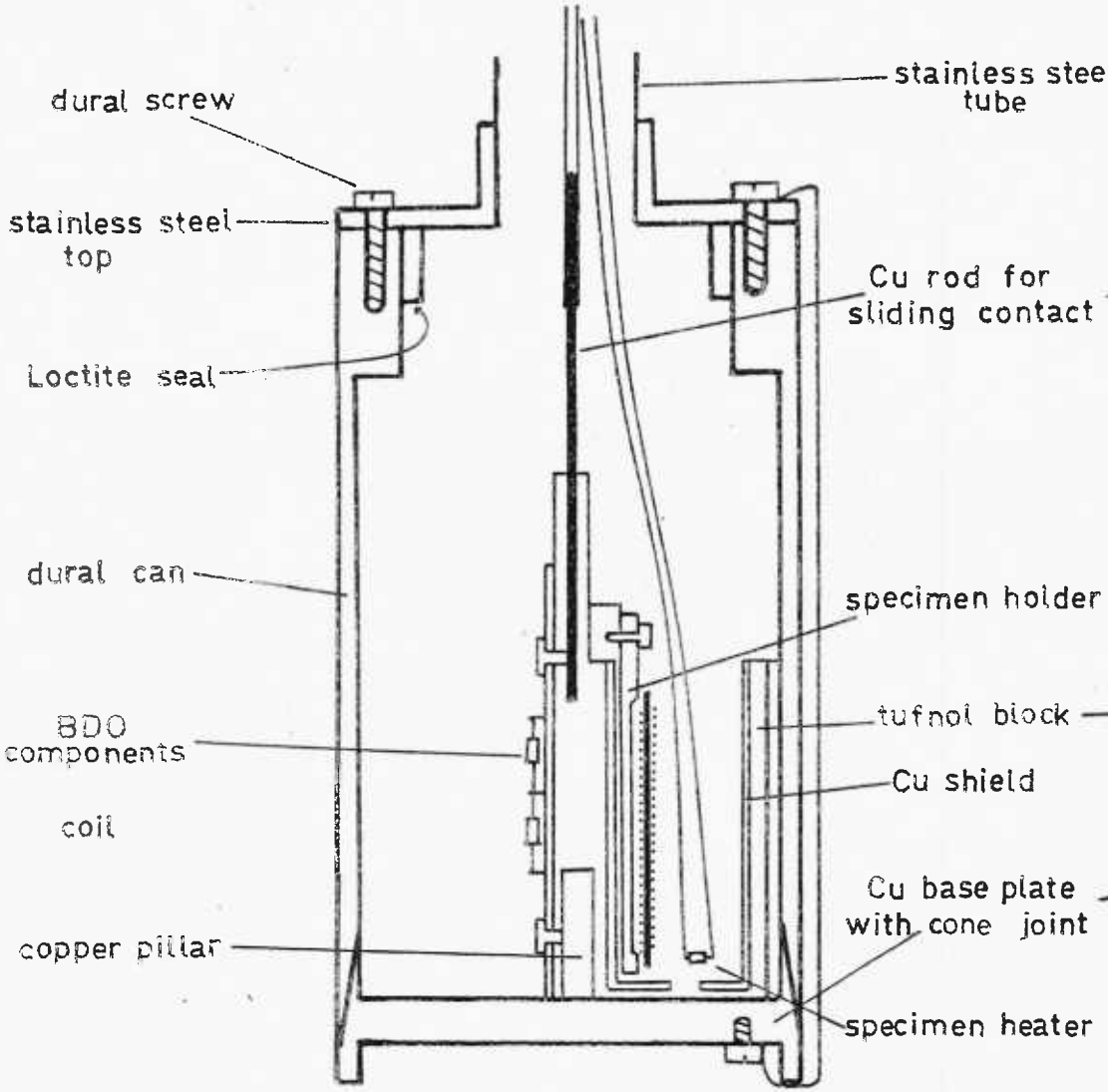

Figure 22(a) - Cross section of the exchange gas chamber and its contents

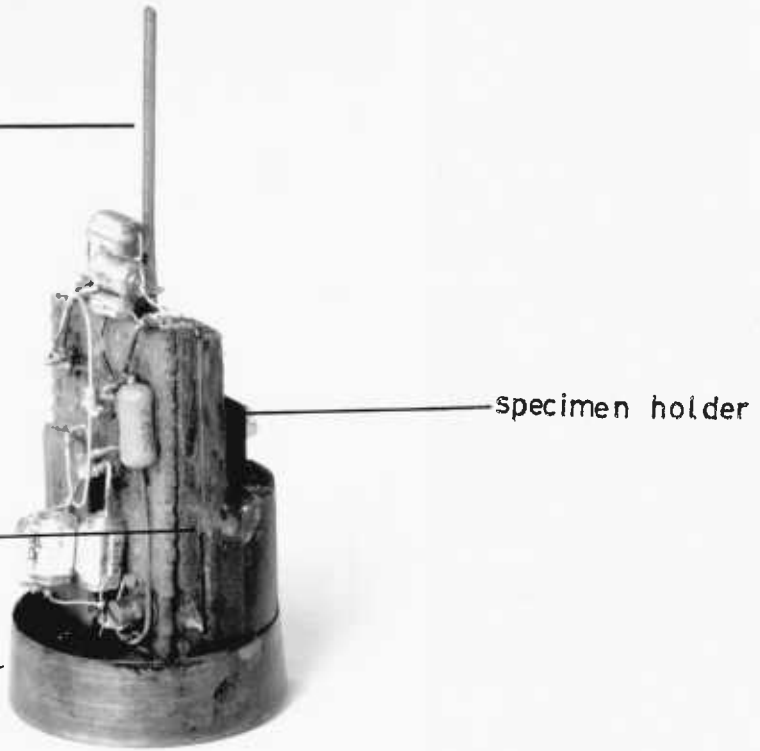

Figure 22(b) - Base plate of exchange chamber supporting the tufnol block with BDO components and specimen holder.

The can was then evacuated so that atmospheric pressure would force the surfaces together. The pressure gauge connected at the top of the insert, (fig. 23) indicated if the joint was leak-tight. Normally, the same gas pressure was maintained both inside and outside the can during a run and this always gave liquid helium tight joints above the λ point but leaks sometimes appeared below this temperature. This, however, was no great handicap from our point of view for reasons explained in §4.5.

The base plate also held four 40 s.w.g. insulated copper wires each leading out from the can through a 0.5 mm. dia. hole and sealed with epoxy resin. These were not normally used and had been installed to study a field alignment technique involving the maximising of film critical current (see §5.4 and fig. 34).

A 22 gauge copper wire, screwed at one end to the base plate and at the other to the top plate of the can, served as an electrical connector and a safety precaution against damage to the dewar in the event of the base coming off. This could happen if the pressure inside the can was allowed to rise well above that outside.

Down the length of the $\frac{1}{2}$ inch tube ran another thin-walled stainless steel tube, o.d. 0.06", held centrally by means of tufnol spacers, the two tubes thus forming a co-axial lead. At its lower end, a one inch length of the inner tube projected into the can (fig. 22(a)), while at the top, it was connected to a hermetically sealed 'n' socket (UG 58A/U) screwed onto the flange. A vacuum tight demountable joint was obtained with the use of 'O' rings as shown in fig. 23. Two 37 s.w.g. copper

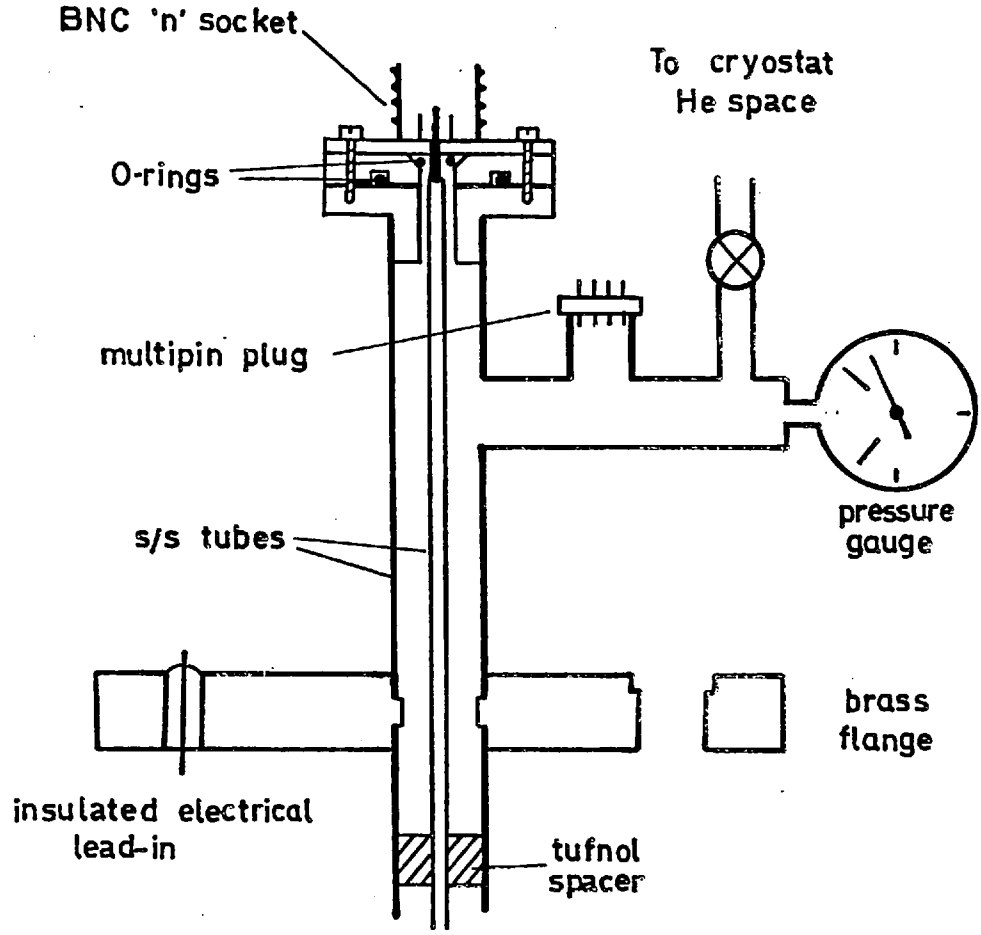

Figure 23 - Top of the cryostat insert

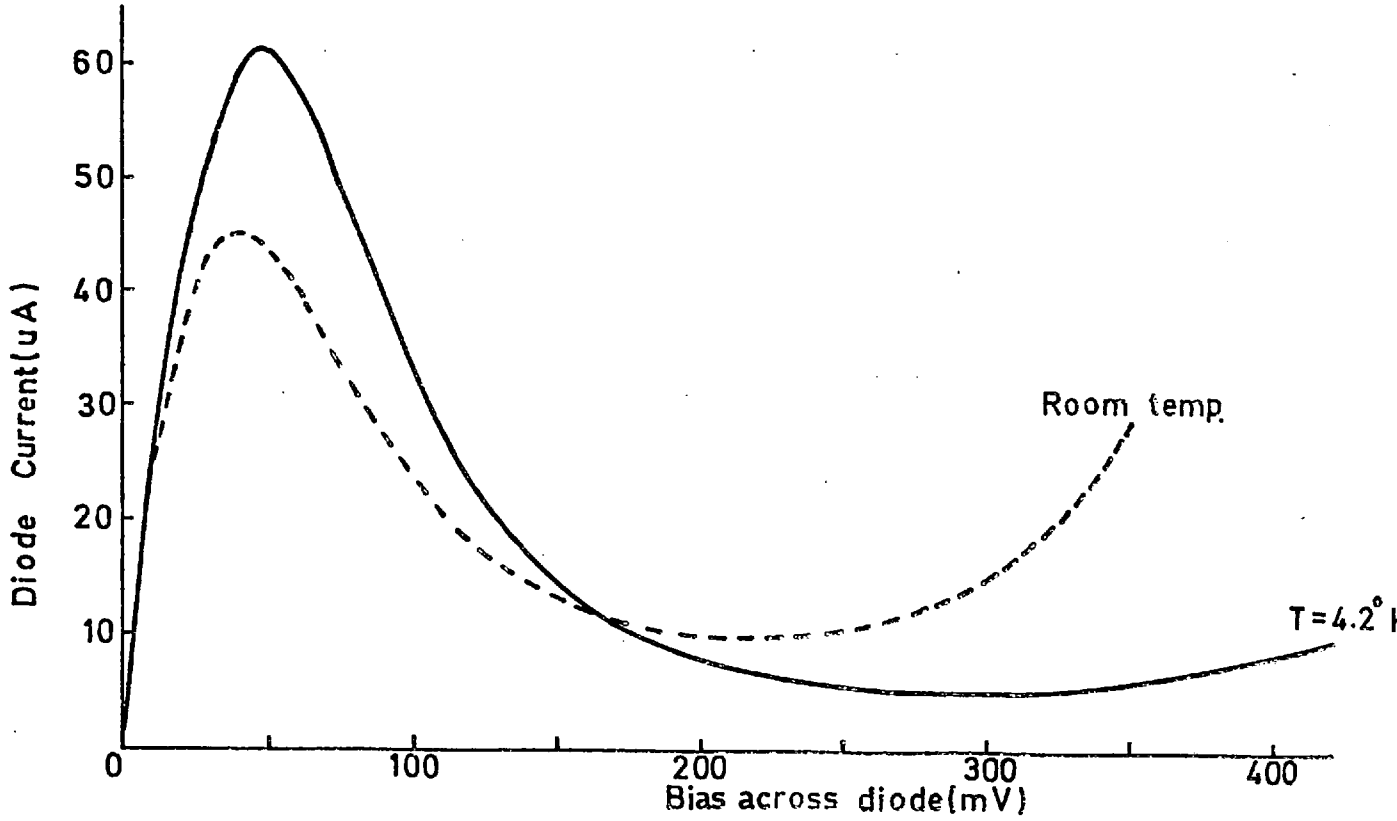

Figure 25 - The d.c. characteristics of the back diode (GE-BD-4).

wires for the heater were led from a sealed multipin connector, down the outer stainless steel tube, into the can.

Two copper pillars, 0.1" dia., 0.5" long, soldered to the base plate acted as supports for a semicylindrical tufnol block. The BDO circuit elements were located on an 'electrokit' pin board attached to the flat side of the block (fig. 22(b)). A 0.5" dia. hole was drilled vertically into the block and contained a close fitting Cu tube with 0.02" thick wall and base. This shielded cavity housed the specimen which was mounted onto its holder, a flat piece of tufnol held to the main block with nylon screws.

One of the Cu pillar supports also served as an r.f. and d.c. return. The inner s/s tube was connected to the positive terminal of the external bias supply and its connection to the BDO was via a sliding contact as shown. This arrangement made the whole assembly easily demountable.

4.5 Reasons for Use of He Gas Chamber

The two primary reasons for using the gas can assembly were as follows:

(a) To eliminate one known source of BDO frequency instability, namely, liquid He bubbling around the circuit elements which causes fluctuations in stray capacities. This effect was observed and corrected by use of gas can assembly. A similar observation was later reported by Slavin (90) for a MOSFET oscillator. Below the λ point, the absence of bubbling in the bulk of the liquid eliminates this problem.

(b) To enable the warming up of the specimen to above T_{CS} for Pb in order to drive out trapped flux (see §5.3).

In addition, the 3 mm. thick walls of the dural can provided an adequate r.f. shield, the skin depth in dural at 4.2°K being ~ 0.1 mm. at a frequency of 1 MHz.

Potting the whole BDO circuit in a resin was also tried in order to eliminate the problem due to bubbling and was found to be satisfactory. However, potting is only convenient when a more or less permanent circuit, without frequent access (for changing specimen coils, for example) is required.

4.6 The Field Coils and Magnet Power Supply

A detailed description of the field coils and auxiliaries and the determination of the coil constant, field homogeneity etc. is given in ref. (91). We shall briefly sketch the main features.

The applied d.c. field was produced by a pair of air-cored, water-cooled helmholtz coils. The current to these was supplied by a 'Wareham' C131 3kW power supply unit with a maximum current capacity of 15 amps. The coil constant was 87.44 ± .01 Gauss/amp and therefore fields of up to 1300 G could be produced. The field was homogeneous to within 0.7 per cent over a distance of ± 3 cm from the centre. The magnet current could be controlled by a ten turn helipot or by means of an integrating linear sweep generator. The latter enabled the field to be increased, decreased or held constant. The sweep rate was continuously variable from 0.005 G/sec to 60 G/sec.

The magnet current was determined by measuring the voltage across a 0.1 ohm standard resistance in series with it by means of a 'Solatron' digital voltmeter type LM 1420.2.

4.7 Back-Diode Oscillator

The back-diode oscillator (BDO) and its d.c. bias circuit are shown in fig. 24. Back-diodes are essentially low-power tunnel diodes but, unlike the latter, the negative dynamic resistance in their current voltage characteristics occurs in the reverse bias rather than forward bias region. A wide selection of these diodes is available spanning a range of specifications, especially the magnitude of the negative conductance which can vary by several orders of magnitude.

We have used a General Electric germanium back-diode BD4 whose d.c. characteristics at room and liquid He temperatures are shown in fig. 25. The change in the characteristics between $77^{o}K$ and $4.2^{o}K$ is so small as to be difficult to show clearly on our scale. The diode is seen to have a negative dynamic conductance g_d, in the near-linear region, of $\sim 3.5 \times 10^{-4}$ mho at $4.2^{o}K$.

The other BDO components are as follows:

1. Tank capacitor C (2100 pf) - three polystyrene capacitors (Radio Spares).
2. Shunting capacitor C_1 (1.4×10^4 pf) - one 3500 pf silver mica + three polysterene.
3. Diode capacitor C_A (10 pf).
4. Tank circuit coil L (20 μH).

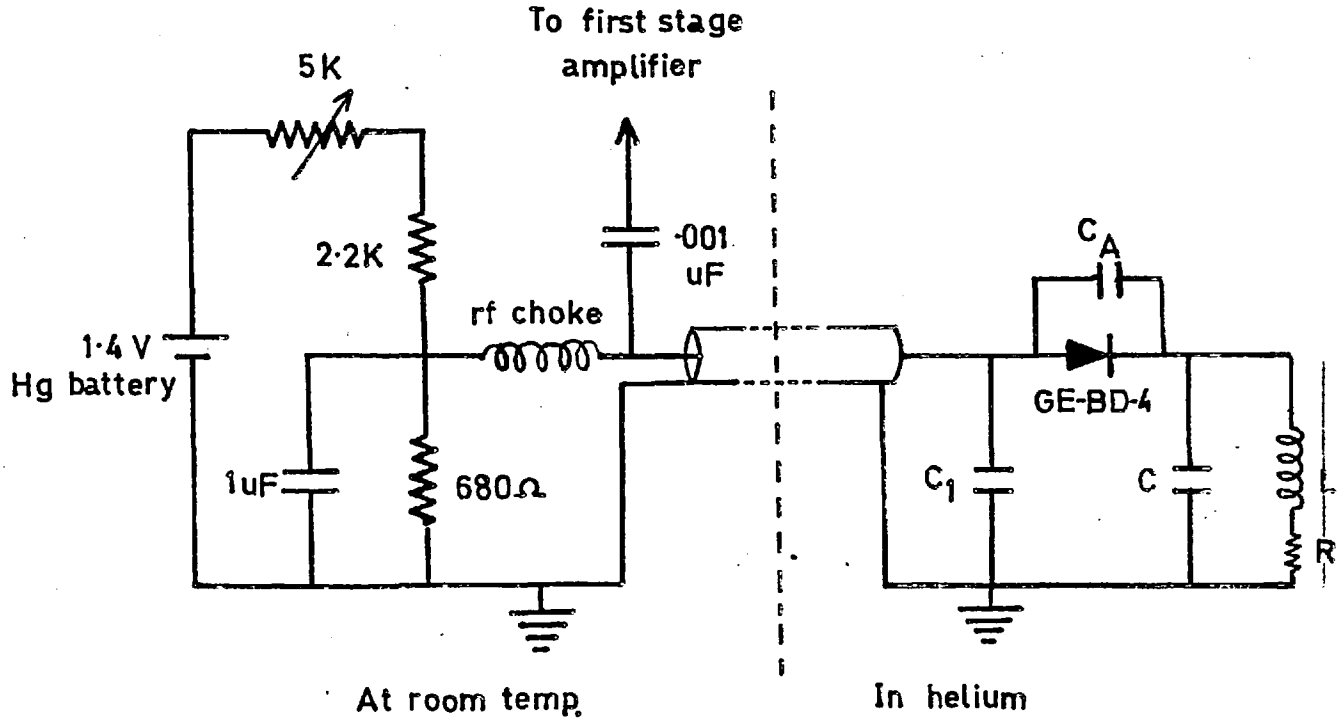

Figure 24 - The back diode oscillator (BDO) circuit and its bias supply.

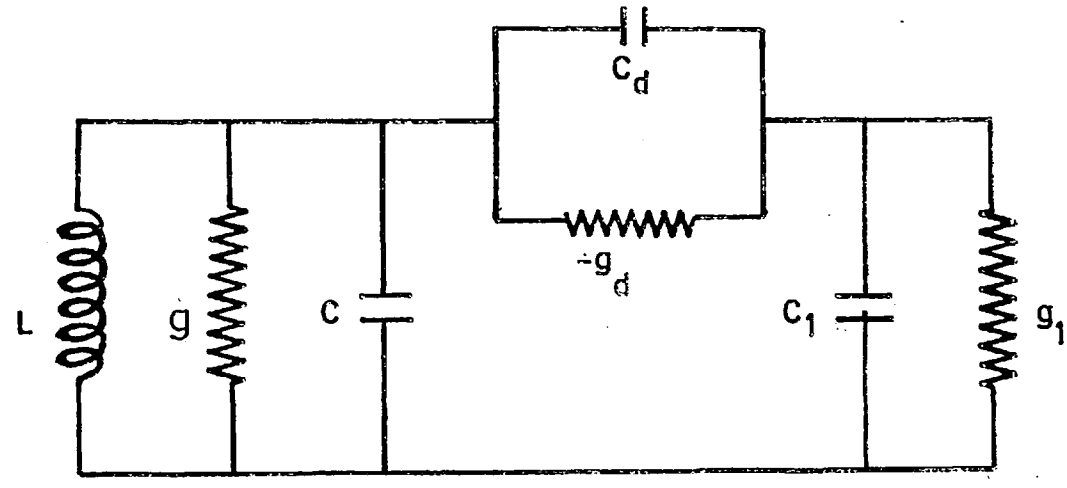

Figure 26 - Low frequency equivalent circuit of the back-diode oscillator.

The silver mica capacitor was used on account of its better thermal conductivity and was connected between the diode and the Cu pillar return by short thick Cu leads.

(a) Low frequency equivalent circuit and its analysis

For r.f. frequencies of up to a few tens of MHz, the circuit characteristics of the diode may be adequately represented by a negative dynamic conductance g_d with the small capacitance C_d in parallel as shown in the equivalent circuit of fig. 26 (87) (C_d is the sum of the diode self capacitance C_s and the added capacitance C_A). In the circuit L, C, R and g are respectively the inductance, capacitance, resistance (of the inductive branch) and the lumped equivalent conductance of the 'tank' circuit which essentially determines the resonance frequency. The back-diode and the large shunting capacity C_1, which isolates the BDO at helium temperature from the bias circuit at room temperature, form the 'active' circuit. g_1 is the equivalent conductance to ground of C_1 and the bias circuit.

The impedance of the active circuit, Z_A at a frequency ω_x is given as

$$Z_A = Z_d + Z_1$$
$$= (j\omega_x C_d - g_d)^{-1} + (j\omega_x C_1 + g_1)^{-1} \qquad \text{(IV-1)}$$

Z_d and Z_1 are the impedances respectively of the diode and the shunting capacitor. For the tank circuit with resistive losses in the inductive branch the impedance Z_T is given by

$$\frac{1}{Z_T} = \frac{R}{R^2+\omega_x^2 L^2} + \frac{j\omega_x(CR^2 - L + \omega_x^2 L^2 C)}{R^2+\omega_x^2 L^2} \qquad \text{(IV-2)}$$

In terms of the circuit Q = $(\frac{L}{C})^{\frac{1}{2}}/R$ the lumped equivalent conductance at resonance becomes

$$g = \frac{R}{R^2 + \omega^2} = \frac{1}{Q^2 R} \qquad \text{(IV-3)}$$

where the resonance frequency ω is defined as that for which the impedance in (IV-2) is purely resistive. Hence for the isolated tank circuit under consideration, the resonance frequency is given by:

$$\omega^2 = \left(\frac{1}{LC}\right)\left(1 - \frac{CR^2}{L}\right) = \left(\frac{1}{LC}\right)\left(1 - \frac{1}{Q^2}\right) \qquad \text{(IV-4)}$$

In terms of Q, the susceptance in Eqn. (IV-2) can be expressed as

$$S \approx \frac{\omega_x L(Q^{-2} - 1 + \omega_x^2 CL)}{Q^2 R^2} \qquad \text{(IV-5)}$$

when ω_x is close to the resonance frequency.

We now consider self-sustaining oscillations of the BDO circuit as a whole. When this circuit oscillates losses in the tank circuit are made up for by the power transferred by the active circuit. Hence the condition for self-sustaining oscillations to occur is

$$Re(Z_A^{-1}) + g \geq 0 \qquad \text{(IV-6)}$$

The resonance frequency is obtained by setting the phase of the total impedance equal to zero:

$$Im(Z_A^{-1}) + \frac{\omega L(Q^{-2} - 1 + \omega^2 CL)}{Q^2 R^2} = 0 \qquad \text{(IV-7)}$$

After rather lengthy but quite straightforward algebraic manipulations, Eqns. (IV-6 & -7) lead to the following results:

(1) For the BDO of fig. 24, the condition for oscillations to occur simplifies to

$$g_d - g \simeq g_1\left(\frac{g_d}{\omega C_1}\right)^2 \geqslant 0 \qquad \text{(IV-8)}$$

on making use of the approximations

$$(g_1 - g_d)^2 \simeq 10^{-8} \ll \omega^2(C_d + C_1)^2 \simeq 2{\cdot}5 \times 10^{-3}\ (\text{mho})^2$$

and

$$C_d \simeq 15\ \text{pf} \ll C_1 \simeq 1{\cdot}4 \times 10^4\ \text{pf}$$

(2) Similarly, by numerical inspection the expression for the frequency may be simplified to

$$\omega^2 \simeq \frac{1}{L(C+C_d)}\left(1 - \frac{1}{Q^2} - \frac{g_d^2 L}{C_1}\right) \qquad \text{(IV-9)}$$

In our case, C = 2100 pf, Q ≃ 70 (see below), L ≃ 20 μH. From these, the magnitudes of the second and third terms (inside the bracket) on the r.h.s. of Eqn. (IV-9) are estimated as ~ 2×10^{-4} and 4×10^{-5} respectively. They are both much smaller than the first term. To relate inductance changes ΔL to changes in frequency Δω only the first term will therefore be significant provided that the $\frac{1}{Q^2}$ term (the 'losses') can be shown not to change significantly when the specimen undergoes a transition (see §4.11).

(b) Amplitude of oscillations

The amplitude of the oscillations is determined by the requirement that the power dissipated per cycle be equal to the power transferred (92) i.e.

$$\bar{g}_d = g$$

where $\bar{g}_d$ is the average value of the diode conductance over an oscillation. When $g << (g_d)_{max}$, non-sinusoidal oscillations of large amplitude ensue, with the voltage swing extending into regions where the diode conductance is positive. This behavior was observed at 4.2°K, if the diode was biased to operate in the high negative conductance region, bias ~ 80 mV (fig. 25). That the voltage swing extended into the positive resistance region was shown by a re-entrant dip in an otherwise smooth waveform as in fig. 27. In normal operation the bias was adjusted to avoid this although, in common with Clover et al. (92), we find no quantitative effects of it in our measurements provided only the fundamental frequency is always measured.

(c) Q of the circuit

The minimum value of circuit Q for oscillations to occur can be estimated by setting the losses equal to the maximum power that can be transferred, i.e. $Q\omega L = {}^{1}/_{(g_d)_{max}}$. This gives $Q_{min} \approx 25$ for our oscillator. We found that the BDO just oscillated at 77°K. Therefore at this temperature $Q \gtrsim 25$. On cooling to 4.2°K we estimate the a.c. resistance of the copper coil to decrease by a factor ~ 3 (allowing for the change in the r.f. skin depth with resistivity). The Q at 4.2°K is therefore ~ 70.

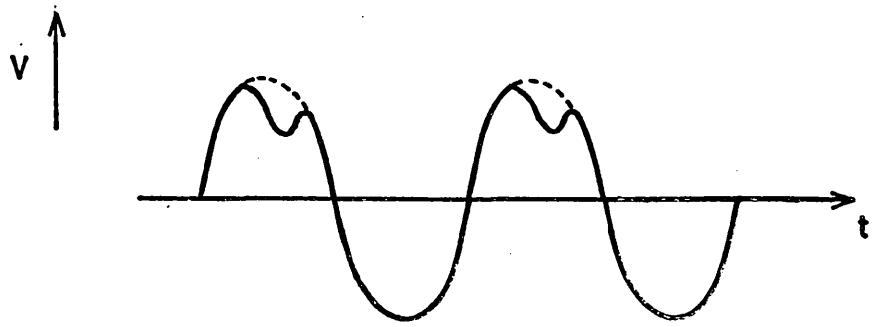

Figure 27 - Oscillator wave form showing 'dip' in otherwise sinusoidal oscillations resulting from voltage swing into positive dynamic conductance region.

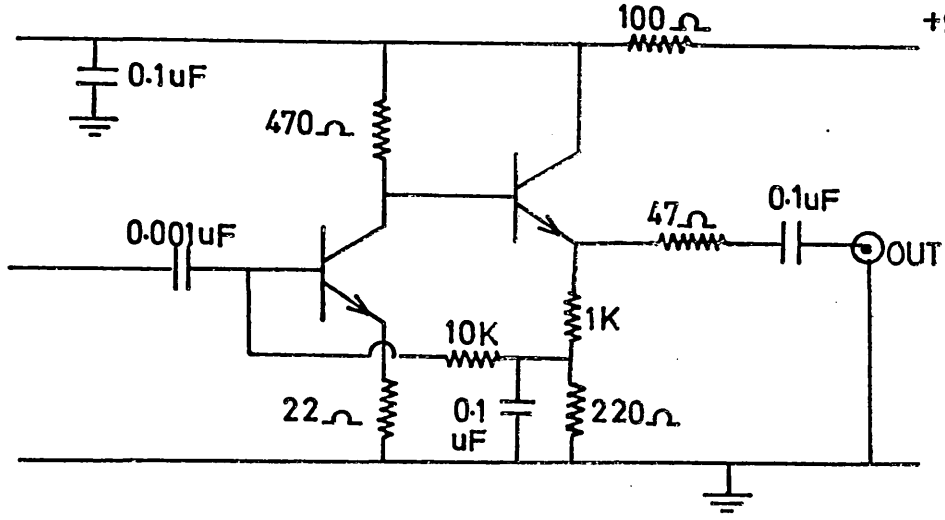

Figure 28 - First stage amplifier circuit.

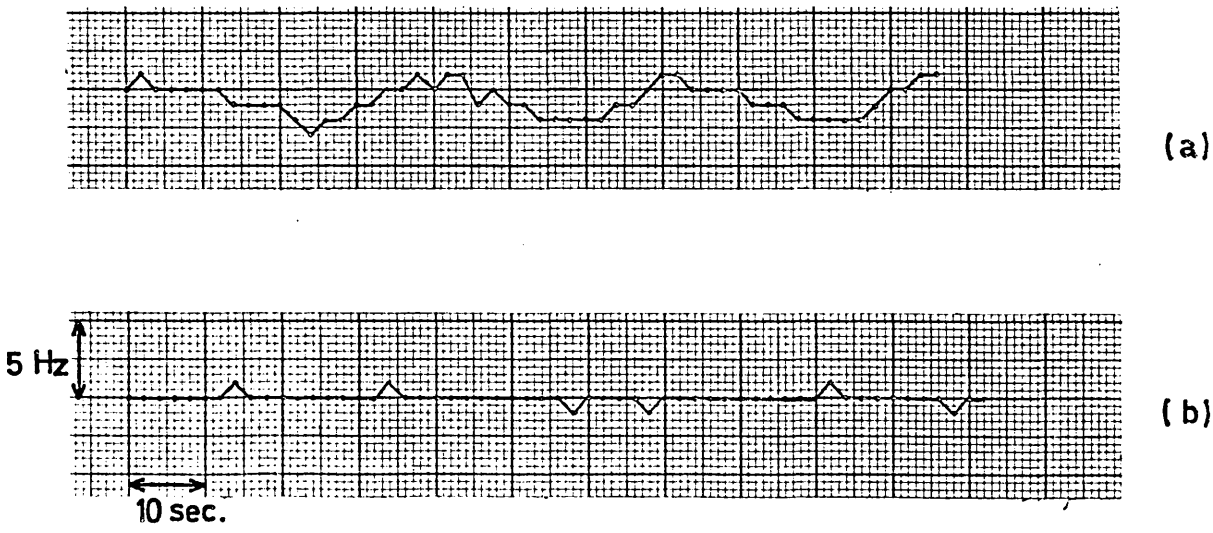

Figure 29 - Frequency counter reading Vs. time for a 6 MHz input from a stable crystal oscillator with (a) internal and (b) external reference frequencies used.

(d) Bias supply

The BDO bias supply of low output impedance is shown in fig. 24. The diode self-capacitance C_s is a function of the bias. The dependence of the frequency on bias is determined by the relative magnitudes of C_d (= C_s + C_A) and the tank circuit capacitance C. In the present case C >> C_d and the average variation of frequency with bias is ~ 10 Hz/mV. A 1.4 V mercury battery (Mallory RM12) gave a bias stability of better than 20 μV over 10 - 15 minutes which was quite adequate for our purposes.

(e) Choice of frequency

It is shown in §4.11 that the higher the frequency, the greater is the sensitivity of measurements. However, we also need to have the electromagnetic skin depth t in the specimens much larger than the thickness d. This consideration dictated the choice of the frequency. The total thickness of a specimen in these experiments could be several microns and the residual resistivity ρ very low. Typical values for Pb at 4.2°K are ρ ~ $^1/_{10}$ micro-ohm cm, yielding t ~ 16 microns at the operating frequency of ~ 800 kHz.

4.8 Estimation of r.f. Field

During oscillations the peak to peak (p - p) 'circuit' current drawn by the tank circuit, or its equivalent conductance g, is equal to the diode current swing. This, in turn, is very nearly equal to the current in the shunt capacitor C_1. The p - p voltage across C_1 is known to be ~ 500 μV, which means that the diode current swing i_d is ~ 35 μa p - p and that the

tank circuit voltage ($= \frac{1}{g} \times i_d$) is ~ 250 mV p - p. The inductance 'branch' current (Q x 'circuit' current) together with the coil geometry (see §5.1) provides an estimate of the r.f. field amplitude of ~ 0.3 G p - p.

4.9 Frequency Measurement

The BDO output signal was amplified in two stages before being fed into a Venner TSA 6636/3 digital frequency counter. The first amplifier (fig. 28) was designed to minimise feedback to the BDO and had a gain ~ 5, while the second one, a Texas Instruments integrated amplifier SN 5510 N had a gain ~ 60.

Several 'gate' times, in decade steps, were available on the counter. However, only the 1 sec. and 10 sec. gates, nominally measuring the frequency to 1 Hz and 0.1 Hz respectively, were used. Normally, an automatic mode of operation, with the gate electronically opened at regular intervals, was employed.

The stated accuracy of the counter was the count error resulting from the instability of its internal reference crystal ± 1 count. The reference crystal stability was stated as ± 1 in 10^6 but was actually found to be ~ ± 3 parts in 10^7. This was done by comparison of continuous sets of counter readings (for a given input signal), with the counter operated in turn on internal and external references respectively. Fig. 29 shows a set of such data for input from a 6 MHz crystal source. The external reference that we used was a 1 MHz signal from an Airmec locking receiver picking up the BBC's 200 kHz Droitwich transmission.

Suppose that ± ΔT is the fluctuation per second in the gate-time when the internal timer is used. Then, even for a stable input frequency F, the counter will indicate a fluctuation in the frequency of $\Delta F = \pm F \times \Delta T$. However, the counter also has a display error of ± 1 count. Therefore on 1 sec. gate the use of an external reference would only be gainful for $F \gtrsim {}^{1}/_{\Delta T}$. For $\Delta T \sim \pm 3 \times 10^{-7}$, this gives $F \gtrsim 3$ M Hz. Our working frequency was about 750 kHz and accordingly the external reference was used on the 10 sec., but not the 1 sec. gate.

4.10 Oscillator Stability

Under quiet laboratory conditions and in the absence of drifts, the BDO frequency fluctuations did not exceed ~ ± 0.3 Hz about a mean value over 15 minutes. A settling down period of about 10 min. just after helium transfer and of up to ½ hr. after lowering the temperature had to be allowed for the drifts in the mean frequency to become ≲ 0.5 Hz/min.

4.11 Effect on Frequency of Circuit Losses

In §4.7 it was shown that the resonance frequency of the BDO with losses in the inductive branch is given by

$$(2\pi f)^2 = \omega^2 \simeq \frac{1}{LC_t}\left(1 - \frac{1}{Q^2}\right) \qquad \text{(IV-10)}$$

where the total effective capacity $C_t = C + C_d$. We shall from now drop the subscript t. The change in frequency produced respectively by small changes in L and R, can be written:

$$\frac{2(\Delta f)_L}{f} \simeq -\frac{dL}{L}$$

and

$$\frac{(\Delta f)_R}{f} \simeq -\frac{1}{Q^2}\frac{dR}{R} \qquad \text{(IV-11)}$$

Thus in order to produce a given Δf, the fractional change in R would have to be $\frac{Q}{2}^2$ times bigger than that in L. Using numerical values, we find that a 1% change in R would only produce a frequency change of ~ 1 Hz, whereas it would change Q and g (= $(Q\omega L)^{-1}$) both by 1%. From the argument of §4.7(c), it can be seen that the corresponding change in the signal amplitude 'a' would be of the same order of magnitude. Monitoring 'a' during a phase transition of the specimen can therefore indicate if the transition is accompanied by a significant change in losses.

Some consideration will show that a knowledge of the operating bias and the amplitude can be used to estimate which portion of the diode I-V characteristic the oscillations span. This in turn can lead to a rough estimate of the change in 'a' for a given dR. Estimates obtained in this way are in good agreement with our observations on Sn In (5 at. %) and Pb In (6 at. %) alloy films where losses dominate and decreases in the amplitude of ~ 30% are observed upon transition from superconducting to normal state. On the other hand, neither of the two pure elements studied i.e. Sn and Pb produce any observable change in 'a' (measured on an oscilloscope). We estimate that of the average Δf_{total} of ~ 1 kHz that we observe for Pb/N specimens upon superconducting to normal state transition, an upper limit of 5 Hz can be put on that due to dR.

We summarise below some empirical observations which also lead us to believe that the magnetic transition of the proximity specimens is not accompanied by a significant increase in losses. We note first of all that the mechanism behind any losses that occur when the specimen is in the normal state must be the power dissipation due to induced eddy currents. Consider a flat plate of thickness d and resistivity ρ placed in a parallel a.c. field of peak amplitude h and frequency f. The eddy current power loss W per unit volume may be calculated when the skin depth t >> d and is given approximately by $W = \frac{\pi^2 h^2 d^2 f^2}{6\rho}$ (93). If this result were to apply to the films under consideration, then losses would be expected to be smaller in an alloy film (larg ρ) than in a film of the pure element. This seems to contradict our findings on Sn and Sn - In films cited in the previous paragraph. The answer to this apparent discrepancy seems to lie in the fact that the sample films, being nearly as long as the coils themselves, were not parallel to the a.c. field near the ends of the coil but were intercepted by it at an angle. Although we do not know of any theoretical treatment of the problem of losses in such a situation, the empirical observations of Cody and Miller (94) seem to lend support to our observations. They find that maximum losses occur when $^{d}/_{t} \simeq 0.1$ and that a departure in either direction of the ratio $^{d}/_{t}$ from the optimum value gives smaller losses. In our preliminary investigation referred to above $^{d}/_{t}$ was ~ 0.3 for Sn films. In this situation, an increase of ρ keeping all the other parameters fixed could indeed lead to increased losses. Before describing the effect

of shortening the films, we consider how the total $\Delta f (=(\Delta f)_L + (\Delta f)_R)$ between superconducting and normal states of the film will be affected by a change in f.

From Eqn. (IV-11) we know that $(\Delta f)_L$ is proportional to f. On the other hand, through its dependence on ΔR (which in turn depends upon t as discussed above) and on Q, $(\Delta f)_R$ will generally be a complicated function of the frequency. Therefore, if the frequency is varied any departure of the quantity $\Delta f/f$ from a constant value would indicate that $(\Delta f)_R$ is significant. Fig. 30 shows $\Delta f/f$ plotted as a function of f for a Sn - In (5 at .%) film. It is clearly seen that the transition to the normal state is accompanied by an increase in losses. On the same figure we have also shown the effect of reducing the length of the film (symmetrically, from either end). The resulting decrease of $\Delta f/f$ is not in proportion to the reduction in the film area but is much greater. From this we conclude that the portions of the film near the ends of the coil account for a greater proportion of losses than those well inside the coil where the a.c. field is parallel to the sample. When the film dimensions are 6.4 x 4.5 mm. not only is $\Delta f/f$ constant as a function of frequency but its value is also close to the expected $(\Delta f)_{L/f}$. The state transition for this case was not accompanied by any change in the signal amplitude.

In order to determine if losses were playing a significant role in the transitions of Pb/N specimens, both $(\Delta f)_N$ and $(\Delta f)_{Pb}$, corresponding to the normal metal and Pb transitions respectively, were measured as a function of f for Specimen 1. The frequency

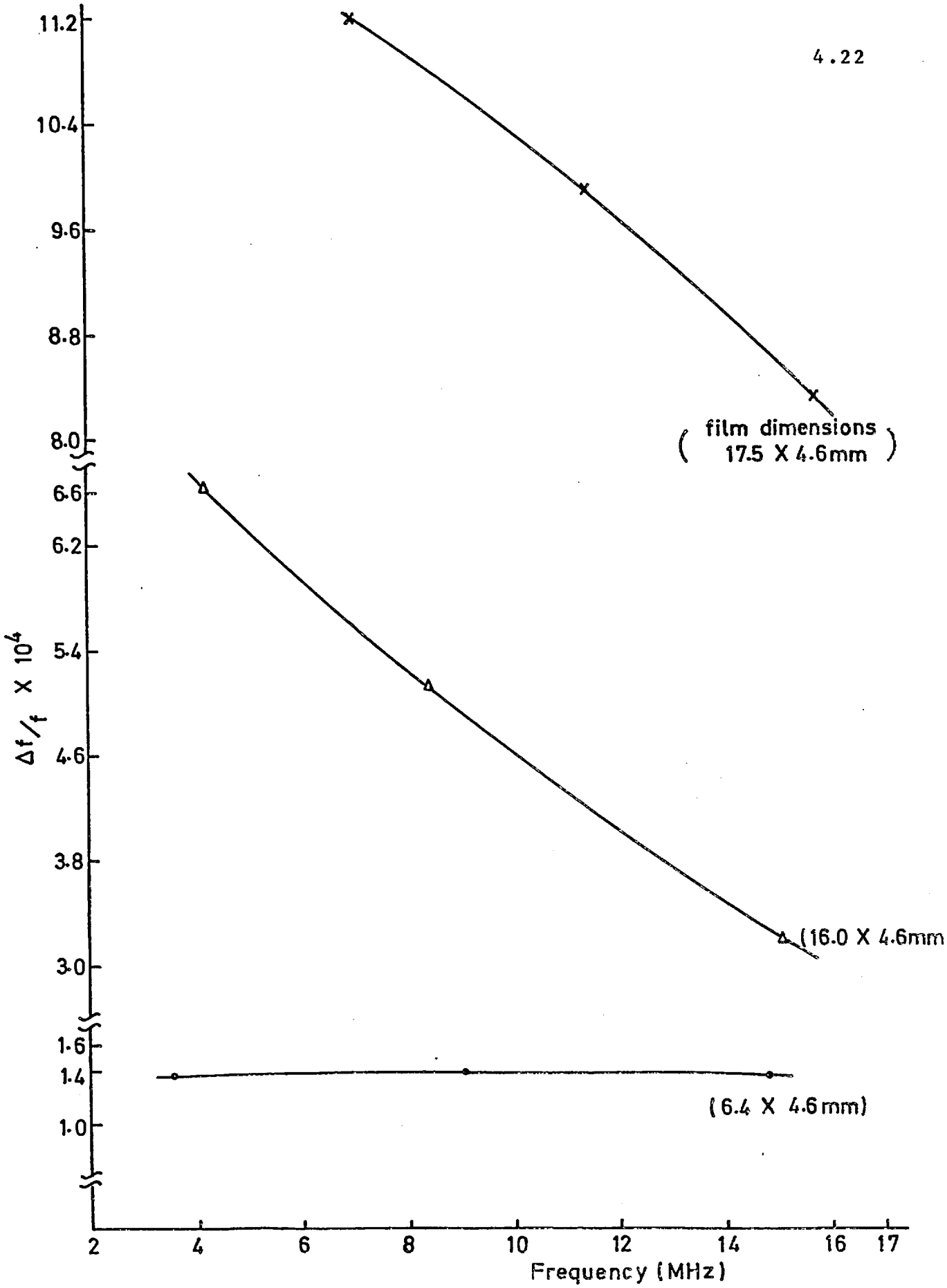

Figure 30 - The quantity Δf/f as a function of the frequency f for Sn In (5 at.%) films of different dimensions.

was varied by ~ 20% on either side of the working frequency. Within the accuracy of the experiment, no evidence for losses was found. The effect of shortening the length of the film (from 17 to 12 mm., cf coil length 19 mm.) was also investigated on the same specimen. $\frac{\Delta f}{f}$ was ~ 5% smaller than the value expected from the change in the filling factor. This is reasonable since near the ends of the coil the film will have a small, non-zero demagnetising factor on account of not being absolutely parallel to the a.c. field.

Not being able to distinguish between inductive and resistive changes is a major weakness of the Schawlow-Devlin technique and it necessitates a careful consideration of losses whenever the technique is employed.

4.12 Specimen Heater and Thermal Contacts

The heater consisted of a 120 ohm tin oxide resistor held close to the specimen coil. Thermal contact with the specimen was by means of vacuum grease. A heat pulse could be applied by momentarily connecting a 10-15 V d.c. source across the connector plug at the top of the cryostat (fig. 23).

The thermal contact of the BDO components (including the specimen coil) in the gas can with the He bath was by means of

(1) metallic conduction through the Cu pillar support and thick Cu leads (§4.7).

(2) vacuum grease between the specimen coil and the Cu base plate (fig. 22).

(3) He gas in the can normally maintained at the same pressure as the bath.

On average thermal equilibrium was re-established within ~ 5 minutes of the application of a heat pulse. The applied voltage and duration of the pulse were adjusted by experimentation to be just sufficient to raise the specimen above T_c for Pb. That thermal equilibrium was re-established was shown by frequency stability and the reproducibility of the specimen magnetic transition curve for that temperature. From the amount of heat generated by the pulse and the time taken for equilibrium to be established the average rate of heat loss from the can was estimated to be ~ $\frac{1}{600}$ watts/^{o}K. This together with the known power dissipation of the BDO yields an estimated maximum temperature difference between the specimen and the bath of ~ 5 mK under equilibrium conditions.

CHAPTER V

EXPERIMENTAL PROCEDURE AND DATA ANALYSIS

Introduction

In this chapter we describe the procedure for setting up the experiments, the collection and recording of experimental data and the interpretation of these data. Some observations made in the course of the experiments e.g. the frozen flux and the empty coil effect are set out. The chapter ends with a description of experiments aimed at determining the effects, if any, of the earth's field on our measurements.

5.1 Coil Winding and Specimen Mounting

To obtain maximum filling factor, a separate coil was wound for each specimen studied. A blank coverslip was placed on top of the one with the trimmed film. This was to protect the film and also ensure that the film was located centrally inside the coil. In some of our early work narrow strips of paper were used as spacers between the coverslips to prevent damage to the films. The spacers were subsequently found to be unnecessary. A single layer coil of ~ 200 turns of 46 s.w.g. insulated copper wire was then wound round the coverslips with its axis parallel to the longest side. Uniformity of windings was achieved by having the turns wound as closely as possible. A thin layer of 'Durofix' spread over the windings held them rigidly together. The coils had a rectangular cross-section of approximately 8 x 1 mm and a length of 18 mm. The inductance was typically ~ 20 μH and the self-capacitance ~ 10 pf.

The specimen coil was held in position on the tufnol holder (fig. 22) by strips of PVC tape. After screwing back the holder in its position, the short coil leads were soldered into the BDO circuit. A small quantity of Apiezon M grease was used to provide contact between the specimen, the copper base plate and the heater. The cone base and the dural can were then reassembled and the vacuum seal and electrical contacts checked.

5.2 Data Recording and Measurement of δ

The basic experimental data consisted of BDO frequency as a function of the applied d.c. fields. Both these quantities were recorded manually. The field was held constant at a desired value during which 3 or 4 frequency readings from the counter, operating on automatic mode, were taken down. The field was then raised (or lowered) to the next value and the process repeated. The size of the field increments varied from a fraction of a gauss to a few hundred gauss depending on the density of points required to plot the particular section of the transition curve.

A typical transition curve, that for specimen 2 (Pb/Ag), is shown in fig. 31. The initial small drop in the frequency Δf_N corresponds to the destruction of superconductivity in N. The field H_N required to achieve this is very nearly independent of temperature but varies with the impurity concentration in N, from ~ 100 G for pure Ag to 150 G for Ag Aℓ (1.5 at %). Above H_N, an increase in the applied field H_{app} produces very little change in the frequency until just before the critical

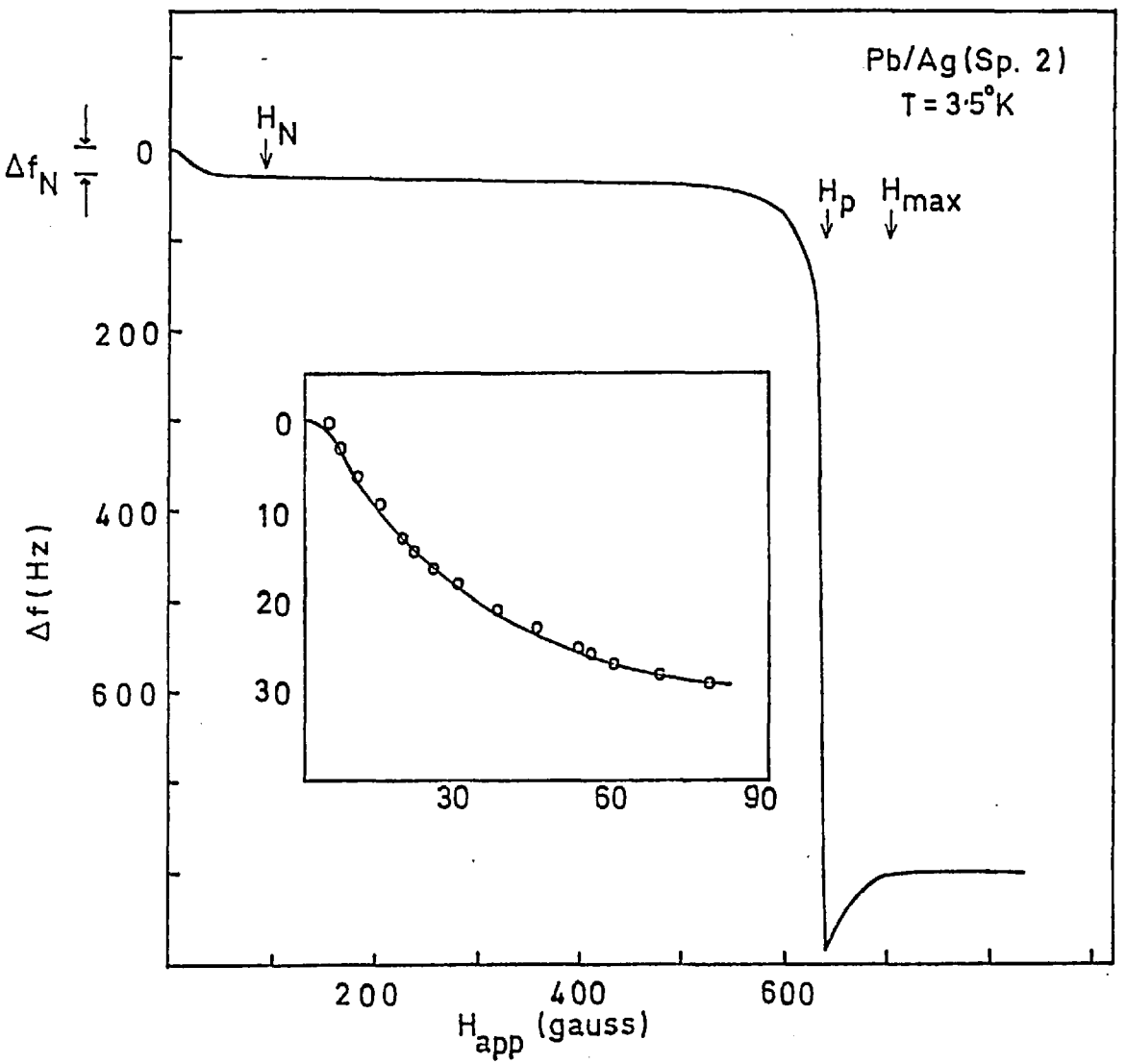

Figure 31 - Typical transition curve for a Pb/Ag specimen showing a plot of Δf Vs H_{app}.

field for Pb is reached. A rapid drop in the frequency is then observed, corresponding to flux penetration in Pb. That the Pb undergoes a first order transition is shown by the presence of a sharp dip in the Δf vs H_{app} curve. The origin of the dip is discussed in the following section. As H_{app} is increased further, all traces of superconductivity in Pb disappear at a field designated H_{max}. For all $H_{app} > H_{max}$, the frequency remains constant. The change in frequency between $H_{app}=H_N$ and $H_{app}\geq H_{max}$ corresponds to complete flux penetration in Pb and is denoted by Δf_{Pb}.

In order to convert Δf_N into the corresponding distance δ, we use the conversion factor A obtained with the help of the known Pb thickness d_s i.e. $A = {}^{d_s}/\Delta f_{Pb}$. A turned out to be ~ 25 Å/Hz (see Table 6.1). Because d_s ~ 2μ the correction to A due to the weak field penetration into a thickness λ ~ 400 Å on the free surface of Pb is small compared to the overall accuracy of the measurements, and has therefore been neglected.

5.3 Magnetic Transitions of Pb of NS Layers

The two critical fields associated with the magnetic transition in the Pb layer of the Pb/Ag specimen (fig. 31) are firstly the field H_p at which the 'dip' occurs in the transition curve Δf vs H_{app} and secondly the field H_{max} at which superconductivity is completely destroyed in the sample. Within experimental error, these two fields coincide with H_c and H_{c_3} respectively for isolated Pb films. This is brought out by the comparison in Table 5.1 of the critical fields of four NS specimens with those of isolated Pb films from the data of Cody and Miller (44). Reference to Table 6.1 (p6.36)

will show that the N material of all the specimens in Table 5.1 is clean enough for $\sigma_N \sim \sigma_S$. The discussion that follows shows that this choice of values of σ in the two materials ensures that H_p and H_c coincide.

Sp 1 Pb/Ag	H_p = 550G	H_{max} = 634G
Sp 4 Pb/Ag Mn(50 apm)	551	629
Sp 7 Pb/Ag Aℓ(0.5 a.%)	552	634
Sp 14 Pb/Zn	552	633
Pb films about 2μ thick (Ref. 44)	H_c = 550G	H_{c_3} = 635G

Table 5.1 Comparison of H_p and H_{max} with H_c and H_{c_3} of isolated Pb films at T = 4.2° K.

Isolated Pb films of the thicknesses we use (~ 2 μ) exhibit a 'sheath state' at temperatures $T \lesssim 6^\circ$ K (45). In an applied field parallel to the plane of the film, H_c is the field at which the bulk of the film undergoes a first-order transition to the normal state. Above H_c, superconductivity persists in a sheath, of thickness of the order of the coherence length, at the surfaces of the film that are parallel to the field. In the geometry being considered, a continuous superconducting sheath will surround the normal bulk of the isolated Pb film for $H_c \lesssim H_{app} \lesssim H_{c_3}$. The sheath is completely destroyed when the applied field equals H_{c_3}, the transition from the sheath state to the normal state being second order (45). We now examine how the sheath is affected by the presence of a normal metal coating on the surface of the superconductor.

A number of experiments have demonstrated that the upper critical field H_{c_3} at the interface of a superconductor with a normal metal is lower than that of the free surface (1a, 48). In the following we shall designate the interface upper critical field by H_{if}. In a theoretical study of the problem, Hurault (48) has shown that for a type II superconductor with an N metal coating $H_{c_2} < H_{if} < H_{c_3}$ when $\sigma_N < \sigma_S$. Here σ is the normal state conductivity of a metal and $H_{c_2} = \sqrt{2}\,\kappa\, H_c$ is the field above which the bulk of the type II material is normal. For $\sigma_N \to 0$ i.e. when the normal layer is an insulator, $H_{if} \to H_{c_3}$. When $\sigma_N > \sigma_S$, he argues that $H_{if} = H_{c_2}$ which implies that no superconducting sheath can exist at the interface. In the case of Pb, H_{c_2} = 373 G at 4.2° K which is less than H_c (= 550 G). In these circumstances, the bulk transition takes place at $H_{app} = H_c$. No surface sheath will exist at the interface unless $H_{if} > H_c$, which in turn requires $\sigma_N << \sigma_S$. For the present, we make the reasonable assumption that no sheath is present at the interface when the bulk of the Pb of an NS specimen undergoes a transition at H_c. On the free Pb surface, however, a sheath persists for $H_c < H_{app} < H_{c_3}$.

The presence of the dip at H_c in the Δf Vs H_{app} curve of Pb coated with a normal material can now be explained as follows. The total field H acting on the specimen is the sum of the applied d.c. field H_{app} and the r.f. field produced by the oscillator coil. Then, the inductance L(H) of the coil is determined by the slope of the magnetisation curve, $\frac{dM}{dH}$, as we now show. Consider a long, uniform solenoid of N turns, length ℓ, and cross-section area A. Let A_s be the cross-section area of a

long, thin superconducting specimen (of zero demagnetising factor) contained within the coil. Then, the total flux linkage Φ through the coil is given by $\Phi = \{(A - A_s)H + A_s(H + 4\pi M)\}N$. Now $L = \frac{d\Phi}{di}$, where i is the current in the coil ; we may therefore write $L = \frac{d\Phi}{dH} \times \frac{dH}{di}$. From the coil geometry we know that $\frac{dH}{di} = \frac{4\pi N}{c\ell}$, where c is the velocity of light. Hence, $L = \frac{4\pi N^2}{c\ell}\{A + 4\pi A_s \frac{dM}{dH}\}$. Using the fact that in a lossless circuit the frequency $f = \frac{1}{(LC)^{\frac{1}{2}}}$ where C is the tank circuit capacitance we have finally,

$$f = \frac{1}{C^{\frac{1}{2}}}\left[\frac{4\pi N^2 A}{c\ell}\left(1 + \frac{4\pi A_s}{A}\frac{dM}{dH}\right)\right]^{-\frac{1}{2}} \simeq \left[\frac{c\ell}{4\pi C N^2 A}\right]^{\frac{1}{2}}\left[1 - \frac{2\pi A_s}{A}\frac{dM}{dH}\right]$$

Eqn.(V-

The figure below illustrates schematically the relation between the oscillator frequency and the changes in the specimen magnetisation in the absence of a continuous superconducting surface sheath round the specimen. The size of the dip in f is related directly to $\left|\frac{dM}{dH}\right|$ which is maximum at the inflexion point in the magnetisation curve; the sharpness of the dip to the rate of variation of $\frac{dM}{dH}$ over fields ~h (the r.f. field) about the inflexion point.

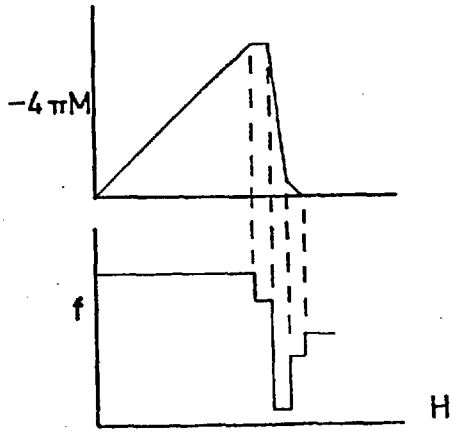

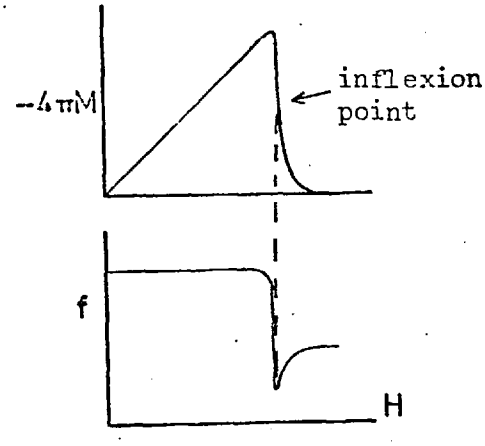

In order to see how the presence of a continuous superconducting surface sheath round an isolated Pb film would alter the response of the oscillator, we consider the magnetisation curve of a Pb film. The magnetisation as a function of the

field undergoes a rapid change at the first order transition at H_c. Then, in the case where there is no continuous sheath round the specimen capable of carrying shielding currents, small changes in H necessitate movement along the steep magnetisation curve producing large changes in $\frac{dM}{dH}$ and hence in the r.f. flux threading the coil. On the other hand, the effect of a continuous sheath round the specimen would be to make the magnetisation move along flux-conserving lines, i.e. lines of slope unity on the plot $-4\pi M$ Vs H. When this is the case, the coil does not see any change in the slope $\frac{dM}{dH}$ and its inductance L (and the BDO frequency) remains constant. In practice, however, we find that in spite of the sheath, a decrease occurs in the frequency at $H = H_c$ (fig. 32) which indicates that the r.f. field is only partially screened out from the bulk of the Pb. This is a geometric effect resulting from specimen films being a few mm shorter than the coil. As the field is further increased, Δf undergoes a very slow decrease showing that only very little additional r.f. flux is able to penetrate the sample. Eventually the total field H reaches a value sufficient to induce critical shielding current in the sheath. The frequency then decreases rapidly with field as more flux penetrates. Above H_c the transition is a second order, continuous one and is complete at H_{c3}.

In fig. 33 we show the transition curves for Pb/Ag alloy specimens for the entire range of values of σ_N^{-1} (ρ_{res} in the fig.) covered experimentally. The behavior of the isolated Pb films ($\sigma_N \to 0$) is seen to be gradually approached as σ_N is decreased. In transition curves of this kind, the critical field H_c of Pb is, in general, identified as that for which $\left|\frac{d(\Delta f)}{dH}\right|$ is maximum. Only when $\sigma_N \sim \sigma_S$ (so that $H_{if} < H_c$) do H_p and H_c coincide.

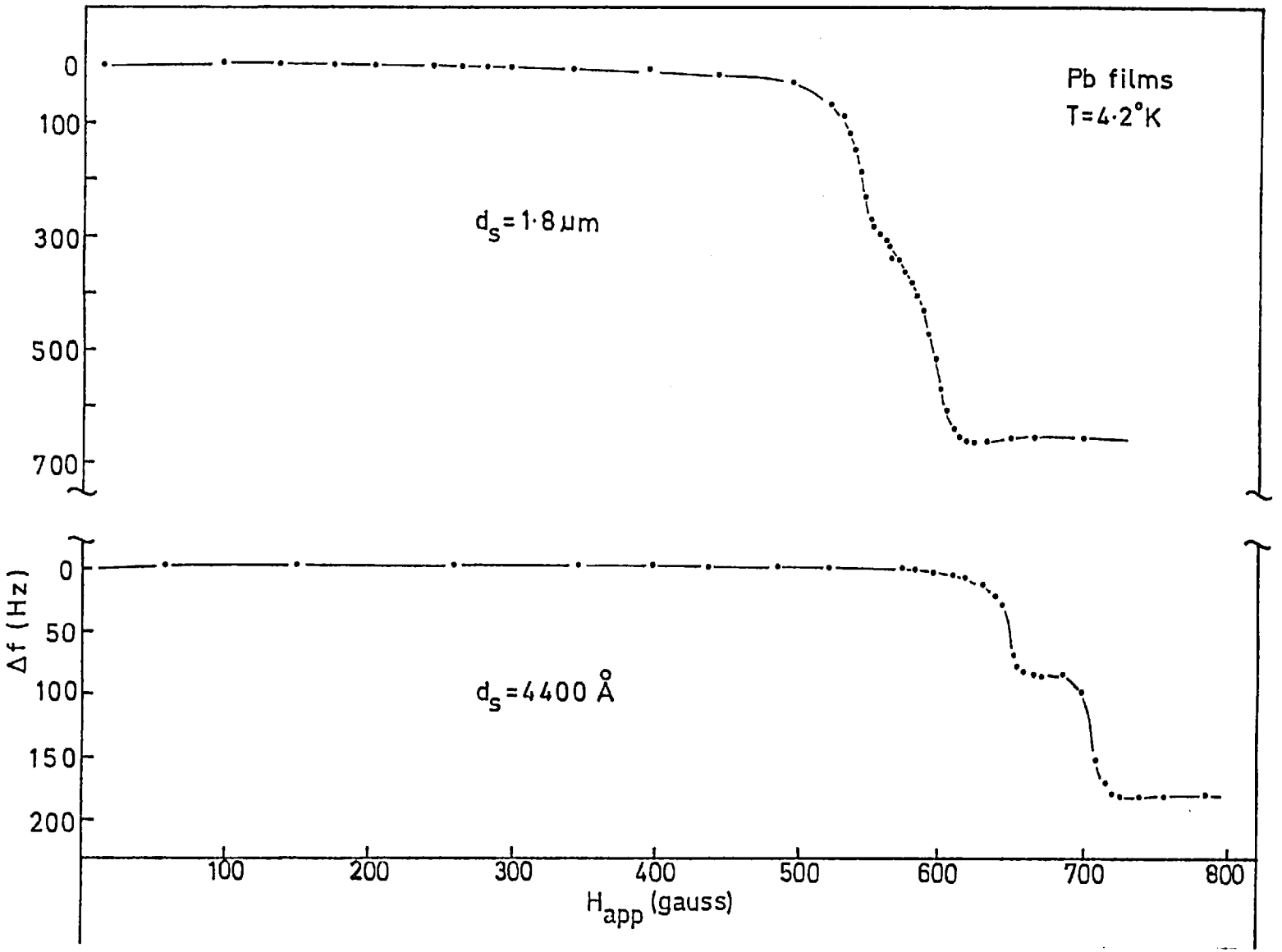

Figure 32 - Δf Vs H_{app} curves showing the magnetic transitions of isolated Pb films.

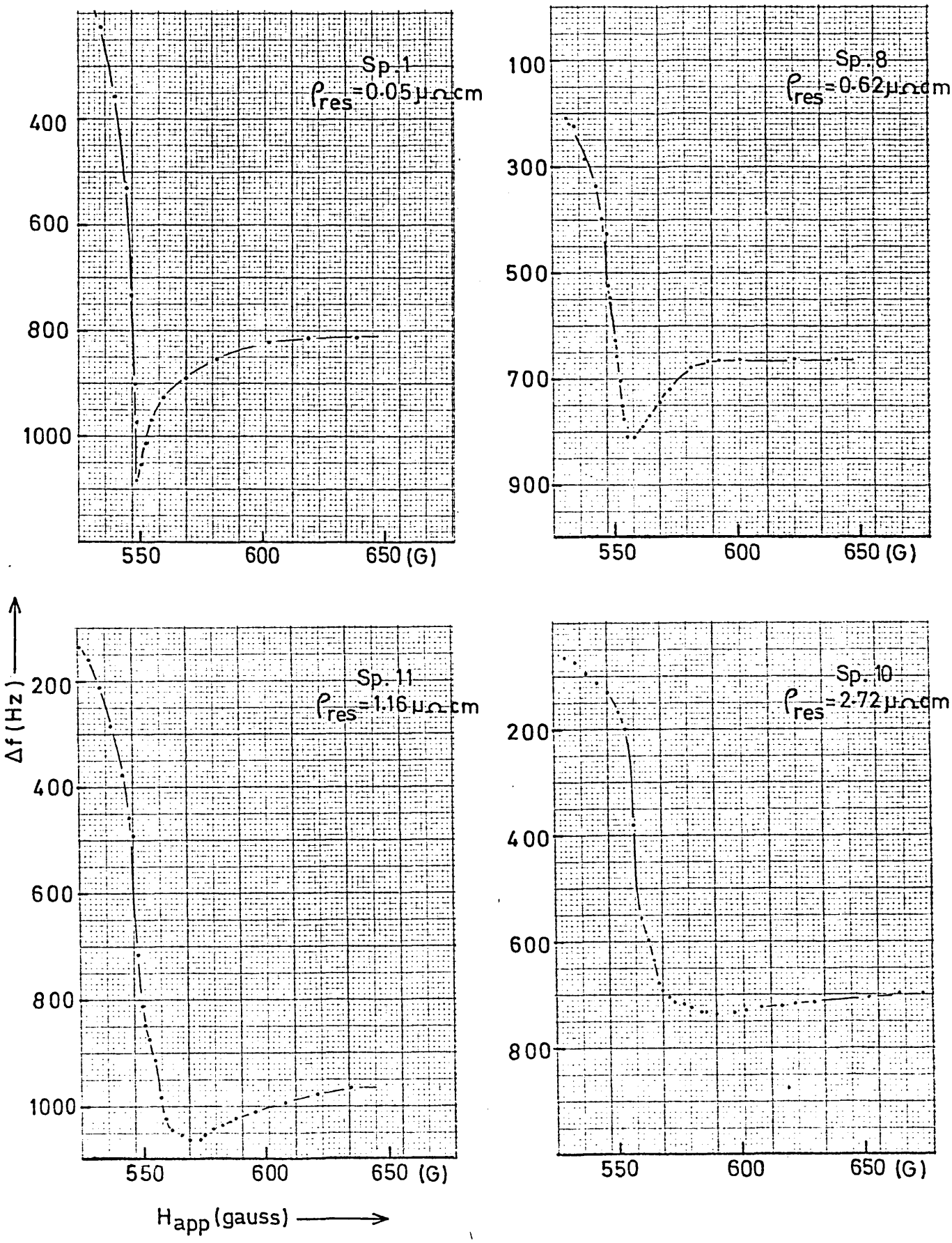

Figure 33 - Magnetic transitions of the Pb of several Pb/Ag alloy specimens for different values of $\sigma_N^{-1} (\equiv \rho_{res}) \cdot \sigma_S^{-1} \sim 0.1\ \mu\Omega cm$.

5.4 Frozen Flux

All the specimens studied showed a tendency to trap flux following a magnetic transition. This was indicated by the frequency returning to a lower zero field value f(0) after the field had been swept once. The decrease in the frequency Δf_F was dependent upon the angle between H_{app} and the film, a fact used to check the alignment of the specimens. The amount of frozen flux as indicated by the magnitude of Δf_F varied from specimen to specimen. For the Pb/Ag specimen (no. 1) whose frozen flux characteristics are typical of all Ag samples, Δf_F at 4.2°K was ~ 8 Hz for H_{app} parallel to the sample, increasing to 14 Hz for a ½° misalignment. At 1.5°K, although Δf_F (parallel) remained nearly the same, $\Delta f_F(\frac{1}{2}^\circ)$ increased to ~ 30 Hz. The Cd and Zn specimens on the whole trapped more flux with Δf_F (parallel) being typically ~ 40 Hz at 4.2° K.

The virgin and subsequent curves for Sp. 14 (Pb/Zn) are shown in fig. 34. In the course of a run, frozen flux could be expelled by momentarily warming the specimen up to above T_c for Pb, in zero field. This was done by applying a heat pulse (as described in §4.12) and on average about five minutes after its application the virgin curve could be reproduced. If the field was raised to a value only high enough to destroy the induced superconductivity (i.e. $H_{app} = H_N$) and then lowered to zero, none of the Pb/Ag alloy specimens exhibited any trapped flux. In contrast, the Cd and Zn specimens trapped enough to change f(0) by ~ 4 Hz.

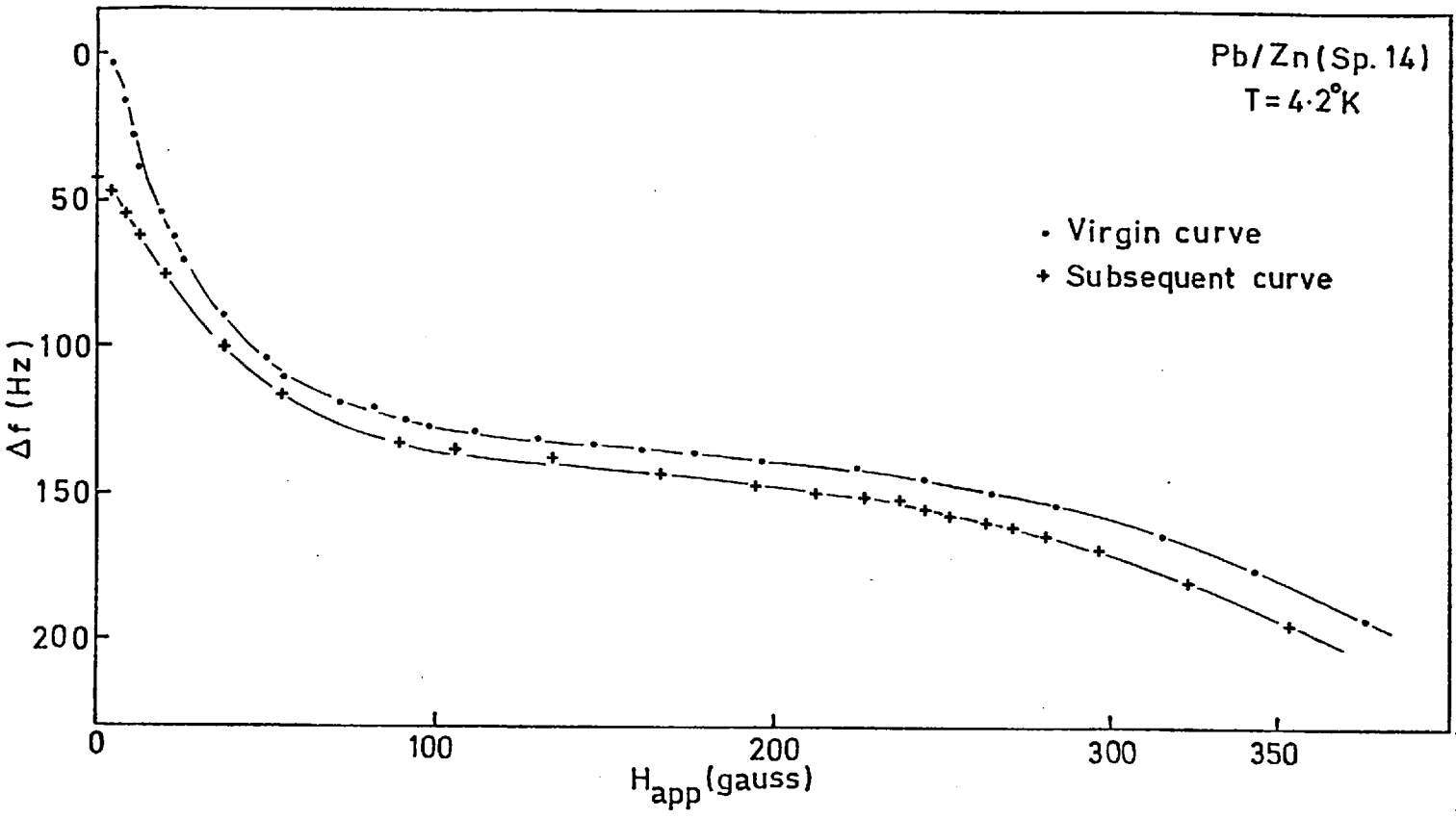

Figure 34 - Typical virgin and subsequent transition curves for a Pb/Zn specimen.

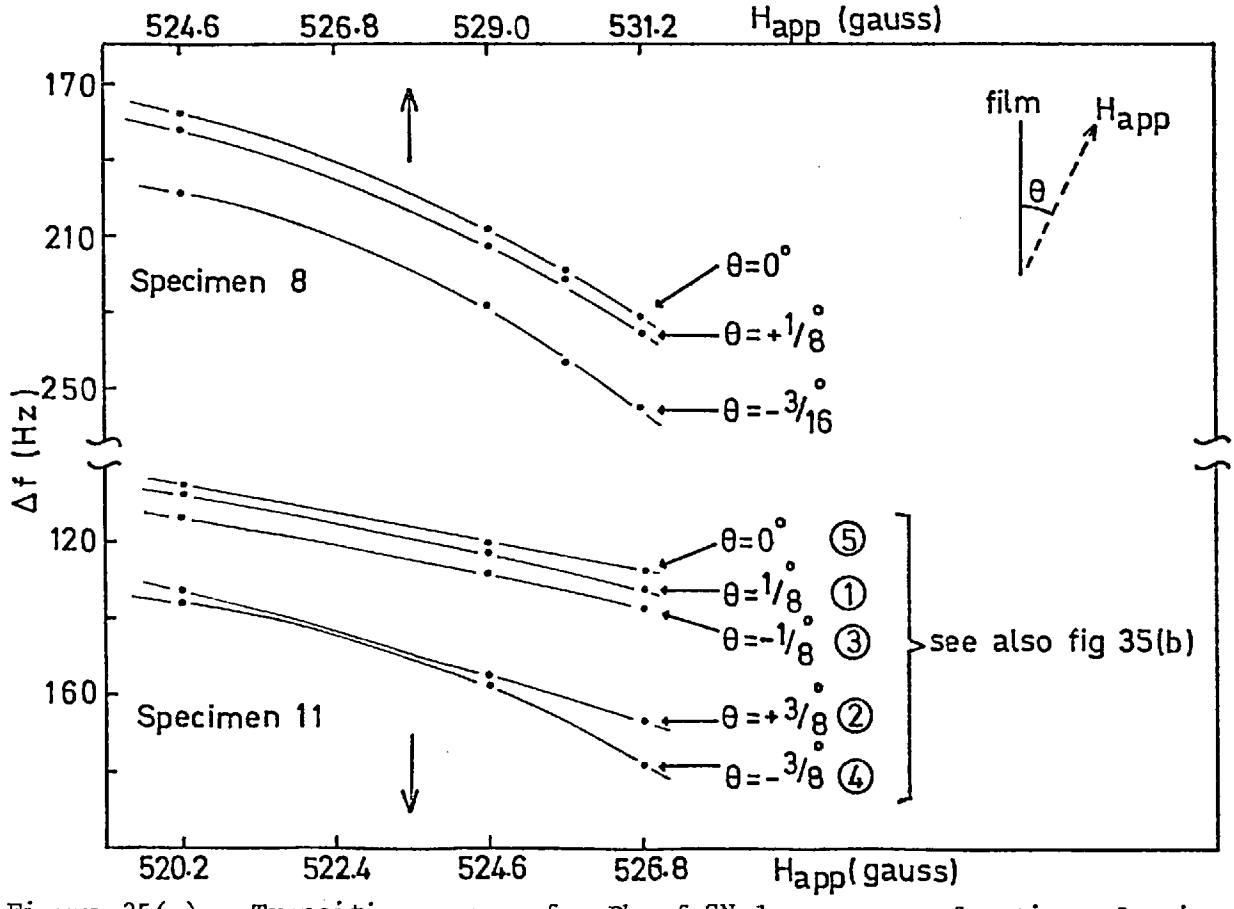

Figure 35(a) - Transition curves for Pb of SN layers as a function of orientation of H_{app}.

5.5 Field Alignment

The air-cored magnet (§4.6) was mounted with the coil windings in the horizontal plane and the dewar tail occupying the core. The magnet rested on three screw supports which enabled the field orientation to be adjusted. The specimens were mounted so that the film plane would be parallel to the line joining two of the screws, reducing the alignment procedure to adjusting the remaining screw.

The technique employed for alignment consisted of measuring $\Delta f(H) = f(0) - f(H)$ at several fixed values of H and minimising $\Delta f(H)$ as a function of field orientation. The values of H were chosen so that a steep part of the magnetic transition curve of Pb was scanned. Because of irreversibility of the transitions, a set of $\Delta f(H)$ values was taken in increasing fields and the specimen taken through a complete transition to its normal state before repeating the procedure with a different orientation, for the same field values, reproduced to within 0.25G. Typical results for two specimens are shown in fig. 35 (a). Fig. 35 (b) shows the various values of Δf at a given H as a function of field angle, each being obtained in a separate sweep. Alignment to better than $\frac{1}{8}^{o}$ was possible. This technique was checked against one employing maximisation of film critical current as a function of orientation for a pure Sn film (Fig. 36).

As mentioned in the last section, the amount of trapped flux was a strong function of the field orientation for all specimens at low temperatures. This property provided a useful check on the orientation.

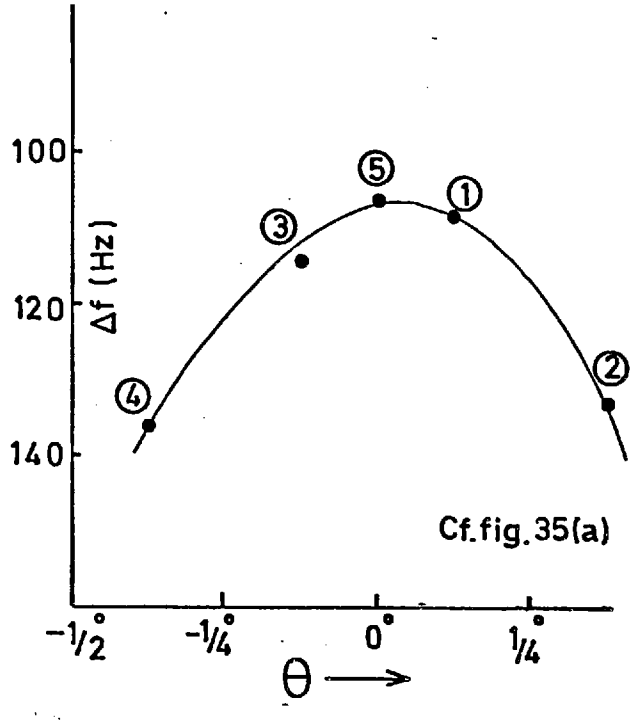

Figure 35(b)- The quantity Δf for a fixed value of H_{app}, as a function of orientation. Each point is obtained from a separate sweep i.e. a full curve of the type shown in figure 35(a).

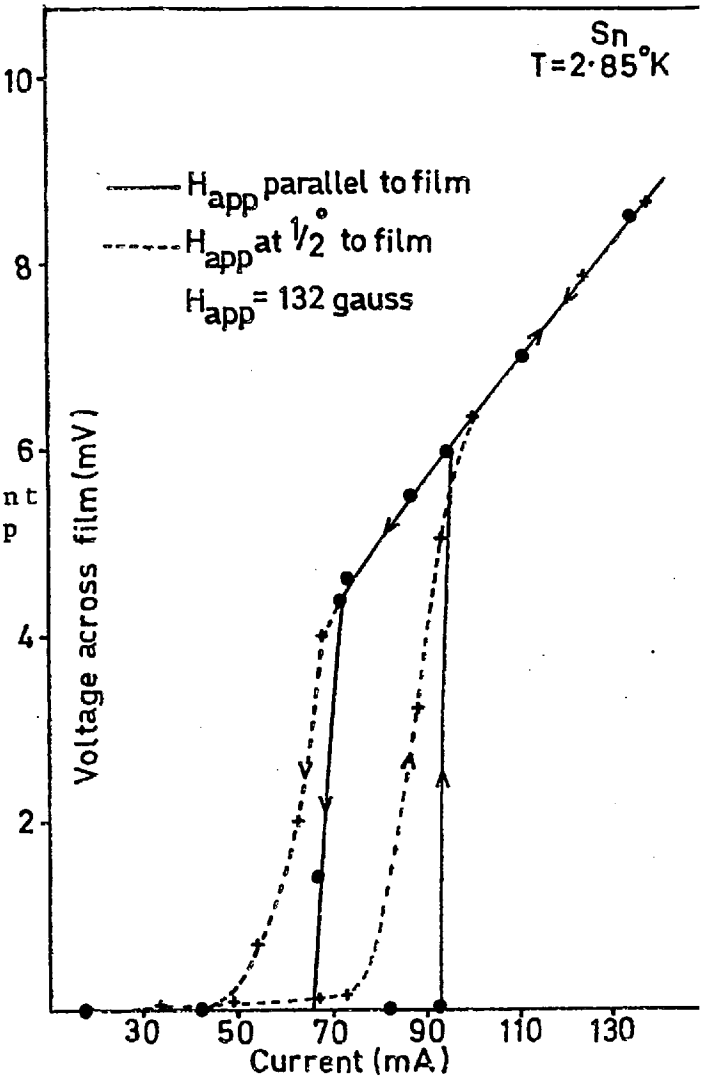

Figure 36- I-V characteristics of a Sn film as a function of orientation.

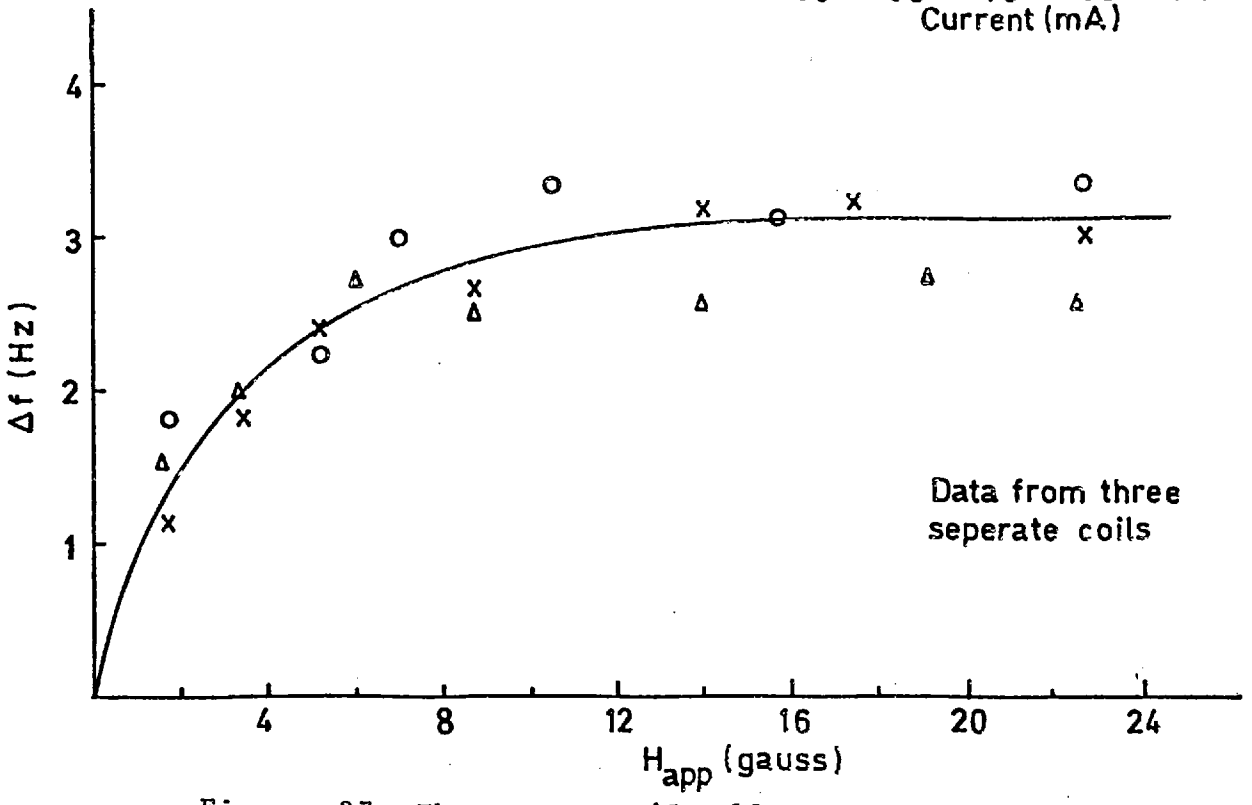

Figure 37- The empty-coil effect.

5.6 The Empty Coil Effect

In the early stages of this work, it was discovered that when the d.c. field was raised from a zero value the frequency of the BDO with an empty tank coil increased by 3 to 4 Hz by the time the field was about 10 G and then remained constant at this value for any further increase of H. The cause of this behavior could not be traced. A similar observation has been made by Shiffman (42). Our experiments showed that this effect existed for coils wound from different batches of Cu wire and for ones made from Aℓ and Nb wire. By experimentation, coil formers and adhesives were ruled out as possible causes and so was any noise pick-up from the magnet power-supply by replacing it with batteries. The magnitude of the empty coil effect, which was proportional to the BDO frequency, did not change with temperature in the helium range although it was smaller by a factor of ~ 3 at 77° K. Any possible involvement of the diode itself was ruled out by shielding it from the applied field by a hollow Nb cylinder in one of the experiments. Fig. 37 shows this effect for three different coils.

For clean N materials e.g. pure Ag, Zn and Cd, the field-induced transition of the N material began at fields as small as ~ 0.5 G (see fig. 38) and the empty coil effect could not be directly measured. In such cases an average empty coil correction of 3 Hz for $H_{app} \gtrsim 10$ G, estimated from fig. 37, was made. From our data for over a dozen coils we have no reason to suspect an error of more than ± 1 Hz in the average correction made. For dirty N materials on the other hand, as indeed for single Pb films, no significant flux penetration occurred up to fields

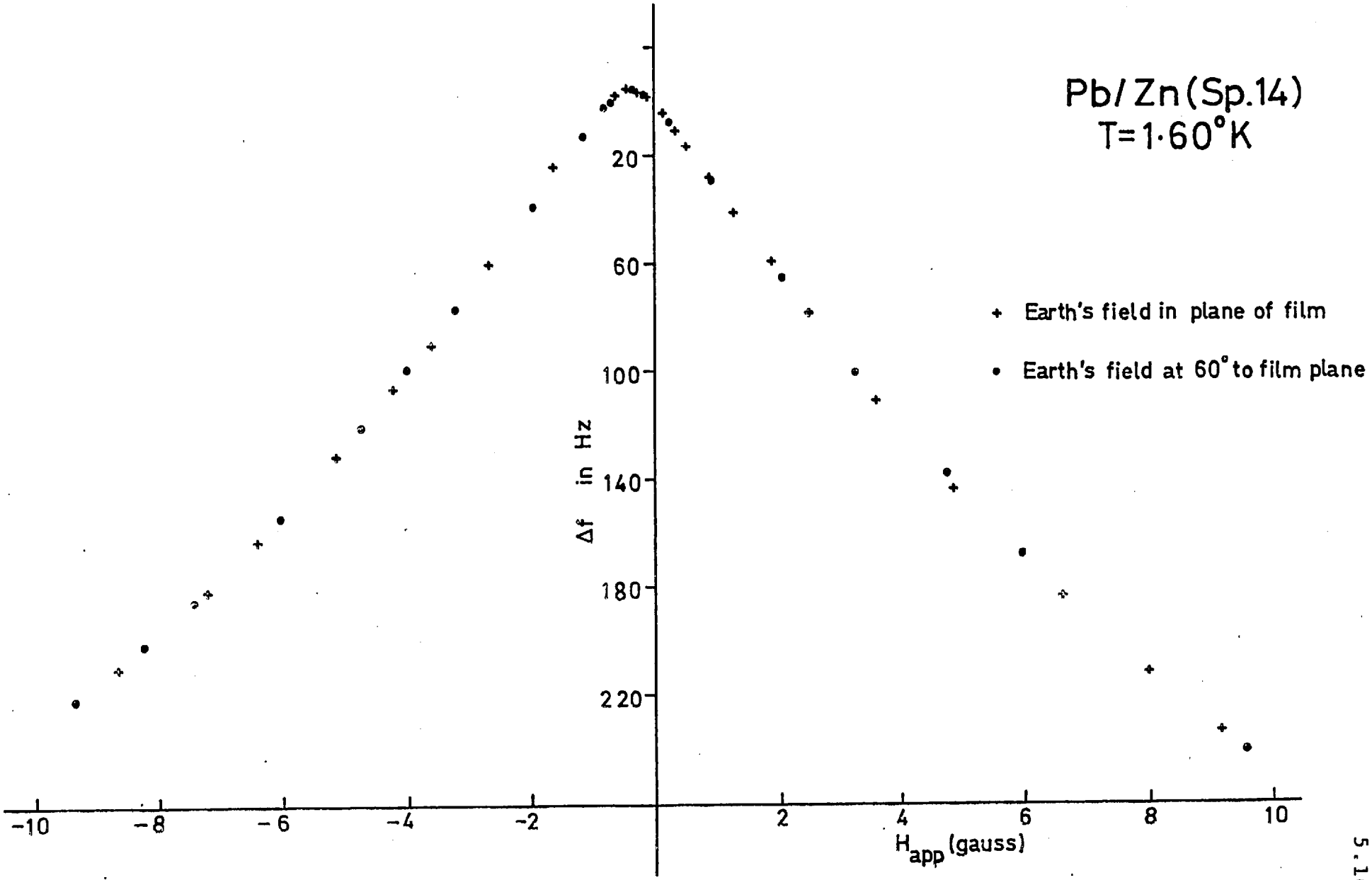

Figure 38 - Low field transition characteristics of Pb/Zn showing the effects of (i) reversal of the direction of H_{app}; (ii) rotation of specimen in earth's field.

of ~ 10 G and in these cases the empty coil effect could be measured directly for each individual coil.

5.7 Measurement of Residual Resistivity

The residual resistivity of the N layers of NS specimens was taken as being the same as that of the separate N strips that were deposited simultaneously (§3.7). The resistance of a strip was measured at room temperature and at 4.2^{o} K. The measuring technique has been described in §3.8. The film holder assembly, attached to a cupro-nickel tube was lowered into a liquid He transport dewar for the low temperature measurement. Care was taken to ensure that the room temperature resistance was reproduced after warm-up, indicating that no structural damage to the film had occurred in the process of rapid cooling. The residual resistivity of the films is given by

$$\rho_{4.2} = \frac{\rho_L}{(R_T/R_{4.2} - 1)}$$

where ρ_L is the intrinsic resistivity of the bulk material which for dilute alloys was taken to be that of the host metal. R_T and $R_{4.2}$ are the film resistances at room temperature and in liquid helium respectively. The residual resistivity of the films includes the effects of boundary scattering. To calculate the corresponding value of the residual resistivity in a bulk specimen of the same material, tabulated results of Toxen et al. (95) based on Fuch's theoretical analysis are used. For this and for the calculation of ℓ the following values of the constant $\rho\ell$ (in units of 10^{-11} ohm cm^2) are used: Ag, 1.16 (96); Zn 1.8 (101); Cd 1.72 (101). Because of the large thicknesses

of our films, correction due to boundary scattering was less than ~ 5% for all Ag Aℓ alloys whereas it was ~ 100% for Sp. 1 (pure Ag), and ~ 20% for Sp.4 (Ag Mn 50 appm).

5.8 Effect of Earth's Field

As remarked in §5.6, the magnetic transition of clean N materials began for fields as low as ~ 0.5 G. In such situations, there is a strong likelihood of the earth's field affecting the measurements. As the apparatus had no facility for compensating this field, we investigated any possible effect of it by reversing H_{app} (which was always in the vertical direction). In its normal mounted position, the specimen film was always parallel to the horizontal component of the earth's field. It could be rotated in the horizontal plane by 60°. The effect of reversing H_{app} in both these positions for a Pb/Zn specimen (Sp. 14) is shown in fig. 38. It clearly shows that whereas the vertical component of the earth's field produces a measurable effect on Δf, the direction of the horizontal component relative to the film plane does not. The Δf Vs H_{app} curve is symmetrical about $H_{app} = -0.4$ G (negative fields oppose the vertical component of the earth's field). The initial (low field) slope of Δf Vs H_{app} transitions always became greater as the temperature was lowered. Accordingly the largest effects were produced by the earth's field at the lowest temperatures. The corresponding correction to Δf_N amounted to ~ 5 Hz (in several hundred) for Zn and 3 Hz for Cd at 1.6° K. For Ag no correction was necessary; the transition curve had zero slope (plateau) at low applied fields.

CHAPTER VI

RESULTS AND DISCUSSION

Introduction

In this chapter we shall present the experimental results for the Pb/Ag alloy system followed by those for Pb/Zn and Pb/Cd. In each case the results will be compared with the predictions of Deutscher's theory (62), discussed in §2.13(b) on the basis of which $(NV)_N$ may be estimated. We shall also show the effect on the screening distance in Ag of the presence of small concentrations of Mn. As a corollary to this part of the experiment, measurements of the Kondo slopes of the films and wires of Ag Mn alloys are presented. A section is devoted to the discussion of our results from the point of view of 'saturation' effects. Although we do not observe any evidence for these in our measurements, they have been reported by the Orsay Group (64, 66). The effect of having trapped flux in the specimen and also of having the N films not thick enough to avoid the breakdown field regime are briefly discussed in this connection We end this chapter with a general discussion of the method, technique, some of the experimental difficulties involved together with suggestions for future work.

6.1 δ for Ag Alloys

(a) Ag and Ag Aℓ

Figs. 39(a) and (b) show the plot of $T^{\frac{1}{2}}\delta$ vs T for all the Ag alloy specimens studied. $T^{\frac{1}{2}}\delta$ is a convenient quantity to

plot because it is proportional to the dimensionless quantity $q_o\delta$, appearing in Deutscher's theory (62), the slope of which as function of temperature, it is claimed (§2.14), would show up the presence of any 'saturation' effects. Confining our attention to Ag Aℓ alloys for the present, the figures show that δ decreases systematically as ρ_{res} is increased which is the correct qualitative behavior as expected from theory.

For comparing the results with Deutscher's theory (62), we have to plot the quantity $q_o\delta$ against κ_{oo}. $q_o^{-1} = \left(\frac{\hbar V_F \ell}{6\pi k_B T}\right)^{\frac{1}{2}}$ has been calculated for Ag using $\rho\ell = 1.16 \times 10^{-11}$ ohm cm^2 (96) and the free electron value of $V_F = 1.38 \times 10^8$ cms^{-1} (102), yielding $q_o^{-1} = \frac{2540}{(\rho_{res} T)^{\frac{1}{2}}}$ Å, where ρ_{res} is expressed in μΩ cm. $\kappa_{oo} = \lambda_{oo} q_o$ (ref. Eqn II-68) may also be expressed as

$$\kappa_{oo} = \left(\frac{6c^2e^2\rho^2\gamma}{\pi k_B^2}\right)^{1/2}\left(\frac{k_B T}{\sqrt{\psi_2(\tfrac{1}{2})}\,\Delta_s}\right) \qquad \text{(VI-1)}$$

where the free electron model identity $\gamma = \left(\frac{\pi^2 k_B^2}{e^2}\right)\frac{1}{V_F \ell\rho}$ has been used. γ is the coefficient of the electronic specific heat per unit volume. Using $\psi_2(\tfrac{1}{2}) = \pi^2/2$, $\Delta_s = 2.15\, k_B T_{cs}$ for Pb (103) and $\gamma = 629$ ergs/cm^3 $^oK^2$ for Ag (104) one obtains $\kappa_{oo} = 0.86\, \rho_{res}\, T/T_{cs} \simeq \rho_{res} T/T_{cs}$ with ρ_{res} expressed in μΩcm. This last approximation is justified by the fact that the calculation assumes $\Delta_S(0^-) = \Delta_{BCS}$ whereas in a realistic situation, $\Delta_S(0^-)$ is slightly depressed near the interface (see fig. 11, also §2.13(c)). The actual value of $\Delta_S(0^-)$ can then be shown to be ∿15 to 20% smaller than Δ_{BCS} (and κ_{oo} correspondingly larger, Eqn.VI-1) depending on the ratio of the conductances in S and N. A plot of $q_o\delta$ Vs ρ_{res} T/Tcs for the Ag alloys is shown in fig.40(a). In order to see how the agreement with the theory depends on ρ_{res} we have calculated $q_o^{-1} \equiv \xi_N$ for all specimens whether clean or dirty by the expression given above which,

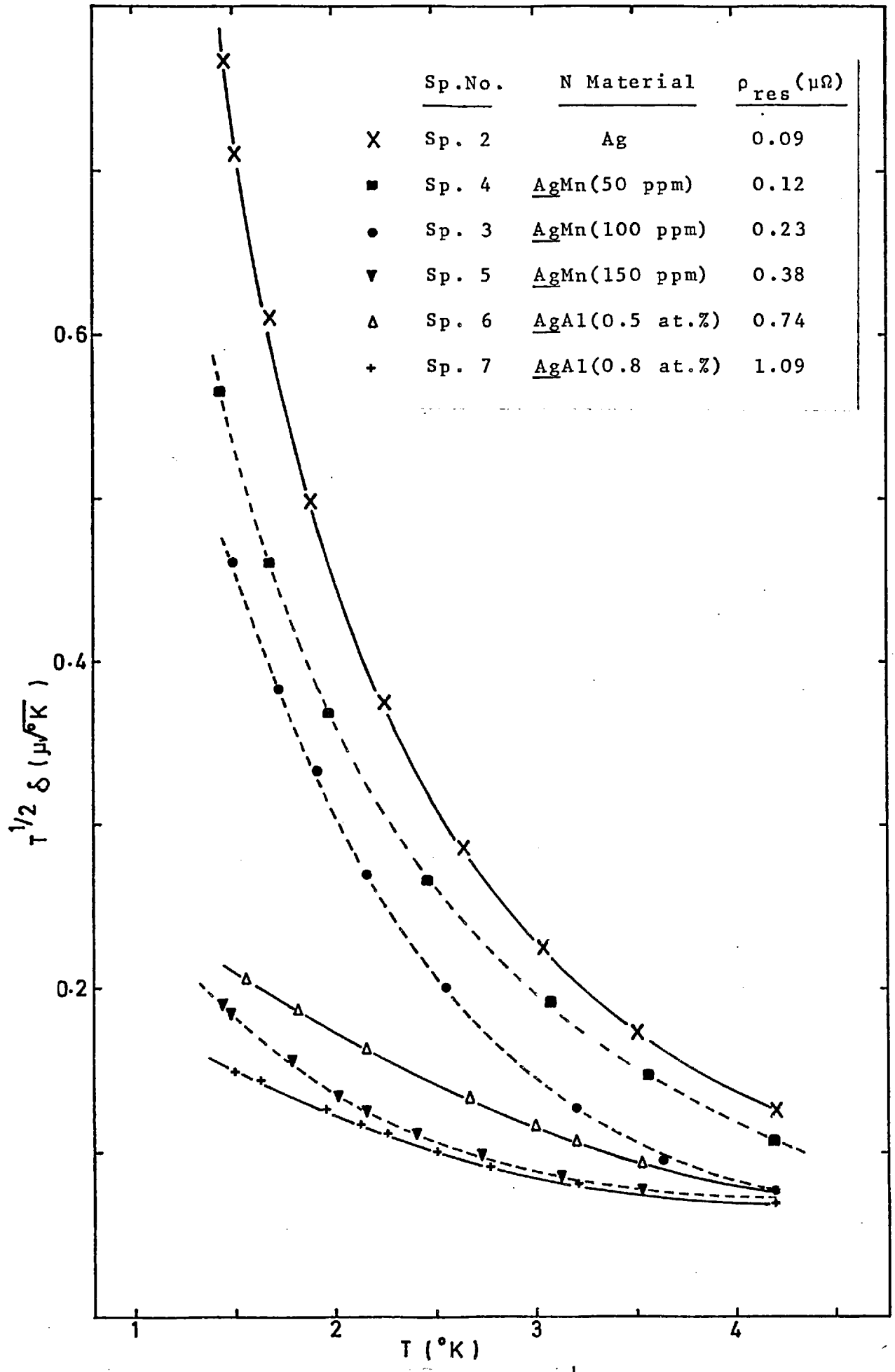

Figure 39(a) - A plot of the quantity $T^{\frac{1}{2}}\delta$ as a function of temperature for the Pb/Ag system.

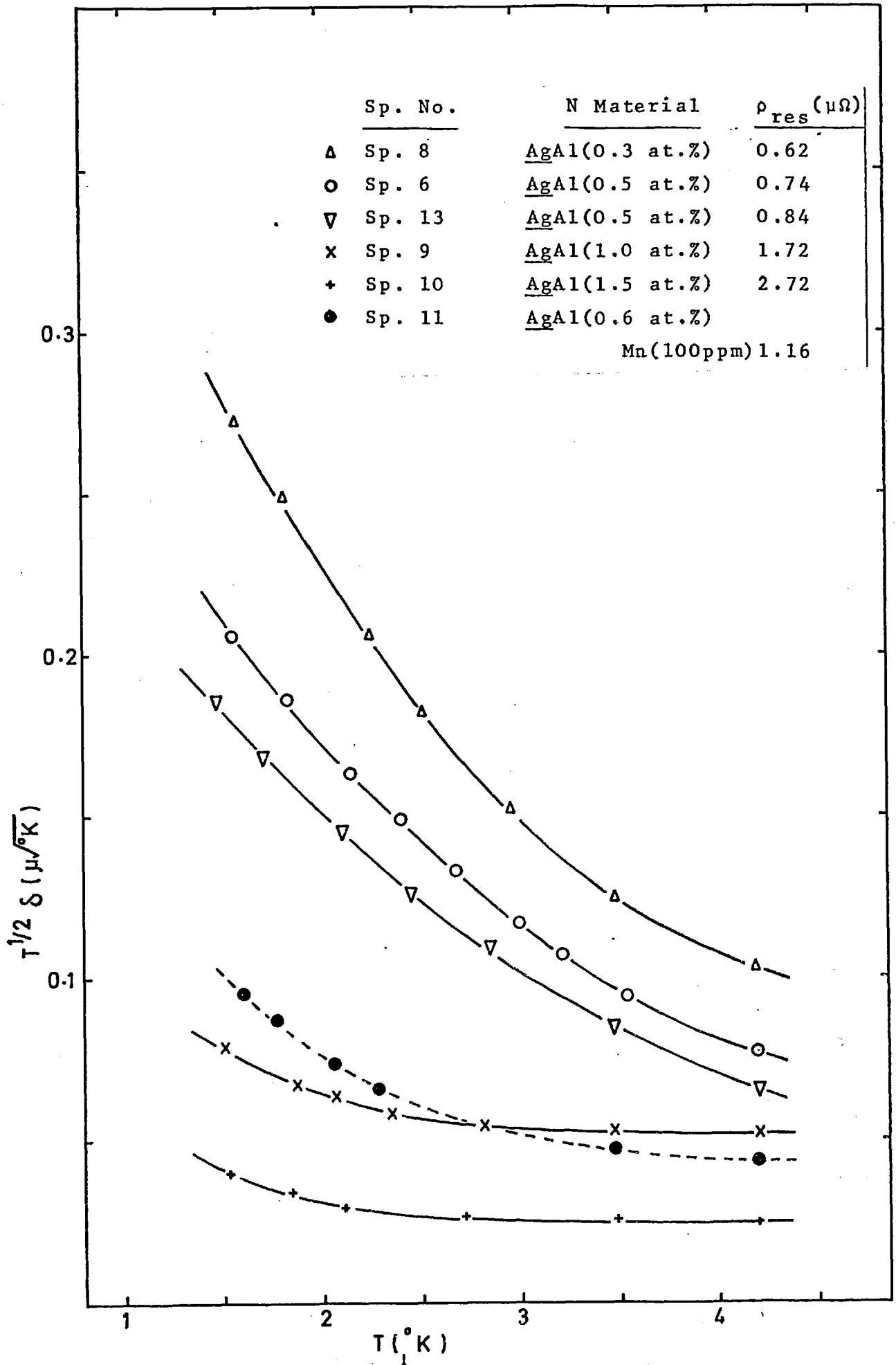

Figure 39(b) - A plot of $T^{\frac{1}{2}}\delta$ Vs T for the Pb/Ag system.

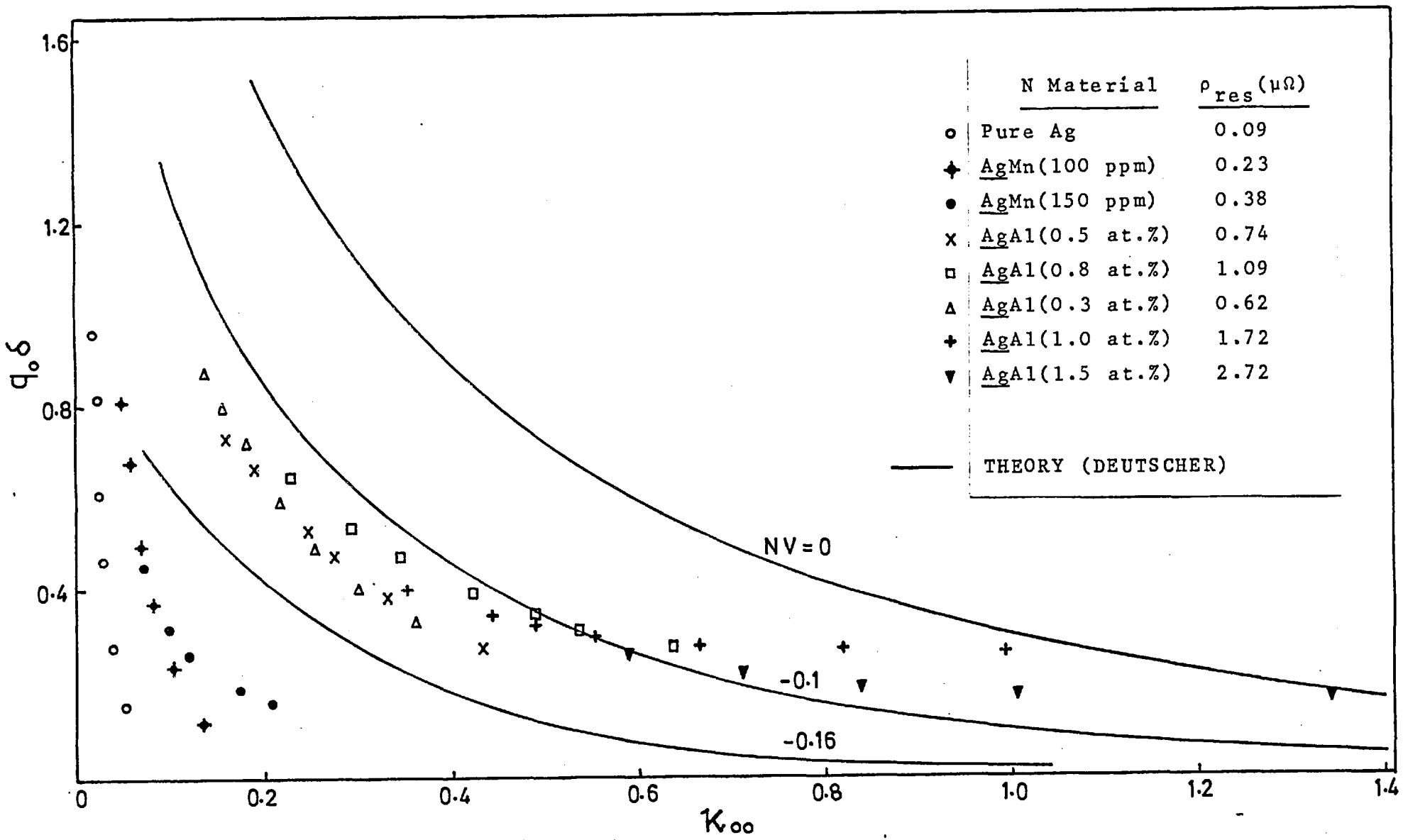

Figure 40(a) - The quantity $q_o\delta$ plotted as a function of κ_{oo} for Ag alloys. Solid curves represent Deutscher's numerical calculation(62)

strictly, is only valid in the dirty limit. The values of q_o^{-1} at 4.2°K for each specimen together with other important characteristics are listed in Table VI.1.For the dirtiest alloy used, Sp.10 AgAℓ(1.5 at %),ℓ∿430 Å and q_o^{-1}(4.2°K) ∿800 Å. From the figure we see that in the clean limit (κ_{oo} small) agreement with the theory is poor, in the sense that $q_o\delta$ does not follow any one of the family of curves obtained theoretically. As we approach the dirty limit, i.e. shorter m.f.p.'s agreement with theory seems to improve, with data points for all Ag Aℓ specimens straddling the curve for $(NV)_N = -0.1$. For $\kappa_{oo} \gtrsim 0.5$, the points cross the $(NV)_N = -0.1$ curve and lie between the curves corresponding to $(NV)_N$ of -0.1 and 0. In this region, the value of $(NV)_{Ag}$ has been estimated graphically as -0.07 ± 0.02.

From experiments similar to ours but conducted on hollow cylindrical films, Valette (63,64) estimates $(NV)_{Ag} \sim +0.06$ with possible limits of +0.01 and +0.09. Part of the discrepancy between our value of $(NV)_{Ag}$ and his arises out of the particular value of $\rho\ell$ that he uses for Ag, i.e. $\rho\ell = 0.733 \times 10^{-11}$ Ω cm^2 reported by Boulesteix (97). This value of $\rho\ell$ was measured at 112°C. Reynolds and Stillwell (98) had earlier obtained $\rho\ell = 0.84 \times 10^{-11}$ Ω cm^2 at room temperature. Boulesteix, in fact, attributes the difference between the two sets of results for $\rho\ell$ to the fact that $\rho\ell$ may not be entirely temperature independent. This makes it all the more necessary to use $\rho\ell$ measured at liquid He temperatures. For this reason we have used $\rho\ell = 1.16 \times 10^{-11}$ Ω cm^2 given by Chambers(96). Use of this value of $\rho\ell$ with Valette's data gives a much lower estimate of $(NV)_{Ag}$ ($-0.04 < (NV)_{Ag} < 0$, see fig.40(b)). The other source of quantitative disagreement between our results and his lies in the measured values of the screening distance which he, on average, finds to be ∿40% larger than ours. There

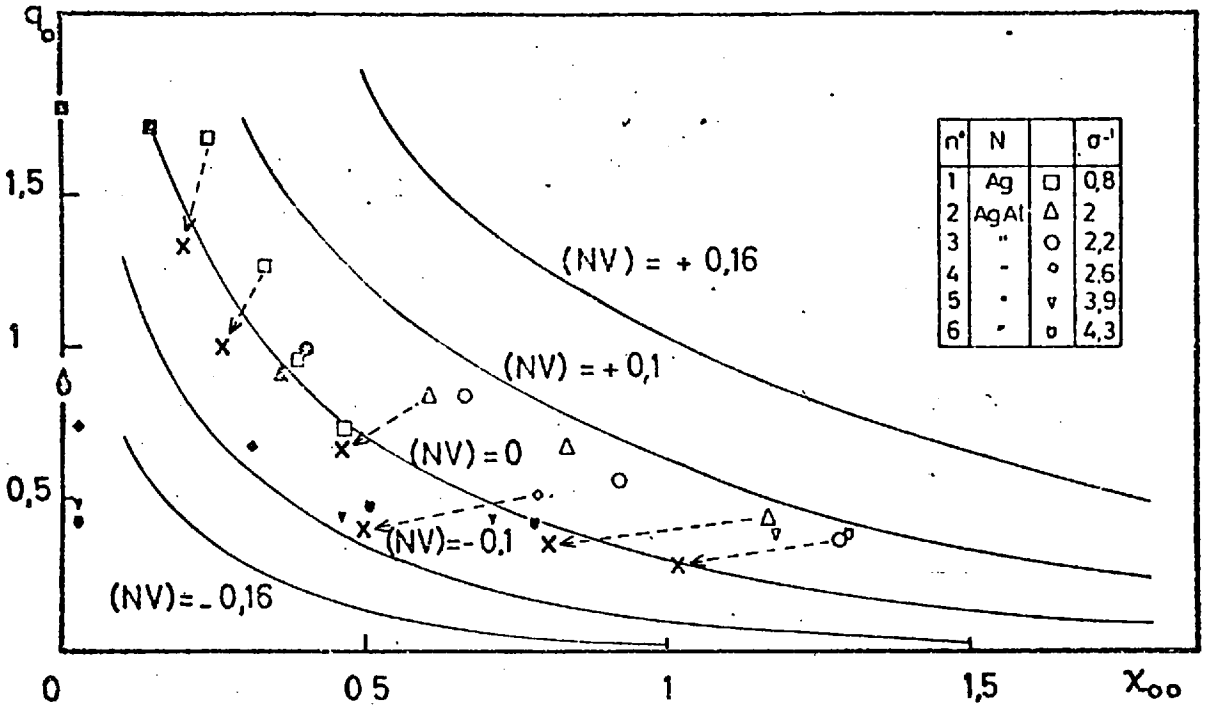

Figure 40(b) - $q_o \delta$ Vs κ_{oo} as reported by Valette (63, 64) Arrows show how a set of typical points would be transposed if the 4.2°K value of $\rho\ell$ (1.16×10^{-11} Ωcm^2) is used instead of the high temperature value used by Valette ($\rho\ell(112^oC) = 0.733 \times 10^{-11}$ Ωcm^2). Points "X" on the figure indicate the new positions of the points.

are several likely explanations for this. Firstly, his alloys were all evaporated en masse rather than in pellets, resulting in a greater likelihood of inhomogeneity. Secondly, for the calibration of the oscillator to convert the observed frequency changes into (corresponding) distances, the cylindrical geometry that he uses (S on the inside) may present special problems. This is so because one is not able to obtain $(\Delta f)_{Pb}$ corresponding to the transition of the entire thickness of Pb. If the entire Pb film were driven normal, the enormous contribution of the hollow cavity of the cylinder to ΔL would be included in the measured Δf. In Valette's experiment, this difficulty was avoided by carrying the magnetic transition of the Pb only far enough to destroy superconductivity in the bulk, leaving a superconducting sheath on the inner surface of S. Uncertainties in the calibration would be introduced by the need to estimate the sheath thickness. Measurement of $(\Delta f)_{Pb}$ could also be difficult if a sizeable 'peak' were present in the transition curve at $H = H_c$ or if, the sheath did not provide total shielding of the hollow cavity. If, or how, these possible sources of error were accounted for is not given in (64) nor indeed does the possibility of electromagnetic 'losses' affecting the results appears to have been considered. All considered, we believe our calibration using flat films to be more reliable than would be possible using cylindrical films. It could be argued, on the other hand, that an oxide layer at the interface in our specimens would depress the value of δ and hence of $(NV)_{Ag}$ that we observe. Although this possibility can never entirely be ruled out in any such experiment, we consider this to be unlikely for the following reasons. For all but one specimen, Ag was deposited first and

as it does not readily oxidise, the chances of oxide formation are diminished. Additionally, if the conditions inside the vacuum chamber were conducive to the oxidation of films, a serious decoupling of N and S would be expected in cases where the Pb was deposited first. No such effect was observed. Although the average interval between N and S evaporations was ~ 15 seconds, this obviously varied from one specimen to another. In fact, on some occasions up to 45 seconds elapsed between the two depositions. If oxidation were occurring, the thickness of the oxide layer would then be expected to vary from specimen to specimen. However, judging by the consistency of the variation of δ with ρ and particularly by the fact that $q_o\delta$ for all the dirty specimens shows a systematic variation with κ_{oo}, the presence of an oxide layer would appear unlikely. Finally, the appearance of the sharp dip in the Δf vs H_{app} curves for NS specimens (§5.3) which implies the destruction of the sheath at the interface also points to good coupling between N and S.

(b) Ag Mn and Ag Aℓ Mn Alloys

From fig. 39(a) we see that although ρ_{res} = 0.38 μΩcm for specimen 5 (Ag Mn 150 ppm), the screening distance is smaller than that for specimen 6 (Ag Aℓ 0.5 at %) with ρ_{res} = 0.74 μΩcm. This is attributed to the additional pairbreaking effect of the Mn atoms on account of their magnetic moment. To investigate this phenomenon in a dirty alloy in which the effects due to shorter m.f.p. and localised moments could be distinguished, we carried out measurements on a Ag Aℓ Mn (0.6 at % Aℓ, 100 ppm Mn) alloy, specimen 11. The quantity $q_o\delta$ vs κ_{oo} for this system is

plotted in fig. 41. The depairing effect of the magnetic impurity (i.e.depression of $q_o\delta$) is clearly seen.Qualitatively, this is the behavior to be expected since the measurements are made at a temperature well above the estimated Kondo temperature $T_K \sim 0.4^oK$ for the Ag-Mn system (60) when the moments are uncompensated. Far below T_K, however, the system would be expected to behave almost as a spinless system. The expected pairbreaking properties both below and above T_K have been confirmed by Hauser et al. (46) in Cu Fe ($T_K \simeq 14^oK$) and Cu Mn ($T_K < 1^oK$) alloys.

6.2 Resistance of Ag Alloys

(a) Ag Aℓ films

The nominal concentrations and residual resistivites of Ag Aℓ films are plotted in fig. 42. Shown in the same figure are the data of Seth and Woods (99) for three concentrations of well-annealed Ag Aℓ alloys in bulk. The agreement between the two sets of data is seen to be fair, perhaps surprisingly so since our films were not annealed. This would seem to indicate, although it cannot be taken as conclusive evidence of, a high degree of homogeneity in these films.

(b) Ag Mn Films and Wires

The resistances of all magnetic alloy films and wires were measured on a sensitive resistance apparatus as a function of temperature between 4.2^oK and 1.5^oK. The results are shown in figs. 43(a) and (b) where the change in resistivity $\Delta\rho$ is plotted

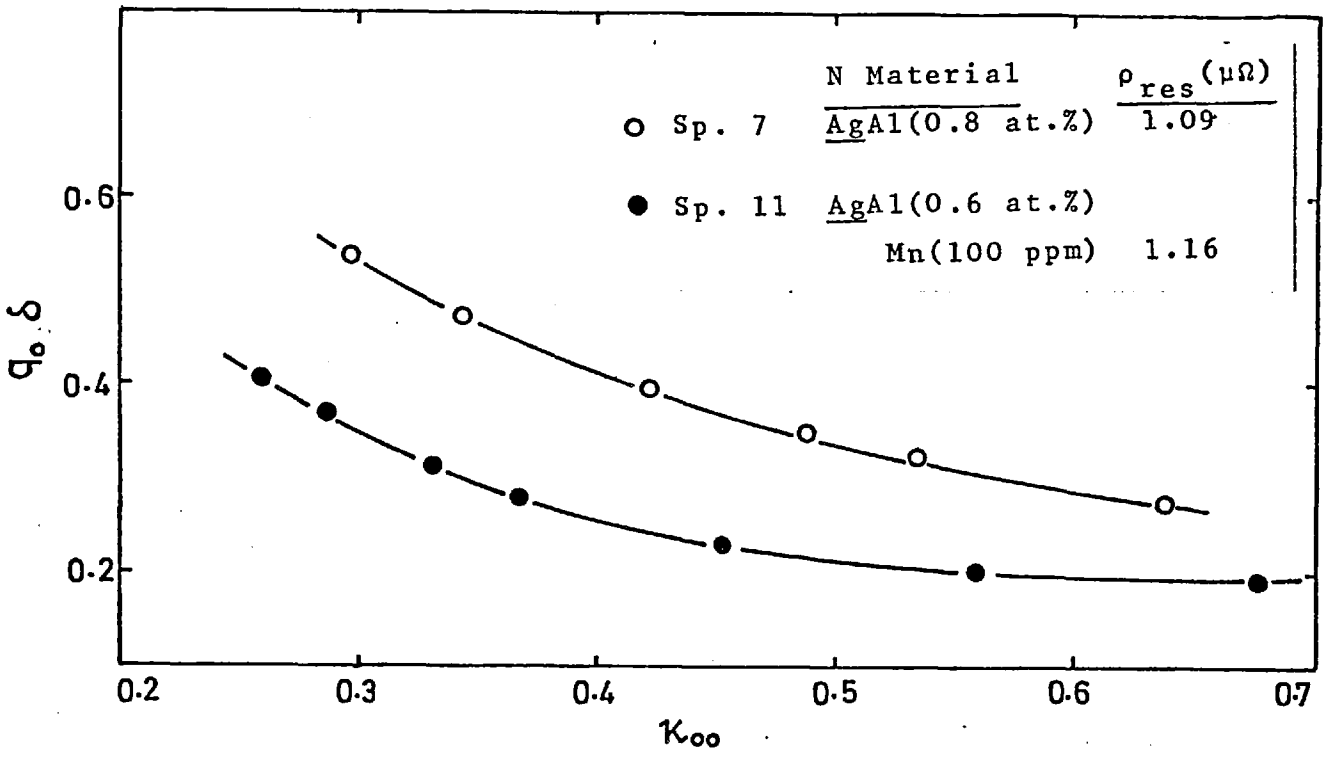

Figure 41 - q_o^{δ} Vs κ_{oo} for Ag Aℓ alloys with and without Mn doping.

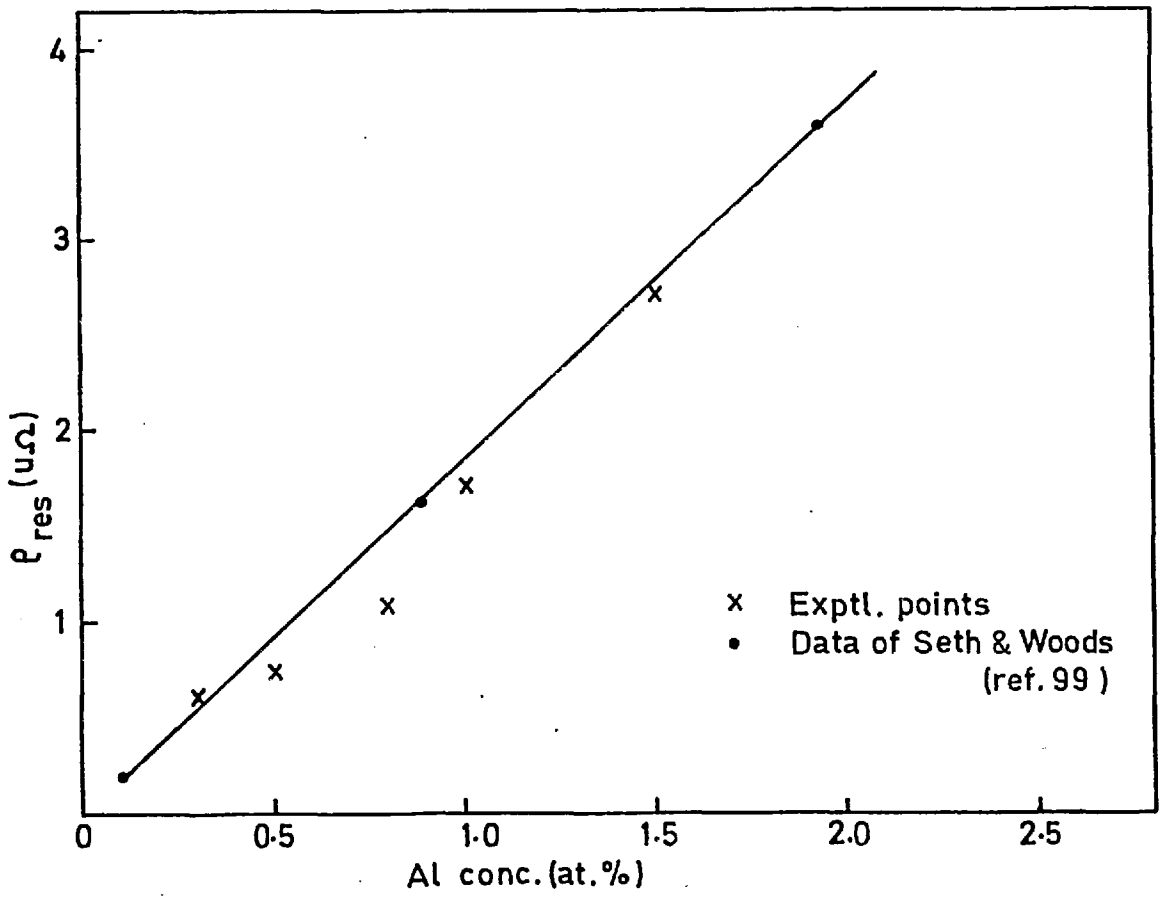

Figure 42 - The residual resistivities of Ag Aℓ films as a function of concentration.

against $\log_{10}T$. The Mn concentrations of the wires were determined from the Kondo slopes $\left|\frac{d\rho}{d \log T}\right|$ by comparison with the data of Jha and Jericho (100). We notice a large discrepancy between the Kondo slopes of the wires and those of the corresponding films, the latter being an order of magnitude smaller. These results are summarised in Table VI-2.

Nominal Conc.	Films $\Delta\rho$	Wires $\Delta\rho$	Mn conc. of wires by comparison with ref. 100	$\frac{\Delta\rho_T(\text{wire})}{\Delta\rho_T(\text{film})}$
50	0.2	2.9	125 ppm	14.0
100	0.29	3.6	160	12.4
150	0.46	4.9	220	10.6

$$\Delta\rho_T = \rho(4^oK) - \rho(2^oK)$$

Table VI-2

The reason for the greatly reduced Kondo slopes of the films is not clear. Before going on to consider two likely causes of this, we point out that the residual resistances in the films are considerably higher than those in the bulk material as the data on the relevant graphs shows. This implies that in the films scattering at defect sites is predominant in determining the residual resistivities which therefore will not be a useful indicator of the amount of Mn in solution.

The possibility of some of the Mn having been oxidised during evaporation suggests itself as a natural explanation for

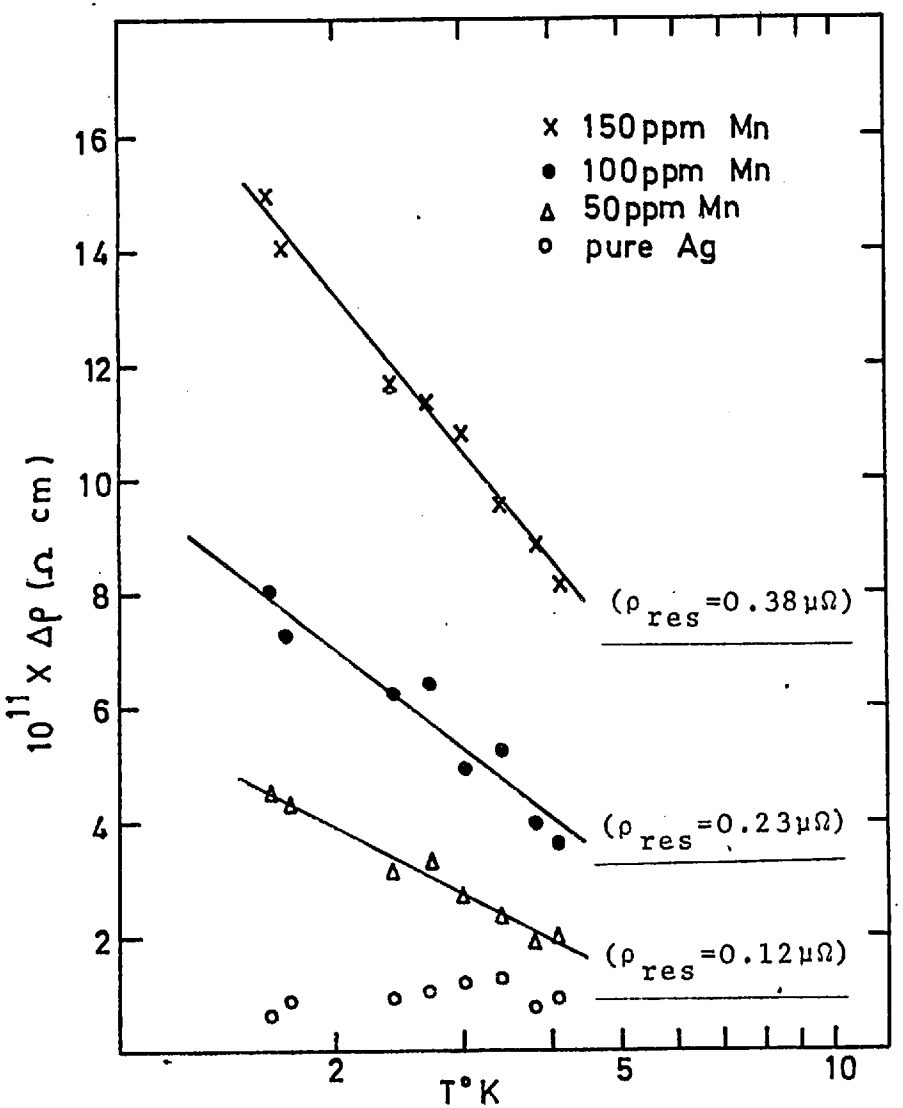

Figure 43(a) - Plot of $\Delta\rho$ Vs $\log_{10}T$ for AgMn films.

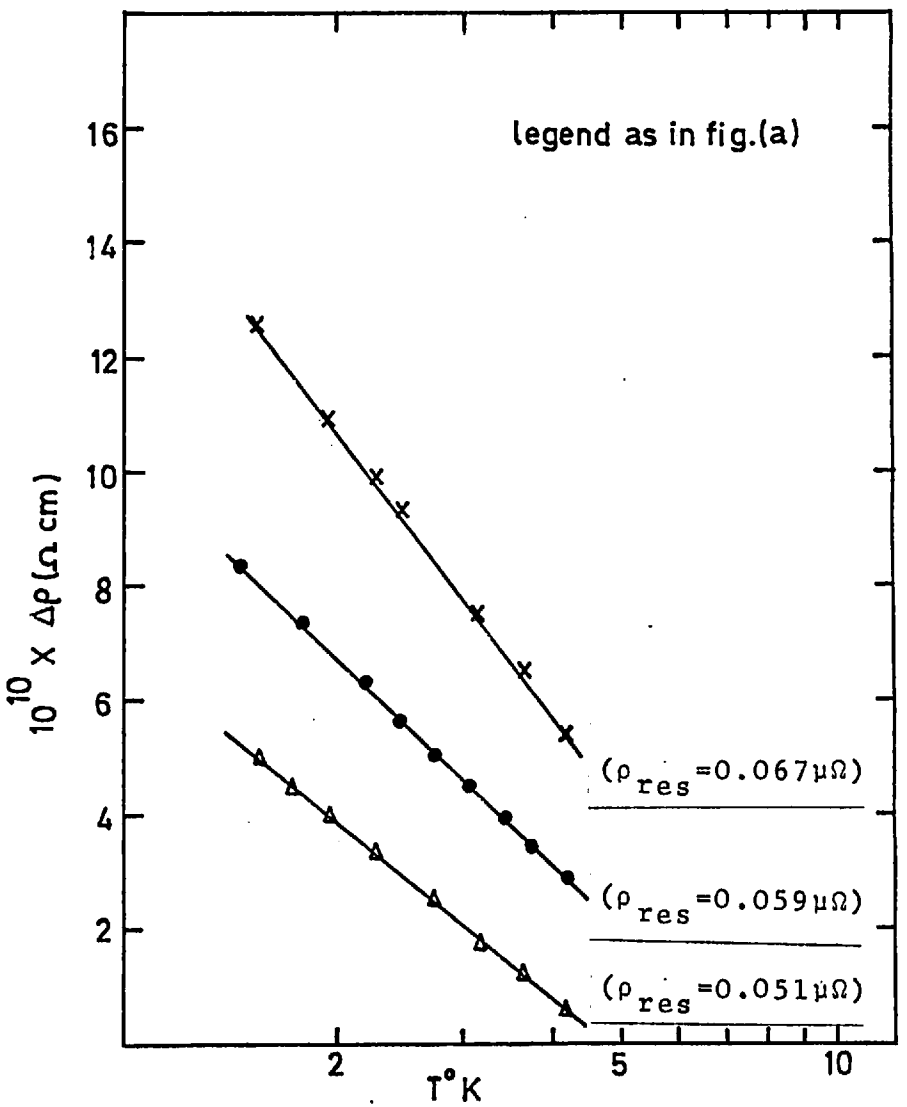

Figure 43(b) - $\Delta\rho$ Vs $\log_{10}T$ for Ag Mn wires.

the behavior of the films. Although it cannot be entirely ruled out, it would seem unlikely to be solely responsible, for two reasons. Firstly a quick calculation shows that even if the residual atmosphere in the evaporation chamber at a pressure of 10^{-5} torr were all oxygen, this would still be one hundredth of the amount required to oxidise all the Mn in a 1.5g charge of a 100 ppm alloy. Moreover, if oxidation of Mn were responsible one would not expect nearly the same proportionality maintained between the slopes of films and wires for all the specimens.

An alternative explanation for the observed behavior is the following. In §3.7 it was mentioned that on average each pellet took ~ 5 secs. to evaporate. Now it is known that when large amounts of Ag Mn are evaporated en masse fractional evaporation occurs with Mn coming off first. Were this to happen in the case of our pellets, the resulting films would be composed of alternate lamellae of comparatively high and low Mn contents respectively. When the resistance of such a film is measured, the lamellae of high Mn concentrations and hence high resistivity would be shorted out by the layers of depleted Mn content. The measured Kondo slopes will therefore indicate a smaller amount of Mn in the alloy. On the other hand all the Mn atoms present will participate in depairing the Cooper pairs that diffuse into the film in a proximity experiment. Unfortunately, the possibility of concentration gradients producing the observed behavior in the films was not thought of at the time of the experiments and hence it was not put to the test by investigating the effect of annealing the films. At this

juncture we add that the homogeneity of the bulk material, which was not annealed either, was tested by making measurements on three different samples of the 100 ppm and two of the 50 ppm alloys. For each alloy the results on different samples agreed to within ~ 5%.

6.3 Zn and Cd

The important characteristics of Zn and Cd specimens are given in table VI-1. By using γ = 690 ergs/cm^2 $^oK^2$ for Zn and 520 ergs/cm^3 $^oK^2$ for Cd (78) the following values of q_o are obtained for the two metals

$$\underline{Zn} \quad q_o^{-1} = \frac{2070}{(\rho_{res}\, T)^{\frac{1}{2}}} \quad \text{Å}$$

$$\underline{Cd} \quad q_o^{-1} = \frac{2360}{(\rho_{res}\, T)^{\frac{1}{2}}} \quad \text{Å}$$

In each case $\kappa_{oo} \simeq \rho_{res}\, T/T_{cs}$. In fig. 44 we have plotted $q_o\delta$ vs κ_{oo} for specimens of pure Zn, Cd and Cd Mg (2 at %). Whereas for Ag with its very low or zero transition temperature the ratio k/q_o is very nearly unity at all temperatures, this will not be so for Zn and Cd.Using (II-9B) and the known value of T_{CN} for each metal, the variation of k/q_o with temperature may be calculated. For instance, kq_o^{-1} for Cd decreases from 0.648 at 3^{o}K to 0.608 at 2.2^{o}K.

In §2.13(b) it was seen that Deutscher's calculation of $q_o\delta$ as a universal function of κ_{oo} was done for fixed values of the parameter kq_o^{-1} (fig. 17). Therefore as the temperature and

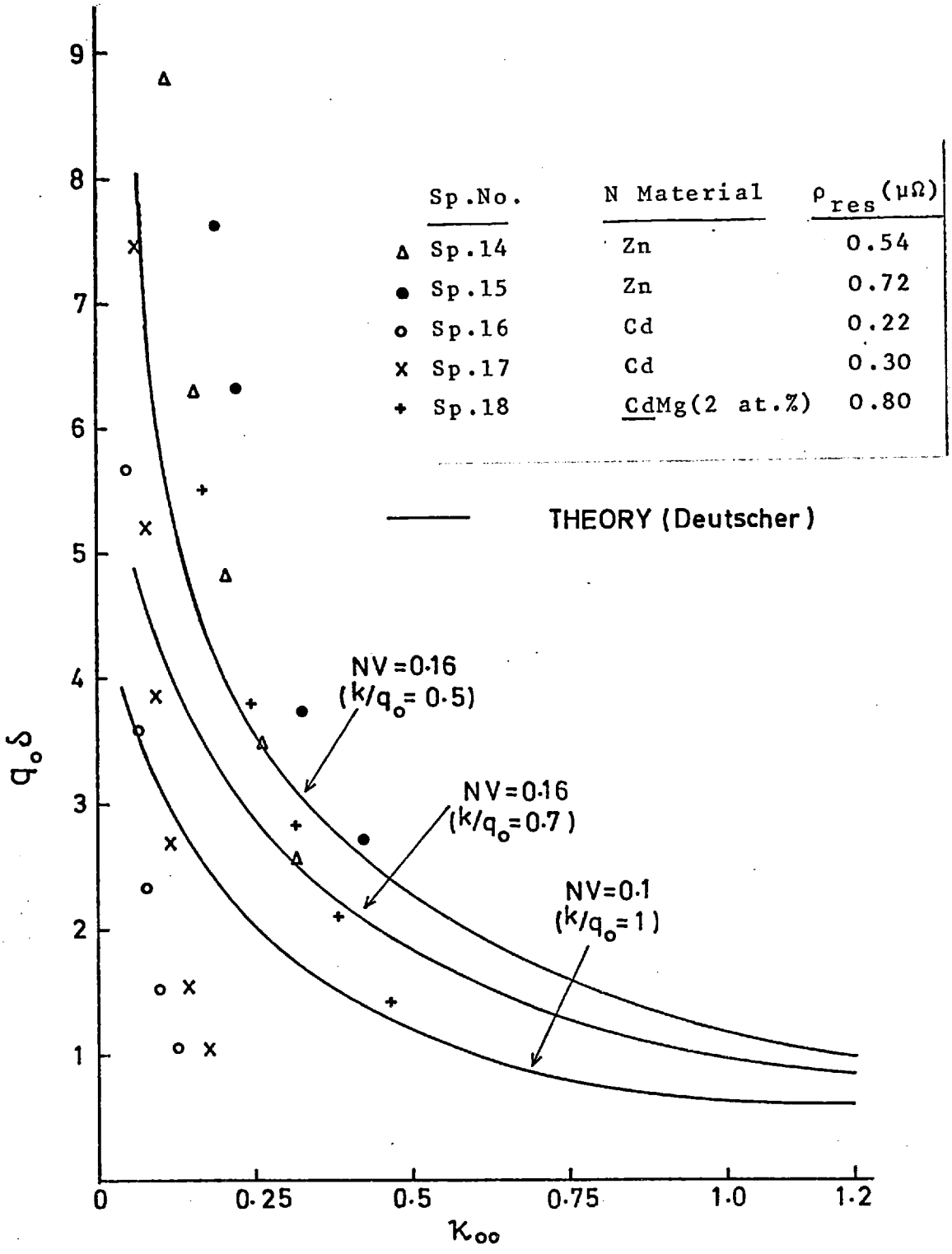

Figure 44 - $q_o\delta$ Vs κ_{oo} for Zn, Cd and CdMg(2 at.%)

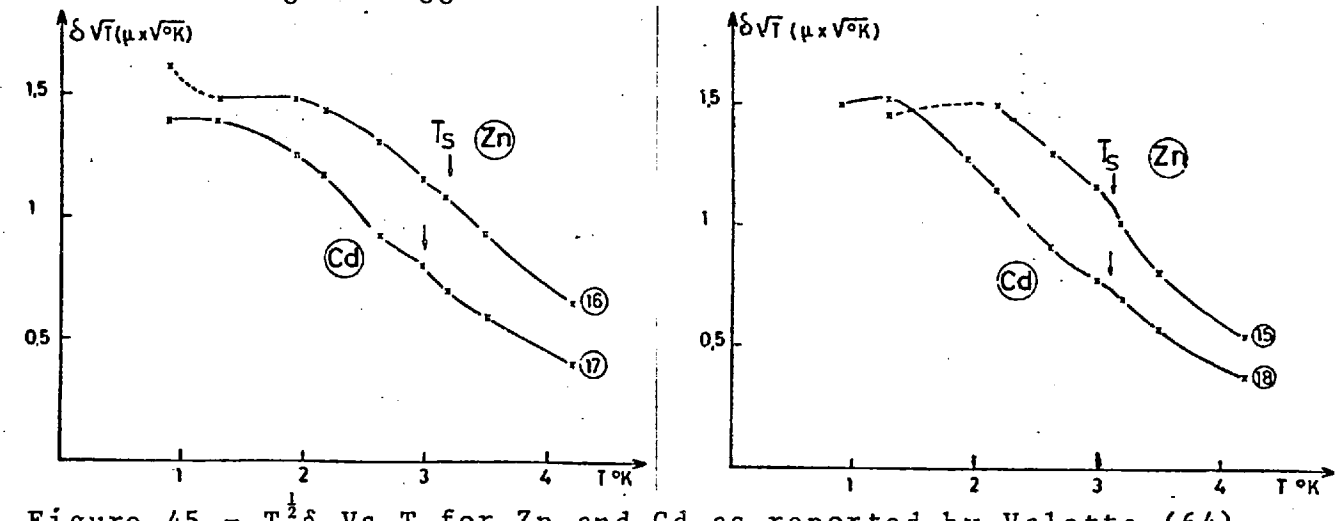

Figure 45 - $T^{\frac{1}{2}}\delta$ Vs T for Zn and Cd as reported by Valette (64).

hence κ_{oo} is lowered the growth of $q_o\delta$ for Zn and Cd will be more rapid than that along any of the solid curves of fig. 17. In fact, the theory would predict $q_o\delta$ to follow a curve of the kind shown dotted on the figure. However, as our measurements were made in the clean limit no quantitative agreement with theory is to be expected. As in the case of Ag, the dirtier material (Cd Mg alloy) seems to produce an improved agreement with theory. Because of difficulties encountered in the preparation of Zn and Cd alloy films (§3.6) we have not been able to study the alloy systems in any detail. The difficulties of preparation are not insurmountable, however, and measurements on specimens well into the dirty limit ought to provide a good test for the theory. The principal reason for our measurements on pure specimens of these two metals was to determine if 'saturation' effects could be observed. These results, together with those for Ag, are discussed in the next section from the point of view of the 'saturation' phenomenon.

6.4 'Saturation' Effects

In §2.14 we had described the Orsay model of 'saturation' and pointed out some apparent shortcomings of it on the theoretical side. Nevertheless, their results on the Pb/Ag system (fig. 10) do show an abrupt change in the slope of the curves $T^{\frac{1}{2}}\delta$ vs T at T ~ $2^{o}K$ for all samples regardless of the m.f.p.. We, however, have been unable to observe this behavior (fig. 39) for any of our Ag or Ag alloy specimens. The Orsay Group's results on Zn and Cd (fig. 45) show a discontinuity in the slope of $T^{\frac{1}{2}}\delta$ vs T curves at around $3^{o}K$. In these cases, the slopes

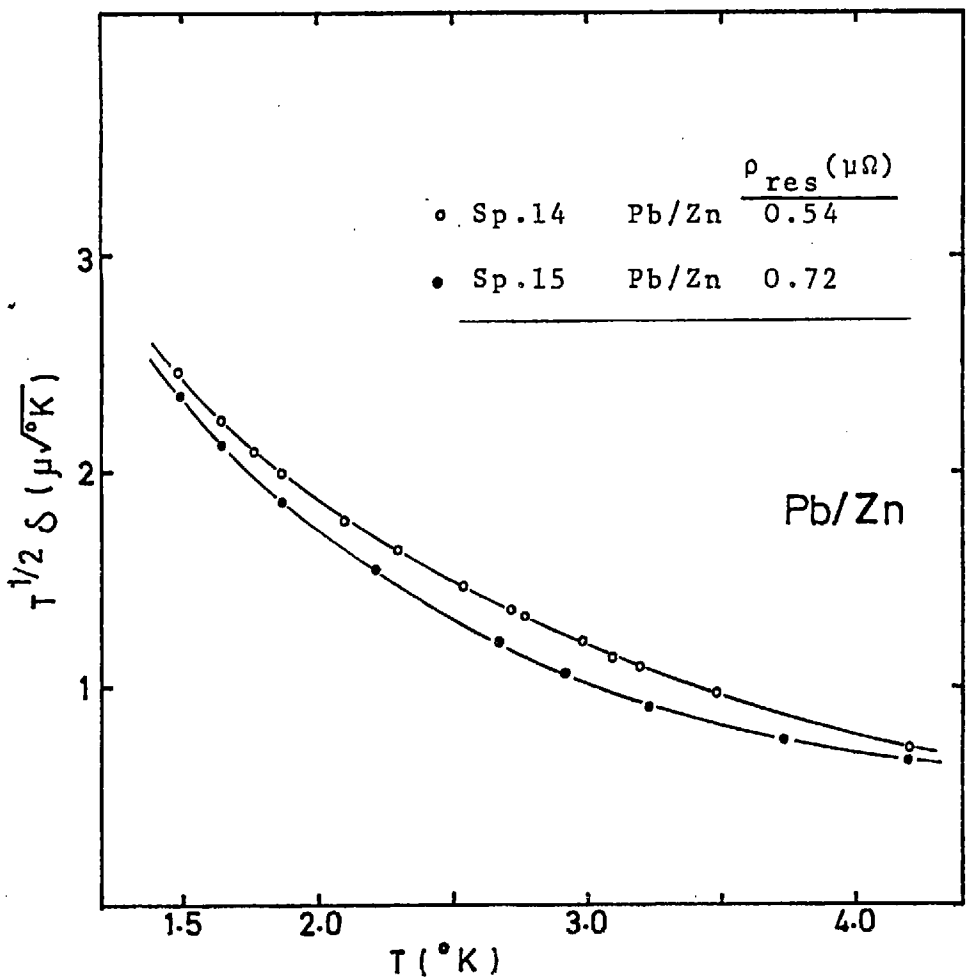

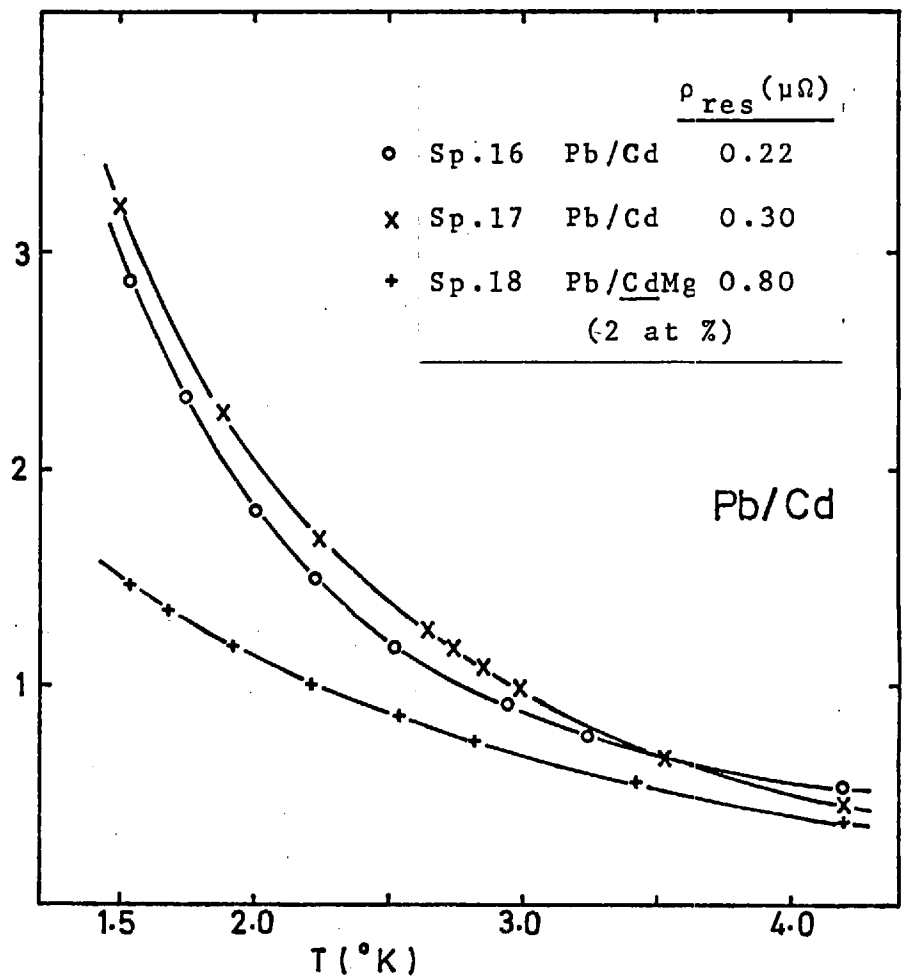

Figure 46 - $T^{\frac{1}{2}}\delta$ Vs T for Zn, Cd and CdMg alloy.

do not become zero but their magnitudes show a very small decrease just below the so called 'saturation' temperature. Our measurements on two Zn, two Cd and a CdMg specimen (fig.46) fail to show, within the accuracy of our measurements, any abrupt discontinuity in the slopes. The temperature range of interest was carefully scanned for all the specimens with the temperature reduced in steps of $\sim 0.1^{\circ}K$. The results for a Cd specimen shown in fig.46(c)(page 6.22) are typical of all these specimens.

Before attempting an explanation of why we think the two sets of results disagree, we refer the reader to §2.14(c) where it was pointed out that the Orsay Group's interpretation of their model as predicting a zero slope in the $T^{\frac{1}{2}}\delta$ vs T curves for Ag at $T < T_s$ was erroneous even if the model itself were accepted. The same criticism applies to their interpretation of the results for Cd and Zn where on assuming that $x_o = q_o^{-1}$ they obtain the following result

$$k\delta = 1 - k/q_o + \text{Constant} \qquad \text{(VI-2)}$$

They explain the difference in the behavior of Ag on the one hand and Zn and Cd on the other by the fact that whereas kq_o^{-1} remains equal to unity at all T for the former, it is a decreasing function of temperature for the latter. It is interesting to compare their results quantitatively with this prediction which the authors do not seem to have done (64). One finds that the predicted increase in δ on lowering T from $3^{\circ}K$ to $2.2^{\circ}K$ for Zn is within ~ 10% of their experimental value (their specimen 15). For Cd, however, the experimental value is more than twice as large as that predicted by (VI-2) suggesting that the good agreement in the case of Zn may be fortuitous.

As already mentioned, we do not observe any saturation effects in any of the systems we have studied. Our experiments

have, however, suggested two possible explanations for the discrepancies between our results and those of the Orsay Group, which are now discussed.

(i) Film thickness - breakdown effects

For the measurement of δ the specimens have to be much thicker than the coherence length k^{-1}. If they are not sufficiently thick, breakdown effects appear, the theory of which was sketched in §2.12.

One specimen for which we observed a breakdown-like (so called for reasons discussed below) behavior was Specimen 1 (Ag/Pb, $d_N \sim 1.2\mu$, $k^{-1}_{Clean} = \frac{\hbar v_F}{2\pi k_B T} \simeq 0.4\mu$ at 4.2^oK). The results for Sp. 1 are shown in fig.47(a). The "breakdown" occurs at a field H_b' of ~ 10 G for all $T < 3^oK$, with H_b' varying little with temperature. Fig.47(b) is a plot of $T^{\frac{1}{2}}\delta$ Vs T for the specimen and a significant decrease in the magnitude of the slope with the lowering of T is clearly seen.

Theoretically, the temperature T^* below which a breakdown is observed is given by (56)

$$d_N / \lambda(0,T^*) = \frac{3}{2}\{\cosh k(T^*) d_N\} \qquad \text{(VI-3)}$$

Eqn.(VI-3) has been derived for dirty specimens and in that limit has been found to be in fair agreement with experiment by Krätzig (10) who studied the breakdown effect in Pb/Al, Pb/Ag and Pb/Cu. If we use Eqn.(VI-3) to estimate T^* for our specimen which is in the clean limit, we obtain a value of $\sim 3.5^oK$ which may at first sight seem to compare favorably with our observation of breakdown-like effects below $\sim 3.1^oK$. We however do not think that the observed temperature of 3.1^oK corresponds to T^* for our specimen, for the following reason. The effect that we observe does not have the characteristics of a true breakdown by which we mean a first order transition accompanied by supercooling and field hysteresis. To the accuracy of measurements all transitions were reversible i.e. no hysteresis was observed in increasing and decreasing fields. The "breakdown" that we observe seems to correspond to the field H_b' shown on fig.48, (which is reproduced from Hurault(47)) and is based on the results of his numerical solutions for the b/d field. H_b' represents the

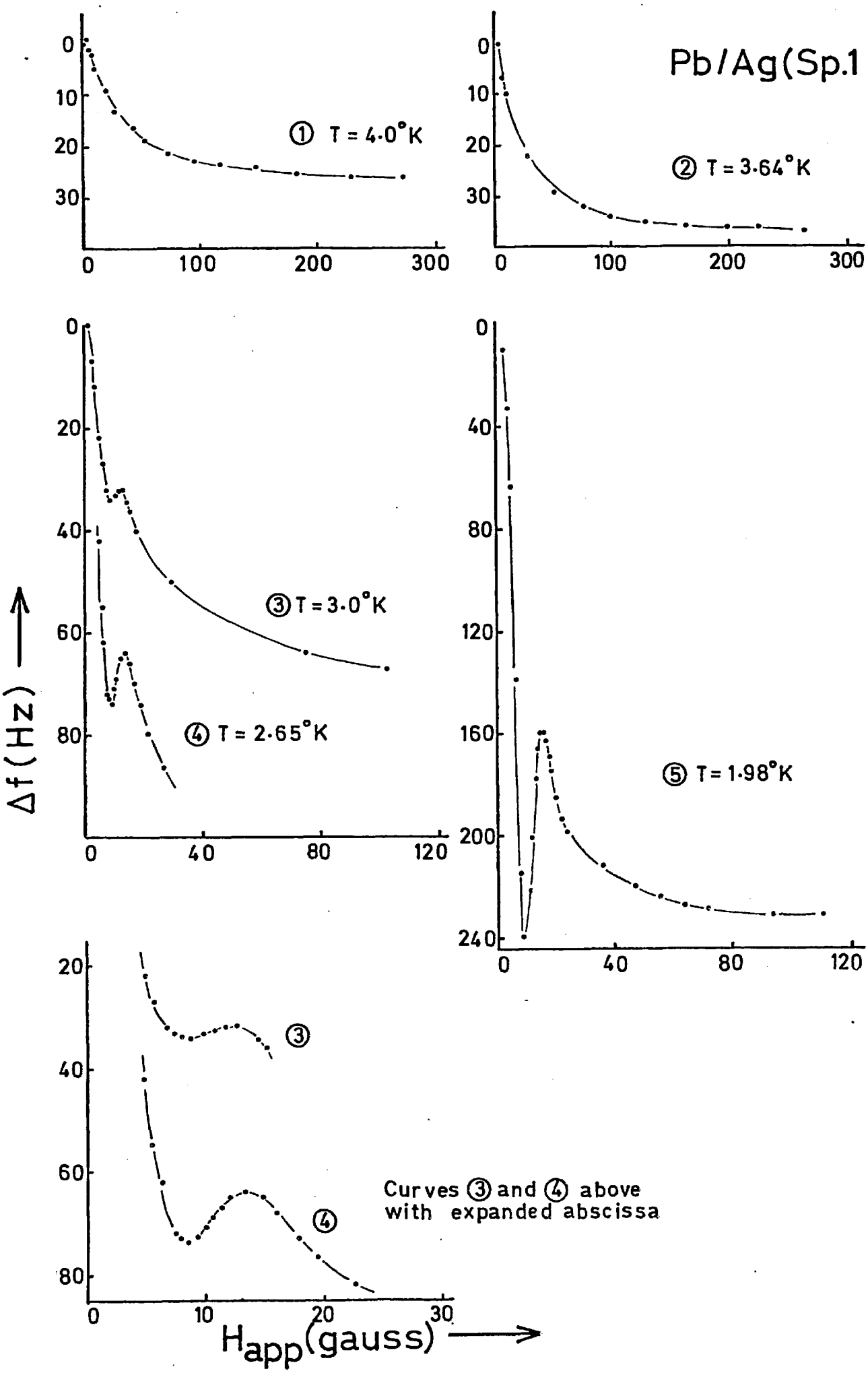

Figure 47(a) - Δf Vs H_{app} curves for a "thin" Pb/Ag specimen at several different temperatures.

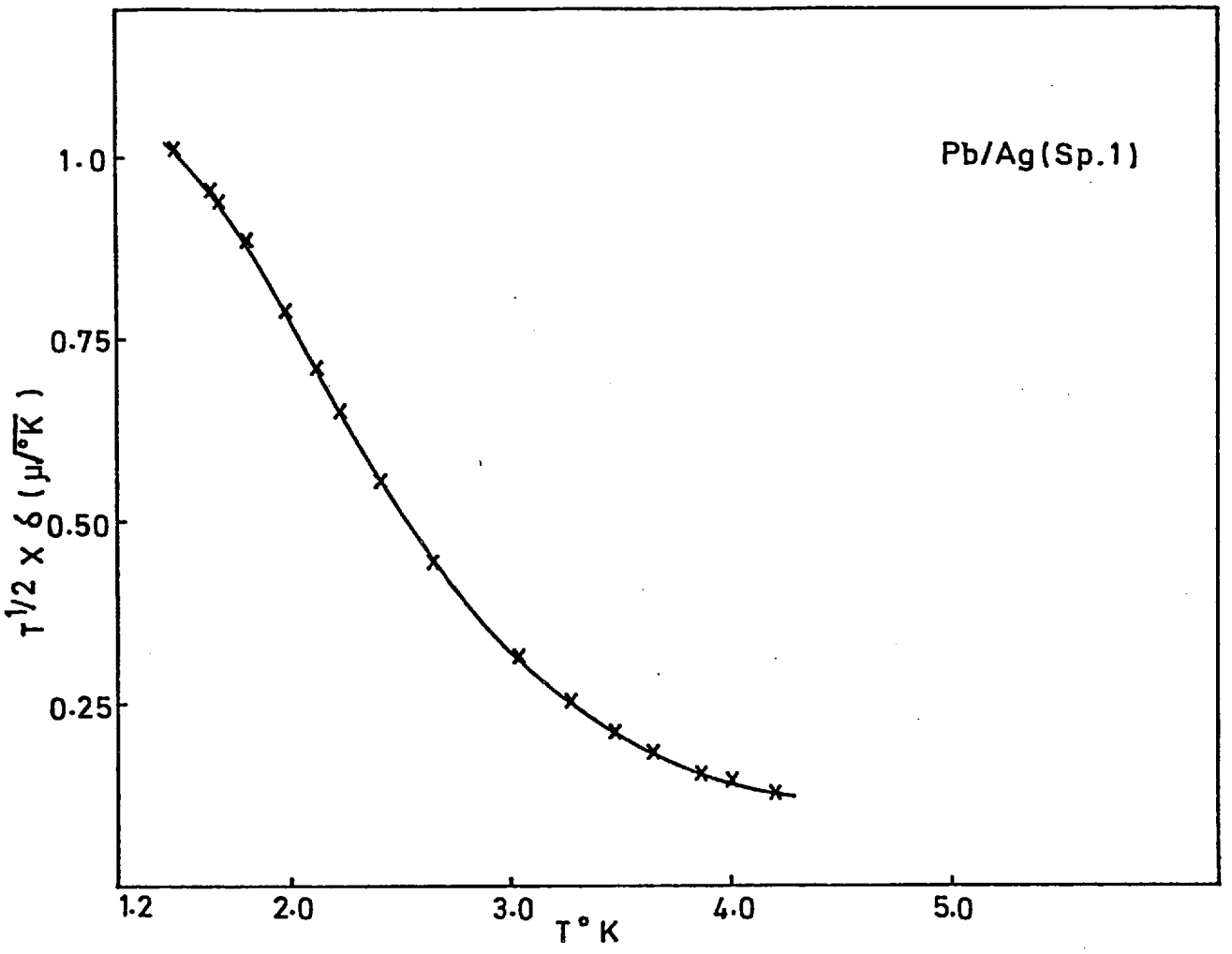

Figure 47(b) - $T^{\frac{1}{2}}\delta$ Vs T for a "thin" Pb/Ag specimen.

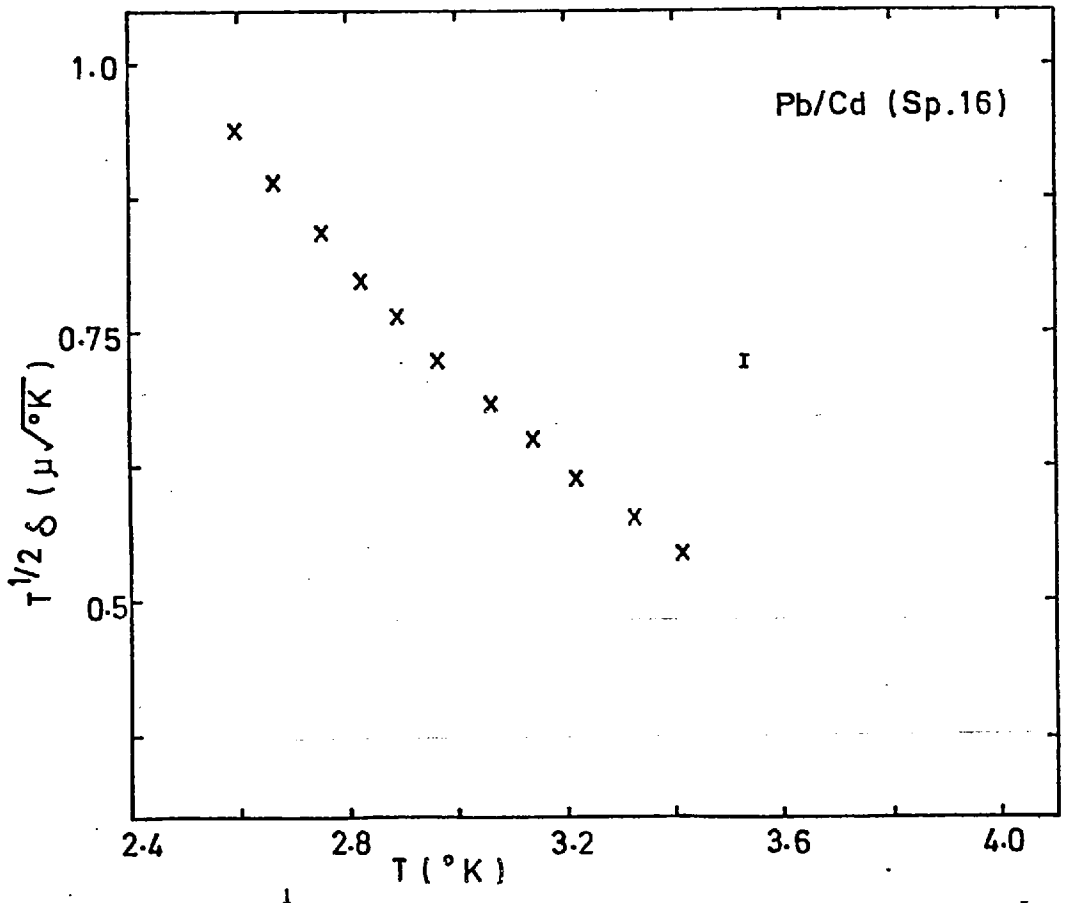

Figure 46(c) - $T^{\frac{1}{2}}\delta$ Vs T for a Pb/Cd specimen with the range $2.5^{\circ}K < T < 3.3^{\circ}K$ carefully scanned.

inflexion point in the variation of the vector potential $A(d_N)$ as a function of the applied field. A large $\frac{dA}{dH}$ produces a dip in the transition curve (§5.3). Such a transition, however, will not be accompanied by any supercooling i.e. hysteresis in the field transition in increasing and decreasing fields. Observations similar to ours have been reported by the Orsay Group (56) whose results for an InBi/Zn specimen are shown in fig.49. It is seen that in the temperature regime $T > T^*$ the magnitude of the dip $\Delta\nu_2$ (in their notation) increases as T is lowered towards T^*, an observation our results support. Moreover, we were unable to observe any field hysteresis. Although we cannot discuss here the subject of breakdown effects in detail, the important conclusion from our point of view is that unless the thickness d_N is much larger than the critical thickness d_N^*, the resulting $T^{\frac{1}{2}}\delta$ vs T plots do indeed show a decrease in the magnitude of the slope at low T.

Now, while the exact normal metal thicknesses of the Orsay Group's specimens are not given in either of their two publications on the subject of 'saturation', it is mentioned in ref. 64 that the thicknesses of their films were ~ 5000 Å for Ag and ~ 1μ for Zn and Cd. Although the critical thickness d_N^* will clearly depend on the purity of the material (longer m.f.p.'s giving larger d_N^*) our results clearly indicate that ~ 5000 Å is not an adequate thickness for screening distance measurements in the range of the m.f.p.'s that their specimens span (ℓ ~ 1400 Å to ~ 200 Å for Ag).

Although we could not carry out a systematic study of the variation of δ as a function of d_N, we have come across some

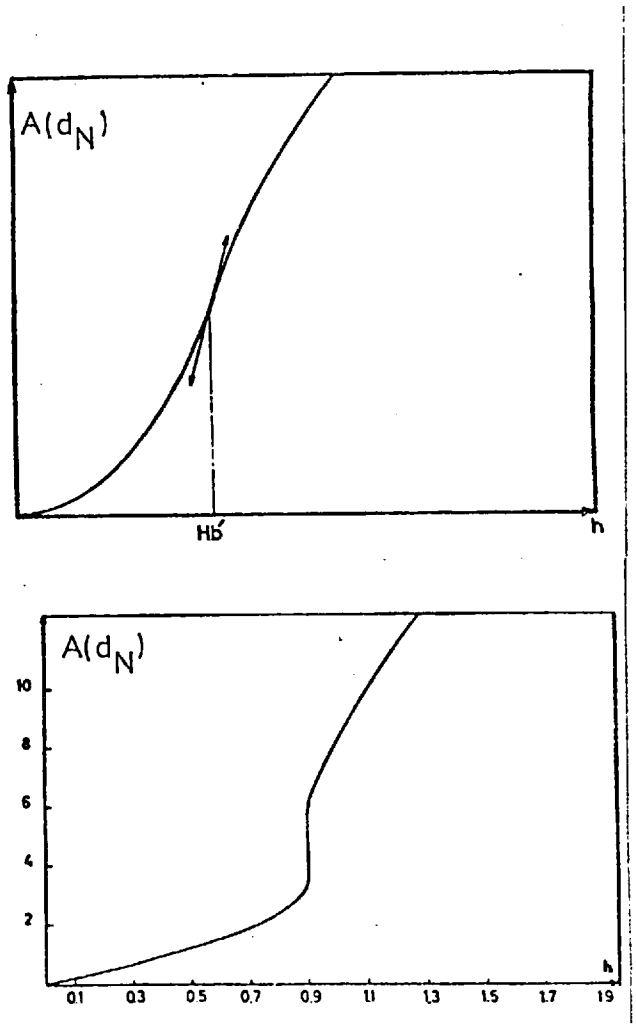

Figure 48 - The vector potential $A(d_N)$ as a function of the applied field h ($= H_{app}/H_c$) (Reproduced from Hurault(47)).

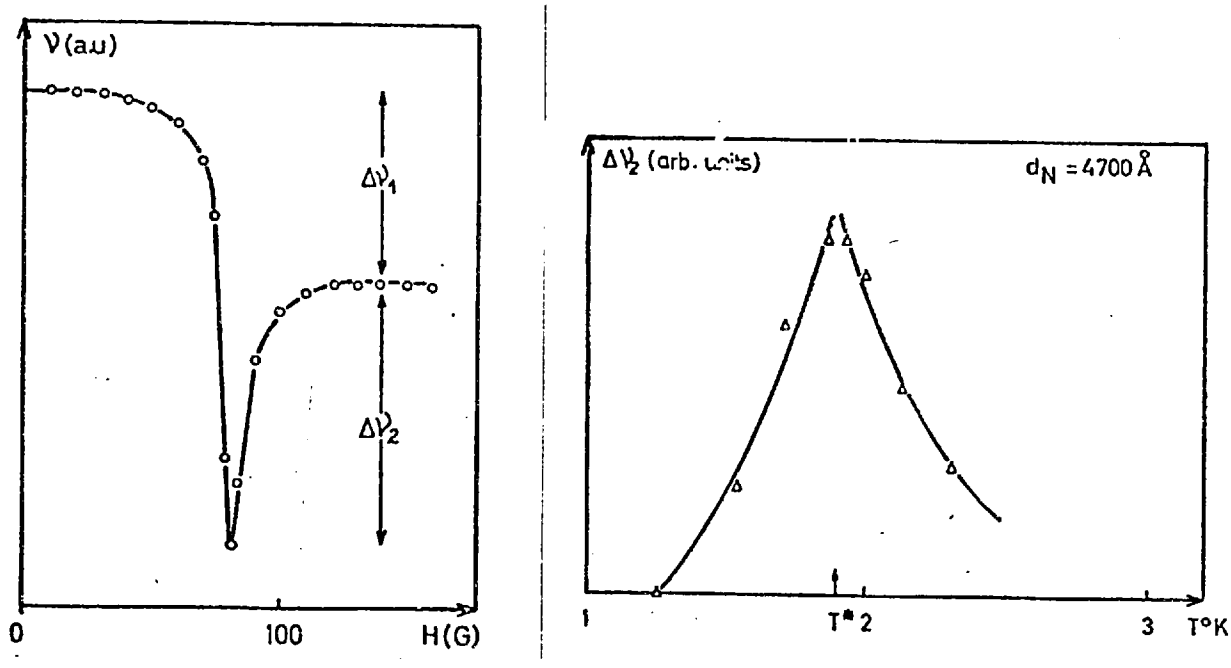

Figure 49 - R.f. permeability measurements on InBi/Zn showing how the amplitude of the peak in the frequency Vs H_{app} curves varies below and above T^*. (Reproduced from ref.56).

early work by Deutscher and Hurault (58) who measured δ in Zn/In Bi for different Zn thicknesses. From their original results shown in fig. 50(a) we have plotted $T^{\frac{1}{2}}\delta$ vs T (fig. 50(b)) and the effect of thickness on the slope of the latter curves is apparent.

It should be mentioned that neither in the above work nor in the Group's latter measurements(64) of δ is mention made of their observing any breakdown effects. In this connection we can only report that we found that the presence of these effects could easily be overlooked unless in obtaining the transition curves, the field increments were kept sufficiently small.In both of the above measurements by the Orsay Group, the field was continuously swept and therefore the rate of sweep would be important in determining whether these effects were observed.

(ii) Frozen flux

It was pointed out in §5.4 that the presence of frozen flux could considerably lower the measured value of δ. In order to determine if this could account for the kind of effects observed by the Orsay Group, a series of measurements were done on Specimen 2 under different conditions. The results (fig. 51) show that if a large amound of flux is left in then the curve does indeed flatten off as T is lowered. However, this results in such a drastic lowering of δ that frozen flux effects do not appear a likely explanation of their results. This explanation cannot however be entirely ruled out without knowing the exact details of their experimental procedure, particularly as all their measurements seem to have been made

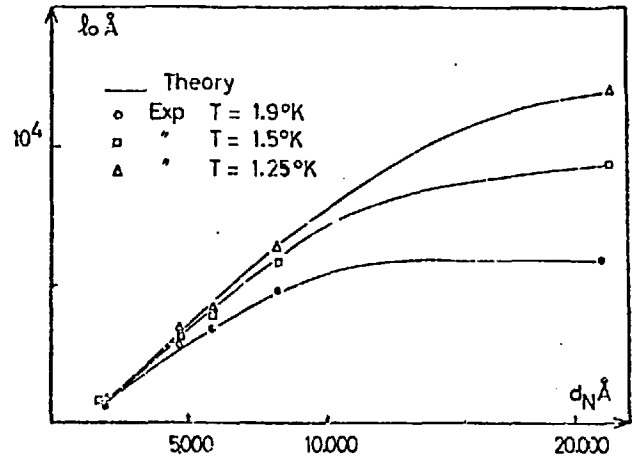

(a)

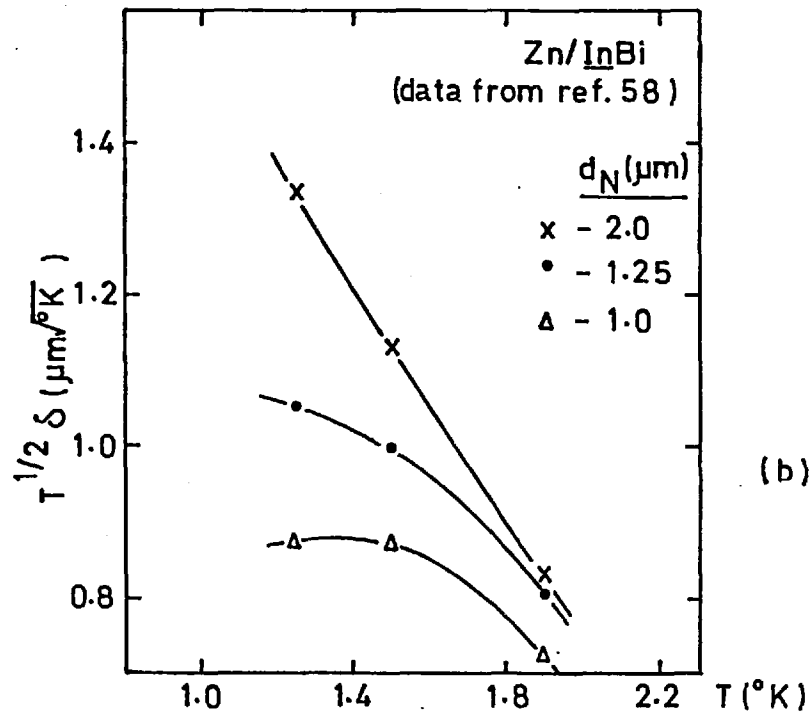

(b)

Figure 50 - (a) The screening distance (ℓ_o) in InBi/Zn as a function of the thickness d_N of the normal film, for three values of temperature.(Reproduced from ref. 58). (b) The quantity $\ell_o T^{\frac{1}{2}}$ obtained from fig.(a) plotted as a function of temperature for different thicknesses.

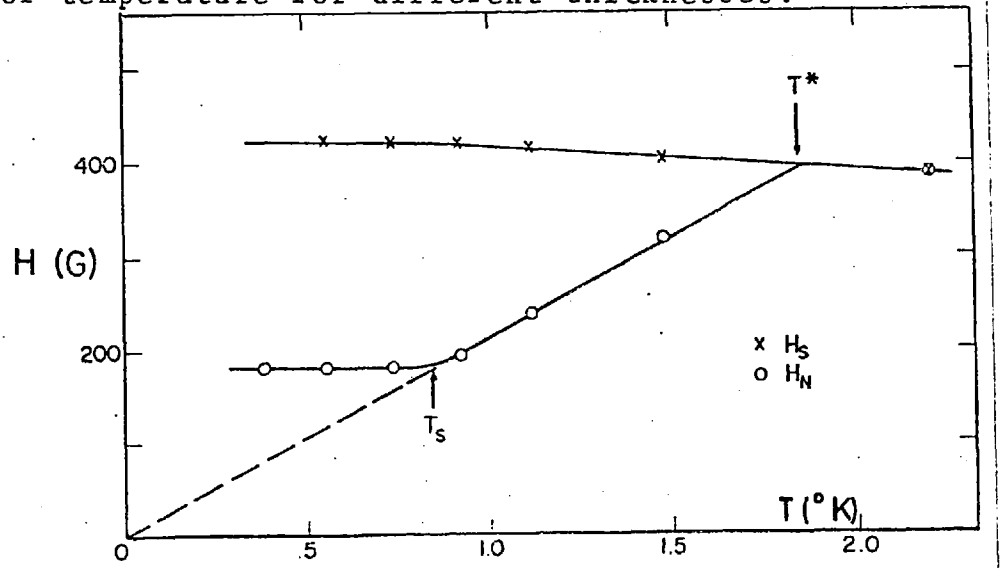

Figure 52-Critical fields of a Ag layer sandwiched between two PbBi layers as a function of temperature.H_S is the field at which normal state is restored in increasing fields, H_N the field at which superconducting state nucleates in decreasing fields.(Reproduced from ref. 53).

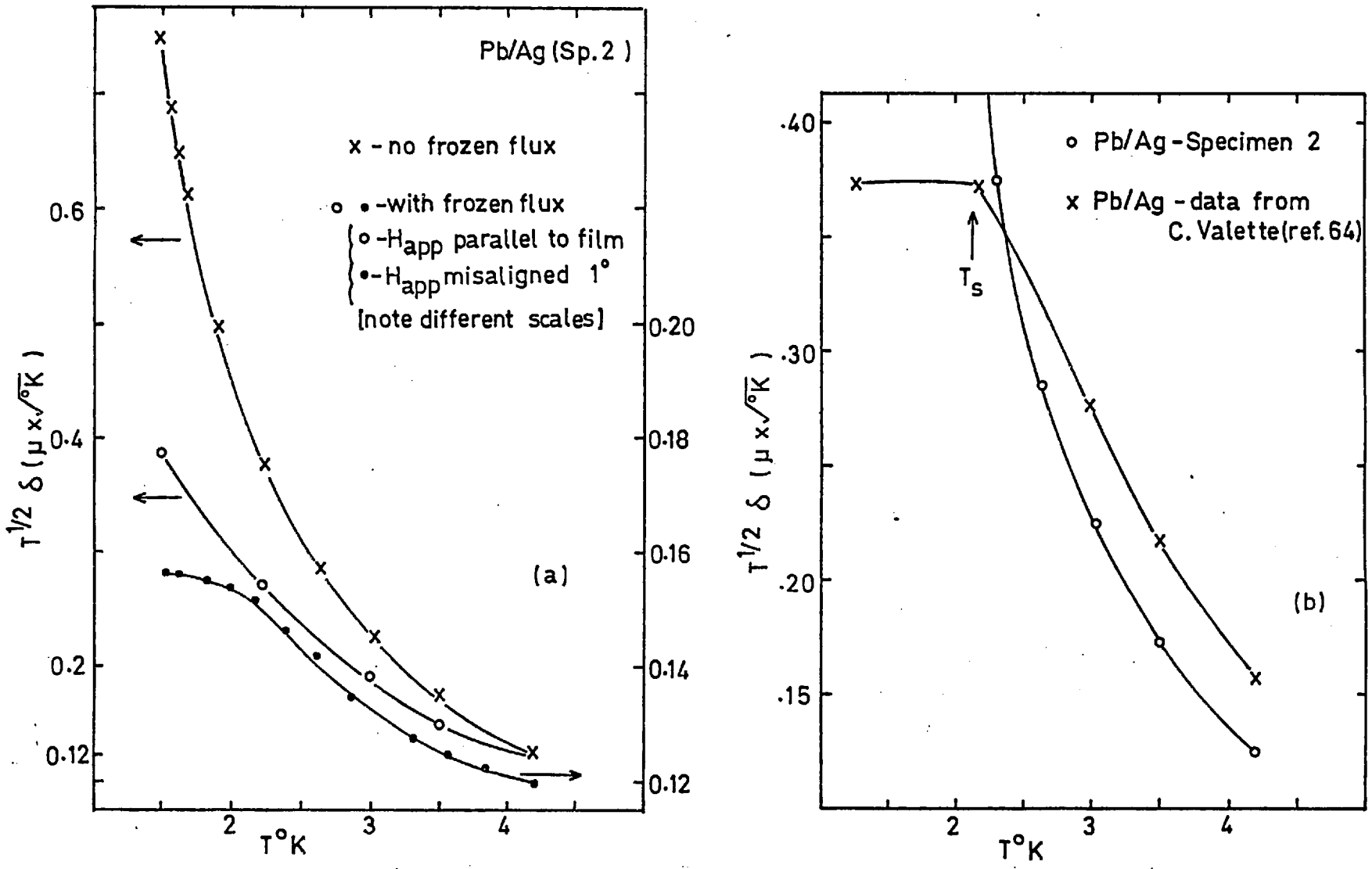

Figure 51 - (a) Plot of $T^{\frac{1}{2}}\delta$ as a function of temperature for Pb/Ag showing the effect of leaving in frozen flux. (b) Comparison of present results with those reported by Valette(64).

at five fixed temperatures.

The only other reported observation of 'saturation' effects is by Deutscher, Hsieh, Lindenfeld and Wolf (53,68). They studied the thermal conductivity of Ag layers sandwiched between layers of Pb Bi. They observed that the field induced transition of the Ag (in the H_e^3 range) was of the first order and identified the field for the transition in increasing fields (from superconducting to normal state) with the breakdown field H_b and that for the transition in decreasing fields (from normal to superconducting) with the supercooling field. Their results for a triple layer are shown in fig. 52. T_s is the temperature at which "the saturation region extends throughout the normal layer". Although an extensive critique of their work is beyond the scope of this thesis, we nevertheless point out certain features of the work which suggest that as evidence of 'saturation', the results be treated with caution.

Firstly, we note that the authors use the Orsay Group's theory of breakdown effects (55, 56) to analyse their results. According to the Orsay theory, the supercooling field H_W (H_N in the notation of ref. 53,68) is given by

$$H_N = \frac{\phi_o\, k}{2\pi\, \lambda_N} \times \frac{1}{\sinh(kd_N)} \qquad \text{(VI-4)}$$

For small values of kd_N, $H_N \propto T^{-\frac{1}{2}}$, which is quite opposite to the temperature variation of H_N in fig. 52. This raises the question of whether their identification of H_N with the theoretical supercooling field is justified. We recall (§2.12) that

H_W has been calculated for a two layer system where the screening properties of N are determined solely by the supercurrents that N can sustain. A three layer system is different in that the bulk of the shielding currents are carried in the outer superconducting layers with the N layer providing two weak links. Such a configuration is likely to trap flux in decreasing fields with the result that the true supercooling field of Ag would be masked.

It is curious that according to the author's analysis, their results are in very good agreement with the theory. The answer to this apparent inconsistency lies in the authors' claim that in a situation where there is no superheating the Orsay theory would lead to the relation $H_W/H_b = \kappa(0,T)/\kappa(0,T^*)$. A careful study of the breakdown field theory has failed to show how the above result can be obtained.

It is therefore fair to conclude this section by stating that the existence of 'saturation' effects in Ag has certainly not been firmly established by any experiments to date.

6.5 Effects of Order of Evaporation and Time Lag

In §3.9 we mentioned the likelihood of the order of evaporation of the S and N materials having a significant effect on the results. The existence of such effects has been known since the early work of Hilsch (9) on the transition temperature of superimposed films. Although in view of all the considerations mentioned in §3.9, the deposition of the normal metal followed by Pb (for the Pb/Ag system) seemed most advantageous we did a

control experiment with the order of evaporation reversed in order to find out how the screening distance would be affected. The results are compared in fig. 53. The control experiment was not, however, expected to provide a conclusive answer as to why the two sets of results differ. The two reasons most commonly advanced to explain such effects are (1) the possibility of a particular evaporation order being more conducive to oxide formation at the interface (2) the change in the morphology of a film resulting from the nature of the substrate onto which it is deposited. Although oxide formation cannot be entirely ruled out, we think it to be unlikely for reasons detailed in §6.1. The reproducibility of results for Zn/Pb and Cd/Pb specimens for all of which Pb was deposited first also leads to the same conclusion. Any major effect arising from a change in the film morphology may, at first sight, be expected to be shown up by the comparison of the resistances of the films. Because of the large difference between the conductivities of Pb and Ag at room temperature (when $\sigma_{Ag} \simeq 13 \times \sigma_{Pb}$) and at liquid He temperature ($\sigma_{Pb} \simeq 2\sigma_{Ag}$) a comparison of the summated conductances of the separate strips with that of the sandwich at those two temperatures should, in theory, reveal any great change in the resistivity of one material or the other when part of the sandwich. However, within the margin of error of ~ 10% arising mainly from the possible differences in thickness between the test strips and the corresponding layers in the sandwich (§3.8) the resistance measurements did not reveal any significant dependence of film resistances on the order of evaporation. This,

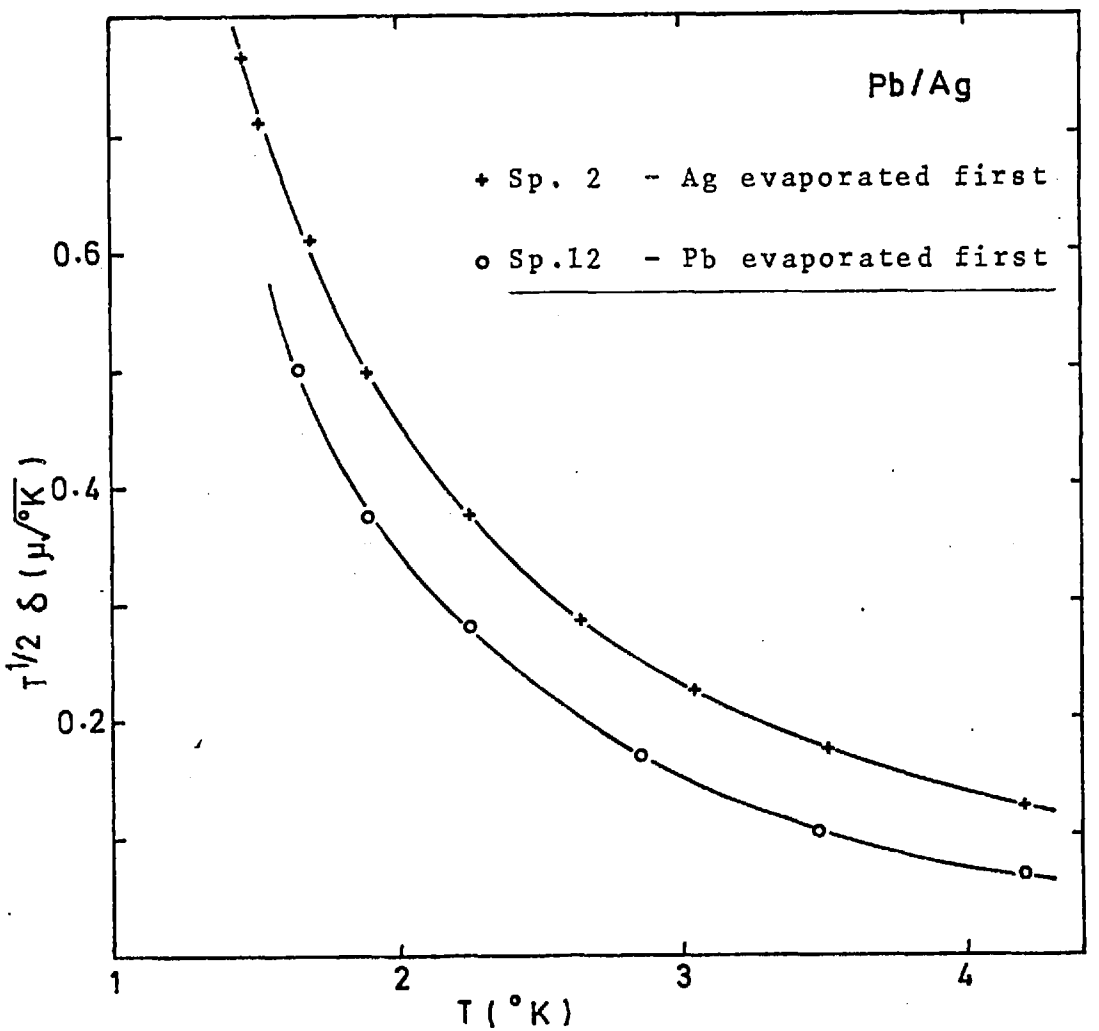

Figure 53 - The effect on the screening distance δ of the order of evaporation for Ag/Pb specimens.

however, does not preclude the possibility that only a thin layer of a film near the interface might be affected by the nature of the substrate, producing the observed dependence of the proximity effect on the order of deposition. This, in fact, was the conclusion that Hauser et al. (22) arrived at after an exhaustive series of control experiments on the depression of T_c in Pb/Pt, Pb/Fe, Pb/Gd and Pb/Cr. Moreover, by comparison of their results with theory they also established that the order of evaporation that produced the greater proximity effect (i.e. greater depression of T_c in their case) always gave a much better fit to the theory and ought to be used. In our experiments, this criterion would amount to adopting the order of evaporation that gives the greater screening distance i.e. N followed by S, which in fact has been used for the Pb/Ag system.

Although the S and N materials studied were chosen for their low mutual solubilities and the absence of any intermetallic compounds, we studied the effects of prolonged time lags on several specimens in the hope that any progressive interdiffusion would show up in the results. For example, the screening distance and film resistances were measured five times over six weeks for a Pb/Ag specimen (Sp. 2) and those for Zn/Pb (Sp. 14) and Cd/Pb (Sp. 16) three times each over a two week period. In each case, no change in the specimen properties was observed, within the accuracy of the measurements. An interesting contrast is provided by our study of two Pb/Au specimens. Pb and Au form two inter-metallic compounds, Au_2Pb and $AuPb_2$, the latter being superconducting with a transition temperature of $\sim 4.4^{\circ}K$(105).

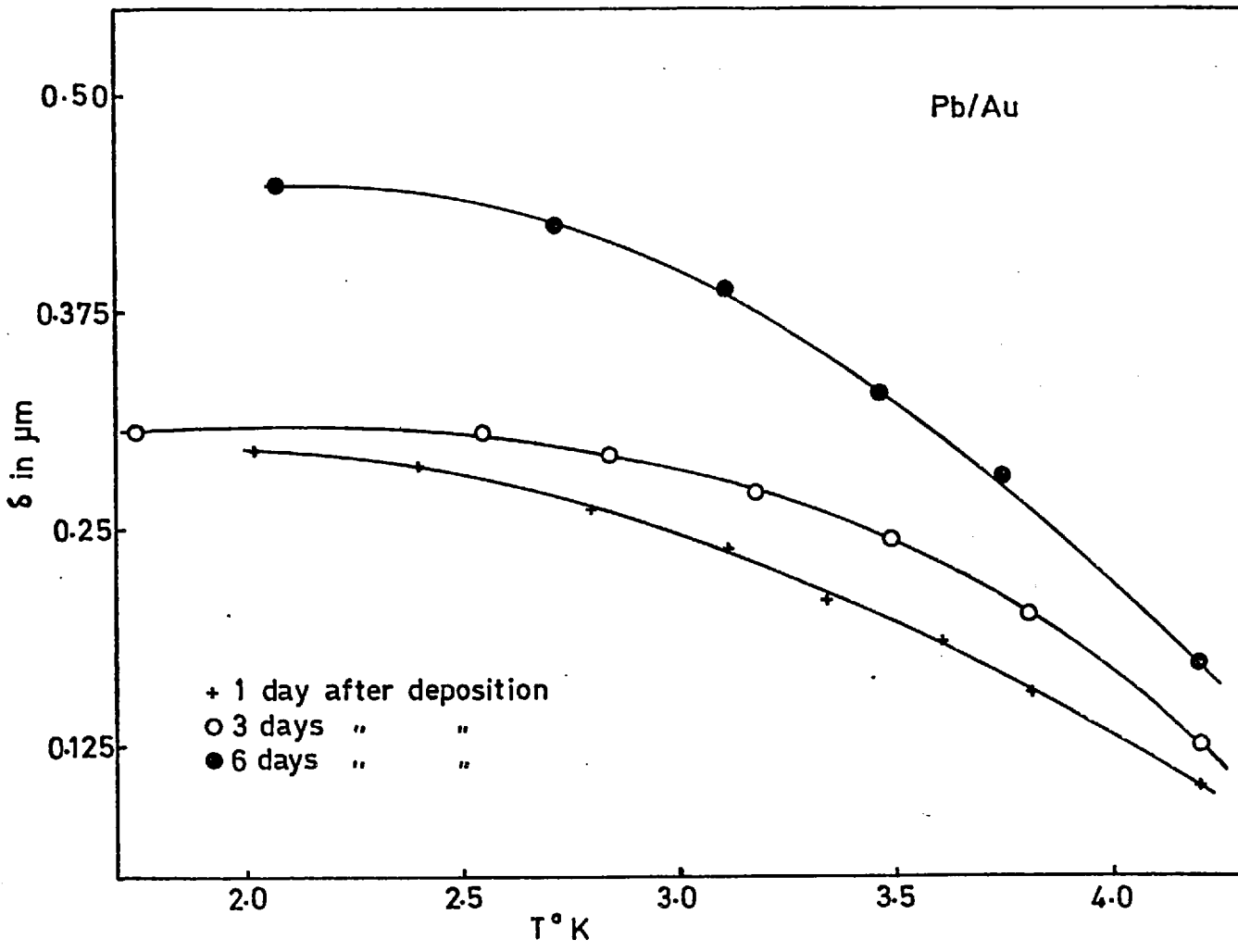

Figure 54 - Effect of prolonged time lag (several days) on the measured screening distance δ in a Pb/Au specimen. The specimen was stored at room temperature between measurements.

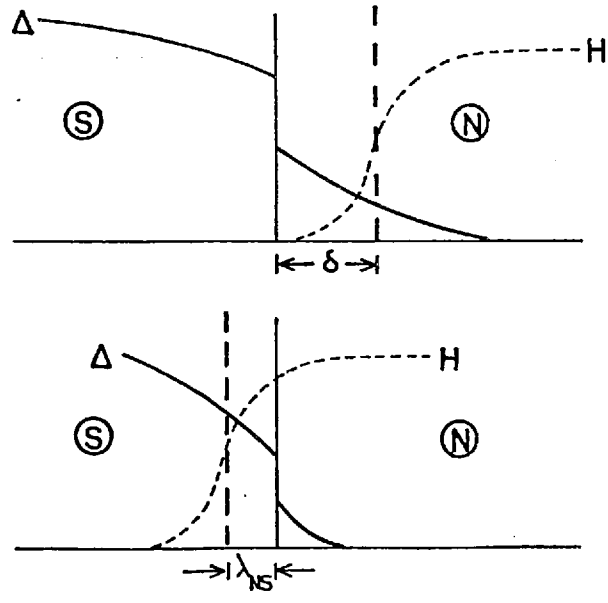

Figure 55 - Schematic representation of the weak field penetration depth λ_{NS} at an NS interface.

The effect of time lag on one of these specimens is shown in fig. 54.

6.6 Assessment of Technique and Suggestions for Future Work

As a means of investigating the interaction parameter NV of a normal metal the measurement of the screening distance is experimentally an attractive technique for reasons enumerated in §1.15. The main problem on the practical side is to improve the sensitivity of the measurements so as to permit the study of alloys well into the dirty limit. For flat specimens the sensitivity is limited by the thickness of the substrates. In this regard, there is room for substantial improvement by the use of thinner substrates several of which coated with the films may be stacked together to give higher filling factors. Measurements with dirty Cd, Zn and Aℓ as the N material of NS systems ought then to provide good data for a thorough comparison with the theory. For this, however, correction will have to be made as described below for an important omission from the present theory.

One major flaw in Deutscher's calculation of δ appears to be the failure to take into account the weak field penetration into the superconductor itself in the vicinity of the interface. The situation is illustrated schematically in fig. 55 from which it can be seen that the quantity measured in our kind of experiment is $\delta+\lambda_{SN}$ where λ_{SN} is the weak field penetration depth in S when coated with N.

De Gennes and Matricon(41) have shown that λ_{SN} is always larger than λ (the penetration depth in the absence of the N material) and that unlike λ it is a strong function of the applied field, particularly near the critical field of S.

In an experimental situation like ours λ_{SN} can be $\sim 2\lambda$ at $H_{app} \simeq 0.5H_c$. This means that λ_{SN} is actually larger than the measured screening distance for many of our Ag alloy specimens. This in turn would imply that although the N material does provide screening, the 'flux front' in zero field may actually exist inside S initially and move further into S as, with increasing field, the capacity of N to sustain screening currents is progressively destroyed. In the case of metals like Zn and Cd the measured screening distances are much larger than λ_{SN} and correcting for λ_{SN} should be straightforward once this quantity has been estimated by the method of de Gennes and Matricon(41). The situation is clearly more complicated for metals like Ag and Cu and a basic refinement of the theory appears necessary.

In view of the omission from Deutscher's theory of this important factor, ours, as indeed any other, estimate of the interaction parameter of a normal metal like Ag based on the theory must be considered unreliable.

With regard to the theory of the "saturation effect", our discussion in §2.14 and the experimental evidence presented in this thesis both call for a fundamental re-appraisal of the subject of "saturation" in normal metals. In this connection, a useful avenue for further investigation suggested by this work is a systematic study of the effect on δ, particularly on the slope of $T^{\frac{1}{2}}\delta$ Vs T curves, of varying the normal metal thickness. Our conclusions in this respect (§6.4(i)) were based on the results from one specimen and on some earlier work by the Orsay Group and a confirmation of these to fully account for the Orsay Group's remarkable observations in this field would be desirable.

Sp. No.	N Material	Res. Ratio	ρ_{res} μΩcm	m.f.p. μ	$k^{-1}(4.2^{o}K)$ μ	d_N μ	d_S μ	Δf_{Pb} Hz	$A \equiv d_S/\Delta f_{Pb}$ Å/Hz
1	Ag	17.8	0.05	2.2	0.54	1.3	2.0	811	25
2	Ag	17.1	0.09	1.3	0.42	3.7	2.1	780	26
3	Ag Mn(100ppm)	7.1	0.23	0.50	0.26	1.3	1.4	566	25
4	Ag Mn(50ppm)	12.0	0.12	1.0	0.36	1.5	2.0	838	24
5	Ag Mn(150ppm)	4.70	0.38	0.30	0.20	1.2	1.8	719	25
6	Ag Aℓ(0.5at.%)	3.20	0.74	0.16	0.14	2.4	2.0	755	26
7	Ag Aℓ(0.8at.%)	2.50	1.09	0.11	0.12	1.6	2.1	815	26
8	Ag Aℓ(0.3at%)	3.65	0.62	0.19	0.16	1.7	1.7	648	26
9	Ag Aℓ(1 at.%)	1.95	1.72	0.07	0.09	1.5	2.1	803	26
10	Ag Aℓ(1.5at.%)	1.60	2.72	0.04	0.08	1.9	1.6	642	25
11	Ag Aℓ Mn(0.6at.% 100ppm Mn)	2.40	1.16	0.10	0.12	1.2	1.8	693	25
12	Ag	14.0	0.13	0.9	0.34	2.1	2.1	770	27
13	Ag Aℓ(0.5at.%)	2.95	0.84	0.14	0.14	1.2	2.1	810	26
14	Zn	12.0	0.54	0.33	0.14	4.2	2.0	788	25
15	Zn	9.3	0.72	0.25	0.12	4.9	2.2	883	25
16	Cd	34	0.22	0.78	0.25	5.7	1.9	753	26
17	Cd	25	0.30	0.57	0.21	3.4	2.0	810	25
18	Cd Mg(2at.%)	8.1	0.80	0.21	0.13	4.2	2.0	815	25

Table VI-1

REFERENCES

(1) Superconductivity, R.D. Parks ed. (M. Dekker Inc., N.Y. 1969):

(a) P.G. de Gennes and G. Deutscher: "Proximity Effects"

(b) N.R. Werthamer: "Ginzburg Landau Equations and their Extensions".

(2) R. Burton, O. Wilhelm and A.D. Misener, Trans. Roy. Soc. Canada, 29, 65 (34).

(3) J. Bardeen, L.N. Cooper and J.R. Shrieffer, Phys. Rev., 108, 1175 (57).

(4) See, for example, P.G. de Gennes: Superconductivity of Metals and Alloys (Benjamin, N.Y., 1966).

(5) E.A. Lynton: Superconductivity (Chapman and Hall, London, 1969), pp. 162.

(6) G. Boato, G. Gallinaro and C. Rizzuto, Phys. Lett. 5, 20 (63).

(7) P.B. Allen and M.L. Cohen, S.S. Comm., 7, 677 (69).

(8) P. Morel and P.W. Anderson, Phys. Rev. 125, 1263 (62).

(9) P. Hilsch, Z. Physik, 167, 511 (62).

(10) E. Krätzig and W. Schreiber, Phys. Kond. Mat., 16, 95 (73).

(11) H. Meissner, Phys. Rev., 109, 686 (58).
H. Meissner, Phys. Rev. Lett., 2, 458 (59).
H. Meissner, Phys. Rev., 117, 672 (60).

(12) J. Clarke, Journale de Physique, Vol. 29 C2, 3 (68).

(13) P.G. de Gennes and E. Guyon, Phys. Lett., 3, 168 (63).

(14) P.G. de Gennes, Rev. Mod. Phys., 36, 225 (64).

(15) N.R. Werthamer, Phys. Rev., 132 2440 (63).

(16) J.J. Hauser and H.C. Theuerer, Phys. Lett., 14, 270 (65).

(17) W. Moorman, Z. Phys. 197 136 (66).

(18) A.E. Jacobs, Phys. Rev. 162, 375 (67).

(19) A.A. Abrikosov and L.P. Gor'kov, Trans. J.E.T.P., 12, 1243 (61).

(20) P.G. de Gennes and G. Sarma, J. Appl. Phys., 34, 1380 (63).

(21) J.J. Hauser, H.C. Theuerer and N.R. Werthamer, Phys. Lett., 18, 222 (65).

(22) J.J. Hauser, H.C. Theuerer and N.R. Werthamer, Phys. Rev., 142, 118 (66).

(23) R.P. Groff and R.D. Parks, Phys. Lett., 22, 19 (66).

(24) P. Fulde and K. Maki, Phys. Cond. Matt., 5, 380 (66).

(25) C.A. Shiffman, J.F. Cochran, M. Garber and G.W. Pearsall, Rev. Mod. Phys., 36, 127 (64).

(26) P. Fulde and W. Moorman, Phys. Kond. Mat., 6, 403 (67).

(27) J. Lechevet, J.E. Neighbor and C.A. Shiffman, Phys. Rev. B, 5, 861 (71).

(28) P. Manuel and J.J. Veyssie, Phys. Lett., 41A, 235 (72).

(29) A.B. Pippard, Proc. Roy. Soc., A216, 547 (53).

(30) J. Clarke, Proc. Roy. Soc., A308, 447 (69).

(31) J. Clarke, S.M. Freake, M.L. Rapport and T.L. Thorp, S.S. Comm., 11, 689 (72).

(32) S.M. Freake, prv. Comm.

(33) I. Giaever, Phys. Rev. Lett., 15, 675 (60).

(34) W.A. Harrison, Phys. Rev., 123, 85 (61).

(35) D.S. Falk, Phys. Rev., 132, 1576 (63).

(36) S. Bermon: The BCS Differential Conductance for a Metal--Insulator-Superconductor Junction (Tech. Report, University of Illinois).

(37) I. Giaever, H.R. Hart and K. Megerle, Phys. Rev., 126, 941 (62).

(38) P.H. Smith, S. Shapiro, J.C. Miles and J. Nicol, Phys. Rev. Lett., 6, 686 (61).

(39) W.L. McMillan, Phys. Rev., 175, 537 (68).

(40) J.J. Hauser, Physics, 2, 247 (66).

(40) K. H. Behrndt, Vacuum (GB), 13, 337 (63)

(41) P. G. de Gennes and J. Matricon, Solid State Comm., 3, 151 (65).

(42) C. A. Shiffman, priv. comm.

(43) P. Fulde and K. Maki, Phys. Rev. Lett.. 15, 675 (65).

(44) G. D. Cody and R. A. Miller, Phys. Rev., 173, 481 (68).

(45) E. Di Crescenzo, P. L. Indovina, S. Onori and A. Rogani, Phys. Rev. B, 7, 3058 (73).

(46) J. J. Hauser. D. R. Hamman and G. W. Kammlott, Phys. Rev. B, 3, 2211 (71).

(47) J.P. Hurault, Ph.D. Thesis, University de Paris, Orsay (1968).

(48) J.P. Hurault, Phys. Lett., 20, 587 (66).

(49) G. Deutscher, J. Phys. Chem. Solids, 28, 741 (67).

(50) G. Deutscher, J.P. Hurault, F. Meunier and D. Saint-James, Phys. Lett., 25, 514 (67).

(51) R.J. Todd, J.T. Chen and Y.W. Kim, Phys. Rev. B, 5, 2518 (71); 7, 150 (72).

(52) S. Wolf, S.Y. Hsieh, G. Deutscher and P. Lindenfeld, S.S. Comm., 10, 909 (72).

(53) G. Deutscher, P. Lindenfeld and S. Wolf, Phys. Rev. Lett., 23, 1102 (69).

(54) J.P. Burger, G. Deutscher, E. Guyon and A. Martinet, Phys. Lett., 17, 180 (65).
J.P. Hurault, Phys. Lett. 17, 181 (65).

(55) Orsay Group on Superconductivity, in Quantum Fluids Proc. 1965 Sussex Univ. Symp., D. Brewer ed. (North Holland Publishing Co., 1966).

(56) Orsay Group on Superconductivity, Phys. Kond. Mat., 6, 307 (67).

(57) K. Maki, Physics, 1, 21 (64).

(58) G. Deutscher and J.P. Hurault, Phys. Lett., 24A, 102 (67).

(59) G. Deutscher, J.P. Hurault and P.A. van Dalen, J. Phys. Chem. Solids, 30, 509 (69).

(60) M.D. Daybell and W.A. Steyert, Rev. Mod. Phys., 40, 380 (68).

(61) Orsay Group on Superconductivity: Proc. LT 12, Kyoto, F. Kanda ed. (Academic Press of Japan, 1971).

(62) G. Deutscher, S.S. Comm., 9, 891 (71).

(63) C. Valette, S.S. Comm., 9 895 (71).

(64) C. Valette, Ph.D. Thesis, Universite de Paris, Orsay, No. A846 (71).

(65) A. Schawlow and G. Devlin, Phys. Rev., 113, 120 (59).

(66) G. Deutscher and C. Valette: Proc. of L.T. 13, Univ. of Colorado, K.D. Timmerhaus, W.J. O'Sullivan, E.F. Hammel, eds. (Plenum, N.Y., London, 1974).

(67) D. Saint-James and P.G. de Gennes, Phys. Lett., 7, 306 (64).

(68) G. Deutscher, S.Y. Hsieh, P. Lindenfeld and S. Wolf, Phys. Rev. B, 8, 5055 (73).

(69) J.J. Hauser, Phys. Rev., 187, 580 (69).

(70) A.C. Mota, P. Brewster and R. Wang, Phys. Lett., 41A, 99 (72)

(71) (a) L.P. Gor'kov, Soviet Phys. JETP, 7, 505, (58);
(b) Soviet Phys., JETP, 9, 1364 (59); 10, 998 (60).

(72) P.G. de Gennes, Phys. Kond. Mat., 3, 79 (64).

(73) W. Silvert and L.N. Cooper, Phys. Rev., 141, 336 (66).

(74) W. Silvert, Ph.D. Thesis, Browne Univ., cit. ref. 73.

(75) E. Guyon, F. Meunier and R.S. Thompson, Phys. Rev., 156, 452 (67).

(76) R.O. Zaitsev, JETP 21, 426 (65); 21, 1759 (65).

(77) P.G. de Gennes and J. Matricon, S.S. Comm., 3, 151 (65).

(78) K.A. Gschneider, S.S. Phys., 16, 275 (64).

(79) A.L. Hinde, Ph.D. Thesis, Univ. of London (1970).

(80) H.L. Caswell in Phys. of Thin Films, 1, 1 (Academic Press, London 1963).

(81) L. Holland: Vacuum Deposition of Thin Films (Chapman and Hall, London, 1966).

(82) W.B. Ittner, Phys. of Thin Films, Vol. 1 (Academic Press, London, 1963).

(83) K. Fuchs, Proc. Camb. Phil. Soc., 34, 100 (38).

(84) G. Fischer and R. Klein, Phys. Kond. Mat., 7, 12 (68).

(85) P. Martinoli, S.S. Comm., 9, 2177 (71).

(86) G.D. Cody and R.E. Miller, Phys. Rev., 173, 481 (68).

(87) C. Boghosian, H. Meyer and J.E. Rives, Phys. Rev., 146, 110 (66).

(88) S. Wipf, Ph.D. Thesis, Univ. of London (1961).

(89) N.B.S. Monograph 10: The 1958 He^4 Scale of Temperatures (U.S. Dept. of Commerce, 1960).

(90) A.J. Slavin, Cryogenics, April 1972 pp. 121.

(91) D.P. Jones, Ph.D. Thesis, Univ. of London (1969).

(92) R.B. Clover and W.P. Wolf, Rev. Sci. Instr., 41, 617 (70).

(93) B. Bleaney and B. Bleaney: Electricity and Magnetism (Oxford Univ. Press, Oxford, 1965).

(94) G.D. Cody and R.E. Miller, Phys. Rev. Lett., 16, 697 (66).

(95) A.M. Toxen, M.J. Burns and D.J. Quinn, Phys. Rev., 138A 1145 (65).

(96) R.G. Chambers, Proc. Roy. Soc. (Lond) A215, 481 (52).

(97) M.C. Boulesteix, Compt. Rend., 260, 6845 (65).

(98) F.W. Reynolds and G.R. Stillwell, Phys. Rev., 88, 418 (52).

(99) R.S. Seth and S.B. Woods, Phys. Rev. B2, 2961 (70).

(100) D. Jha and M.H. Jericho, Phys. Rev. B3, 147 (71).

(101) J.L. Olsen, Materials Sci. Engng., 4, 61 (69).

(102) C. Kittel: Intro. to Solid State Phys. (J. Wiley and Sons, 1966).

(103) J.M. Rowell, P.W. Anderson and D.E. Thomas, Phys. Rev. Lett., 10, 334 (63).

(104) J.G. Daunt in Progress in Low Temperature Physics, C.J. Gorter ed., Chapter XI (North-Holland, Amsterdam, 1955).

(105) M.F. Gendron and R.E. Jones, J. Phys. Chem. Solids, 23, 405 (62).

(106) P. M. Hansen: Constitution of Binary Alloys, (McGraw-Hill, 1958).